TEXAS INSTRUMENTS

INCORPORATED

HEAT STERILIZABLE AND IMPACT RESISTANT
· Ni-Cd BATTERY· DEVELOPMENT

SECTION III.
TASK IX IMPACT TESTING SECTION

Jet Propulsion Laboratory
Contract No. 951972, Modification No. 14

Final Report, Volume III
January 1969 -- January 1970

AUTHOR: J. M. Gondusky

PROJECT MANAGER: P. V. Popat

TEXAS INSTRUMENTS INC.
Research and Development·Laboratories
Attleboro, Massachusetts

SECTION III.

TASK IV IMPACT TESTING SECTION

TABLE OF CONTENTS

metallurgical
materials division

TABLE OF CONTENTS -- CONT'D.

TABLE OF CONTENTS -- CONT'D.

metallurgical
materials division

SECTION III.

TASK IV IMPACT TESTING SECTION

LIST OF FIGURES

metallurgical
materials division

SECTION III.

TASK IV IMPACT TESTING SECTION

LIST OF TABLES

metallurgical
materials division

SECTION III.

IMPACT RESISTANT COMPONENTS AND CELL DEVELOPMENT

A. DEVELOPMENT OF HIGH-IMPACT TESTING FACILITY

1. Introduction

In support of the unmanned exploration of the planets, the Jet Propulsion Laboratory has been actively interested in the development of electronic equipment capable of hard landing survival since 1959. Of immediate concern was the development of a battery power supply required for a proposed hard landing on Mars in 1973. Based upon entry conditions calculated from information about the gravitational and atmospheric conditions on Mars, a design goal has been selected by JPL for all equipment aboard this hard landing capsule. At present, a shock level of approximately 4000 g (square pulse for 1 msec) from an impact velocity of 120 ft/sec is anticipated as the kind of environment to which capsule components will be subjected. Texas Instruments, as a developer of heat-sterilizable Ni-Cd space batteries, has long been interested in the cell's resistance to shock and vibration environments. During 1969, over 100 high-capacity cells (25 AH) capable of heat sterilization were manufactured for evaluation. Under the same contract with JPL, development work concerned with prime cell components was conducted to further extend the knowledge required for high-impact cell design. In order to carry out this devel-

metallurgical
materials division

opment work and the evaluation of complete cells, it was
necessary to simulate the anticipated shock environment.
The scope of this section is to describe in detail the exist-
ing impact facility at Texas Instruments. We wish to
describe its development and the resultant capabilities at
our disposal.

2. Mechanical Design of Testing Equipment

a) General Description:

In the design of the test facility, prime concern was
given to the means of achievement of the specified
shock pulse (the desired shape, magnitude and length).
Secondary concerns were the great number of cell con-
figurations (shapes and sizes) that must be accommodated.
Finally, a facility with enough versatility to permit
the variation of the shock pulse was needed for a com-
plete study of the dynamic response of components. The
testing method selected to meet these demands consists
of the following arrangement: The specimen is mounted
within a sliding carriage by means of adjustable fix-
turing. Carriage and specimen are then accelerated to
the desired velocity. The sliding carriage is finally
impacted against an expendable target and massive anvil
to produce the desired shock pulse. The overall system
is shown in Figure 1.

metallurgical
materials division

HYGE GUN

SLIDING CARRIAGE

ANVIL
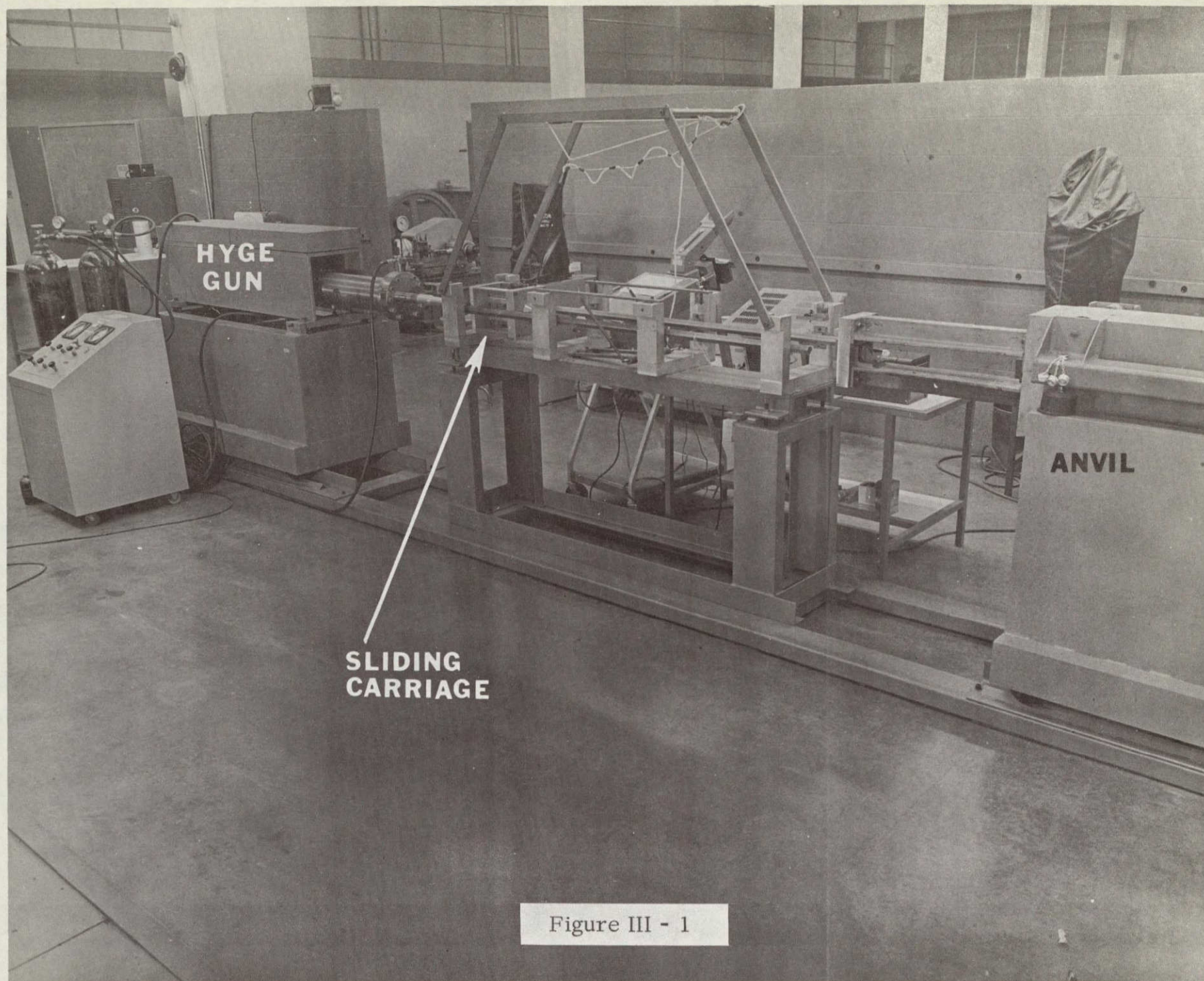
Figure III - 1

b) HYGE ·Gun:

The accelerator is a commercial unit produced by the
Consolidated Electro-Dynamics Corp., and called a, HYGE
gun. It·is essentially a pneumatic cylinder with the
piston operated by a pressure differential. The· gun
used. at·present has a 6" dia. bore with a piston area
ratio of 5'.2:1 and compressed N_2 is the operating
fluid. Thus with approximately 2000 psi N_2 supply this
unit is rated at 40.,000 lbs. thrust and capable of ac-
celerating a 40 lb. mass to a· velocity of 125 ft./sec.
In order to gain more complete firing. control than pro-
vided by automatic unbalance of ·equilibrium, we have
added an auxiliary firing valve. Repeatability of ±1
ft./sec. is attainable on a given sequence· of testing
using the manual firing valve. ·Oscillograph traces of
acceleration – time were recorded to examine the car-
riage input.

c) Carriage & Specimen:

The sliding carriage mass is approximately 32.5 lbs.
All structural members were machined from 7075-T651
aluminum alloy plate. The carriage itself sustains
repeated central impacts during acceleration and more
importantly. at impact. Of prime interest is the· ver-
satile fixture arrangement. We are able to accommodate
various cell configurations and sizes in any orientation.

metallurgical
naterials division

Changes between tests involve very little time and ensure a more rapid evaluation of particular cells or components. Potting material has been unnecessary with the obvious exception of impact at the terminal end of a cell. This ensures a true evaluation of the cell in the absence of most shock attenuating material. The impact end of the carriage is fitted with a hardened steel (M2) impact tool. Several penetrater diameters have been ground and the design has proven quite satisfactory in resisting the repeated impact energy of over 7000 ft.-lbs. As will be shown, the tool diameter is the prime variable affecting the g-level attained at impact and the ability to change this tool readily is of great convenience.

d) Anvil:

The anvil, against which the sliding carriage impacts, is shown on the extreme right of Figure 1. It is basically a 2000 lb block of steel mounted on a steel framework that is free to roll on tracks. At full impact conditions, the entire mass (approx. 2500 lbs) will move 2-3 inches while shock absorbers arrest its motion and return it to the original position. A structural steel extension is fastened to the main anvil block and serves to position the main copper target block. This copper block is our means of achieving the desired uniform

metallurgical
materials division

deceleration of the carriage mass as we plastically
deform the copper. Typically, the target is annealed
copper (#110) 3" x 3" x 1-1/2" thick.

3. Instrumentation System

a) General Description:

In order to fully evaluate a cell during shock environ-
ments, it is desirable to monitor the cell's voltage
during impact and an acceleration-time history for a
full description of the event. The acquisition of data
from a projectile experiencing this kind of motion is
not straightforward. The lead wire arrangement found
most satisfactory is a combination of high strength
steel slide-wire and the two-point suspension loop of
1/4 inch dia. elastic shock cord (bungee). Combined
with an abrasion resistant harness, this system provides
adequate progressive restraint to control the lead wire
motion.

b) Cell Voltage:

Ni-Cd cells present a nominal 1.3 volt open circuit
signal. A signal of this magnitude presents no particu-
lar measurement problem once the lead wire motion has
been controlled. Thus, we are able to display this dc
voltage level directly on the upper beam of the oscillo-
scope. Hence, a cell which is truly impact resistant

metallurgical
materials division

will exhibit a constant potential (straight line at dc
level) throughout the impact period. Complete failure
at impact (plates and tab fracture or complete shorting)
will exhibit a drop to a lower dc level line. In addi-
tion we are able to observe any momentary shorts that
may occur within the cell only during the period of im-
pact. Should it be desirable, an external load is
easily placed across the cell and thus discharge voltage
(or charge voltage) can be measured during the actual
impact.

c) Velocity:

The velocity of the carriage at impact is accomplished
essentially by measuring the actual time of travel
between two points of known distance apart. The moving
carriage momentarily completes two circuits during its
travel and the two voltage pulses are used to start and
stop an electronic counter which records the time
interval (μ sec) between the known distance. Although
basically very simple, this technique is highly reliable
and possesses several advantages over other methods.
Accuracy is better than 0.5 ft/sec.

The velocity measurement itself is made only one inch
before the point of impact. This system readily sup-
plies an equally reliable trigger pulse for the

metallurgical
materials division

oscilloscope as shown in Figure III-2.

d) Acceleration:

(1) Instrumentation:

The measurement of the shock pulse associated with the deceleration of the carriage and specimen is obtained by a piezoelectric accelerometer mounted on the main carriage plate. The high impedance charge output of the transducer (Kistler 808A or 805A) is converted by an electrostatic charge amplifier (Kistler 504A) to the low impedance voltage signal desired for display on an oscilloscope (Tektronix 555). A passive transducer resonance filter is also provided at the amplifier. With this conditioning, the signal is connected to a Tektronix 1A7 plug-in at the scope.

(2) Low Frequency Response:

Good low-frequency response of the system is a necessity in order to follow the long duration of the rectangular pulse created. In the present instrumentation system, the dominant time constant is determined by the product of the feedback capacitor and resistor within the charge amplifier. With the present instrument settings we have a time constant of 5.0 seconds (< 0.1HZ) which is nearly

metallurgical
materials division

Figure III - 2
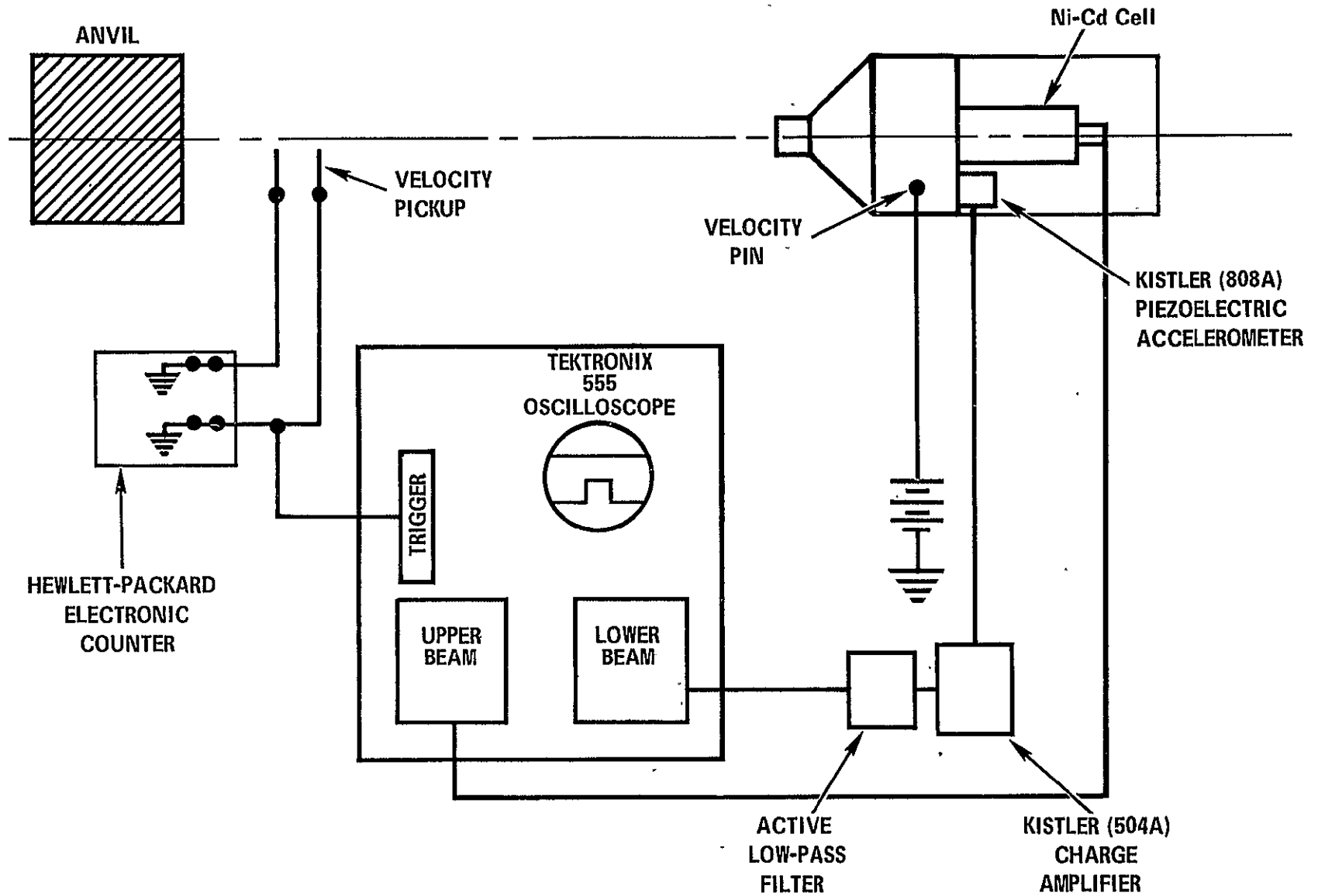
100 times better than the requirement for 2%
accuracy.

(3)   High-Frequency Response:

A Fourier spectrum analysis of a rectangular pulse
shows that most of the energy of that pulse is
contained in the frequency band from zero to 1/T
(T=pulse length). It has also been shown that in
order to prevent excessive rounding of corners,
$f_H \geq 10/T$. In the present case (T=.001 sec) it was
felt that f_H=10KHZ would be quite adequate to
accommodate the rectangular pulse and rapid rise·
time. The high frequency response of the instru-
mentation is theoretically limited by the first
mechanical resonance of the accelerometer (mass-
spring) itself. Manufacturers generally trust
approximately $f_n/5$ as the useable (± 5%) frequency
range and this implies approximately 8KHZ for our
system. This value approached the desired 10KHZ
and we expected fairly good performance. The rise
time of our pulse is approximately 30 µ·sec and
the system seems to have more than adequate high-
frequency response to follow this pulse.

(4)   Effect of Vibrations:

It was felt that lower frequency vibration might
be a disturbing influence and we calculated the

natural frequencies of key structural elements.
within the carriage for several modes of vibration.
Later in the testing program, one rather important
design or structural modification was made to the
sliding carriage which significantly improved the
overall performance. The original 8½" x 8½" x 2"
thick aluminum main plate was replaced by a conical
block of the same aluminum alloy. The shape is
best described as a conical frustrum with a square
base (8½"x 8½") and a circular top (4" dia.). The
conical included angle is 80° providing a 6" height
or "thickness" replacing the original 2" thick
plate. This angle is the same as the tool angle
and the 4" dia. top matches the tool's base exactly.
Thus, we have a smoother transition from tool to
specimen mounting and have essentially eliminated the
vibration problems that previously existed. Because
of the increased weight and associated momentum,
tools of larger diameters were required to maintain
the upper g-levels. However, the resultant shift
in calibration was fully compensated by the increased
structural rigidity and the resultant improvement of
system performance.

metallurgical
materials division

(5) Filtration & Calibration:

Alternatively, such vibration and the frequencies involved were best eliminated from the system by electronic filtration. Thus, an active low-pass filter network was designed and employed to attenuate all but the fundamental vibration frequency.

4. Overall System Analysis

Oscillographs were taken during the development phase. and indicated the g-levels and pulse lengths typically achieved. They were used as the basis for calculations to check the overall system accuracy. Our present collision into copper closely approximates the perfectly plastic collision yet we experience some rebound. Considering the applicable relations:

Impulse = Δ Momentum:

$$\int_{t_o}^{t} F \, dt = m \, (V_{m2} - V_{m1}) \tag{1}$$

Conservation of Momentum:

$$m \, V_{m1} + M \, V_{M1} = m \, V_{m2} + M \, V_{M2} \tag{2}$$

Conservation of Total System Energy:

$$KE_{m1} + KE_{M1} = KE_{m2} + KE_{M2}$$

$$+ \, E \text{ Absorbed in} \quad + \, E \text{ Heat Light.} \tag{3}$$
$$\text{Deforming Copper} \quad \text{Sound}$$

metallurgical
materials division

Equation (1) may be solved for V_{m2} by using the measured V_{m1} and the area of the acceleration-time trace. This would permit the solution of equation (2) for V_{M2} directly assuming m and M were known. Finally equation (3) could be solved for the force required to deform the copper since the depth of penetration is measured. Thus we can compare this calculated force to that force associated with the test's mean g-level. The results are given in Table III A-1.

In the tabulated calculations we have noted the very small anvil velocity that is implied (ref. col. V_{M2}) and the fairly low carriage rebound velocity (ref. col. V_{m2}) that follows the collision and thereby established the system's proximity to the classical plastic case. Late in the testing program high speed photographic analysis was also used to investigate the overall system.

5. System Calibration

During the development phase and the initial testing program, a large amount of data was generated by this testing facility. Many separate studies were employed to extend the typical range of values and the total of this information constitutes the overall system calibration. The blunt-end cylindrical tools are responsible for achieving a square deceleration pulse with excellent

metallurgical
materials division

TABLE III A-1

Tool Dia. (in)	Meas. Impact Velocity V_{m1} (ft/sec)	Calc. Rebound Velocity V_{m2} (ft/sec)	Calc. Velocity V_{m2} (ft/sec)	(1) F_{mean} Calc. from full System Analysis as Described Above	(2) $F_{mean}=ma_{mean}$ a_{mean} Meas. from Photo	(3) $F_{mean}=ma_{mean}$ from uniform decelleration $a_{mean}=\dfrac{(V_{m1})^2}{2S}$	(4) F_{mean} Impulse Time %	(5) $F_{pk}=ma_{pk}$ a_{pk} Measured From Photo
5/8	82	4.5	1.1	56,800#	55,200#	57,800#	51,400#	65,000#
3/4	91	0	1.1	78,700#	74,800#	79,700#	68,800#	87,700
7/8	108.5	3.8	1.5	104,000#	104,000#	105,000#	103,000#	122,000#
1	115.5	10.8	1.6	135,000#	119,000#	138,000#	110,000#	140,000#

rise times. The actual g-level·and pulse length,
however, remain flexible and are under the control of
the operator within certain bounds. It is this capa-
bility (calibration) that is best shown in Figures III-3
and III-4 which illustrate the effects of changing the
main·system variables.

a) g-Level vs Tool Diameter

As indiated earlier, tool diameter or the area of
the penetrator is the prime variable affecting
g-level. Assuming a fairly constant state of three-
dimensional stress during copper deformation, the
total force (g-level) would be directly proportional
to the area. Figure III-3 shows this linear rela-
tionship as exhibited over many impact tests.

b) g-Level vs Velocity

The carriage mass, equipped with any given tool
diameter may be fired at any desired velocity as
regulated by the selection of differential pressure.
The practical limits are: 1) low velocity provides
a short (time) pulse length which was not of inter-
est in this study, 2) high velocity provides a very
deep penetration (tool may be embedded in the
copper) and if a very long (time) pulse length is not.
required, it is avoided as a matter of convenience.

metallurgical
materials division

FIG. III-3

PRELIMINARY IMPACT LEVEL CALIBRATION

ACCELERATION VS TOOL AREA

○ CALCULATED AVE

× MEASURED AVE

ACCELERATION @ 10² @ X10²

TOOL AREA (IN)

MEASURED PULSE TIME
VS
VELOCITY

Tool Dia.
5/8
3/4
7/8

PULSE TIME mSEC

2.0

1.5

1.0

.5

0

CALCULATED PULSE TIME
VS
VELOCITY

Tool Dia.
1/2
5/8
3/4
7/8

PULSE TIME mSEC

2.0

1.5

1.0

.5

0

Fig. III-4

VELOCITY (ft/sec)

0   15   30   45   62   75   90   105   120
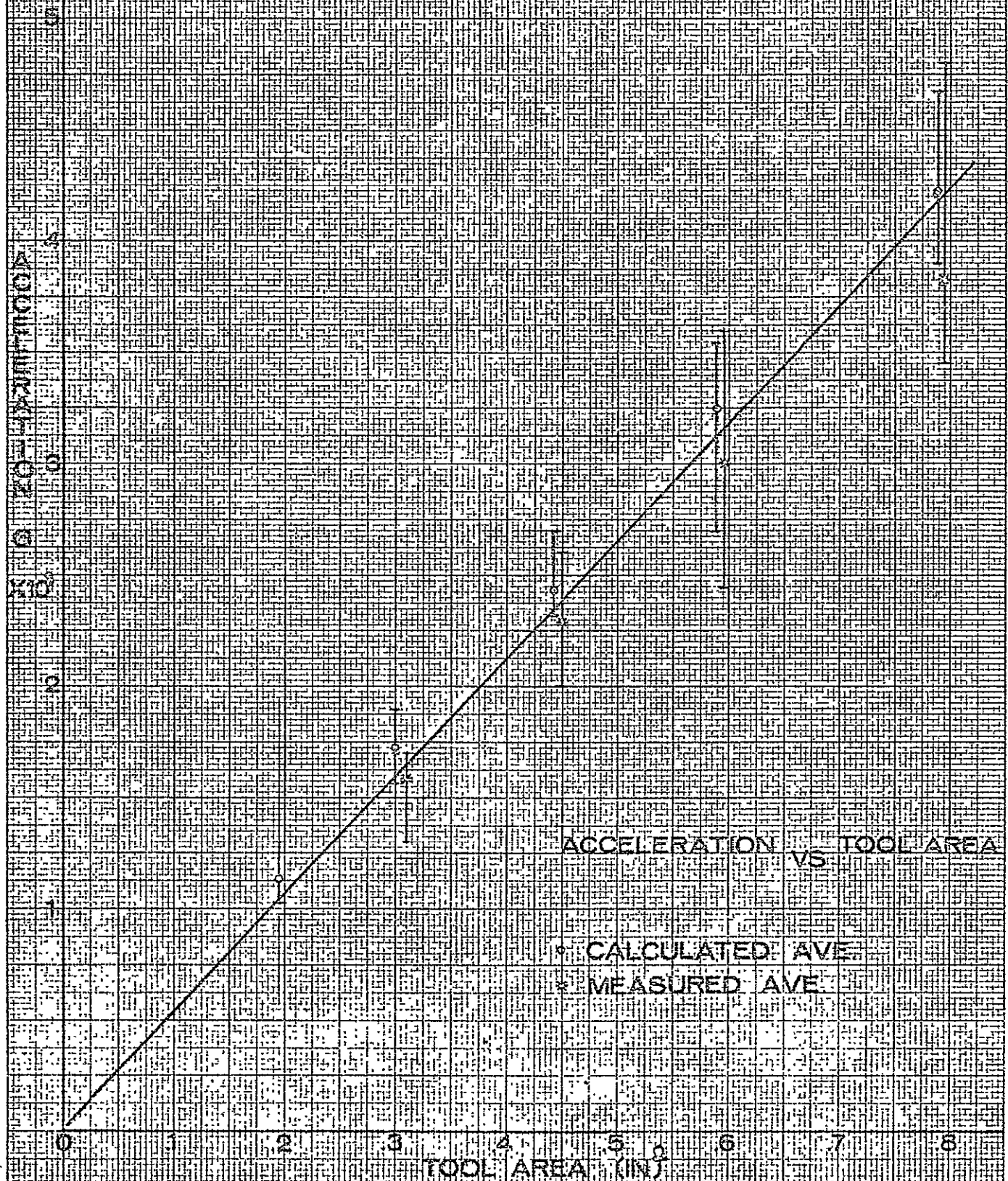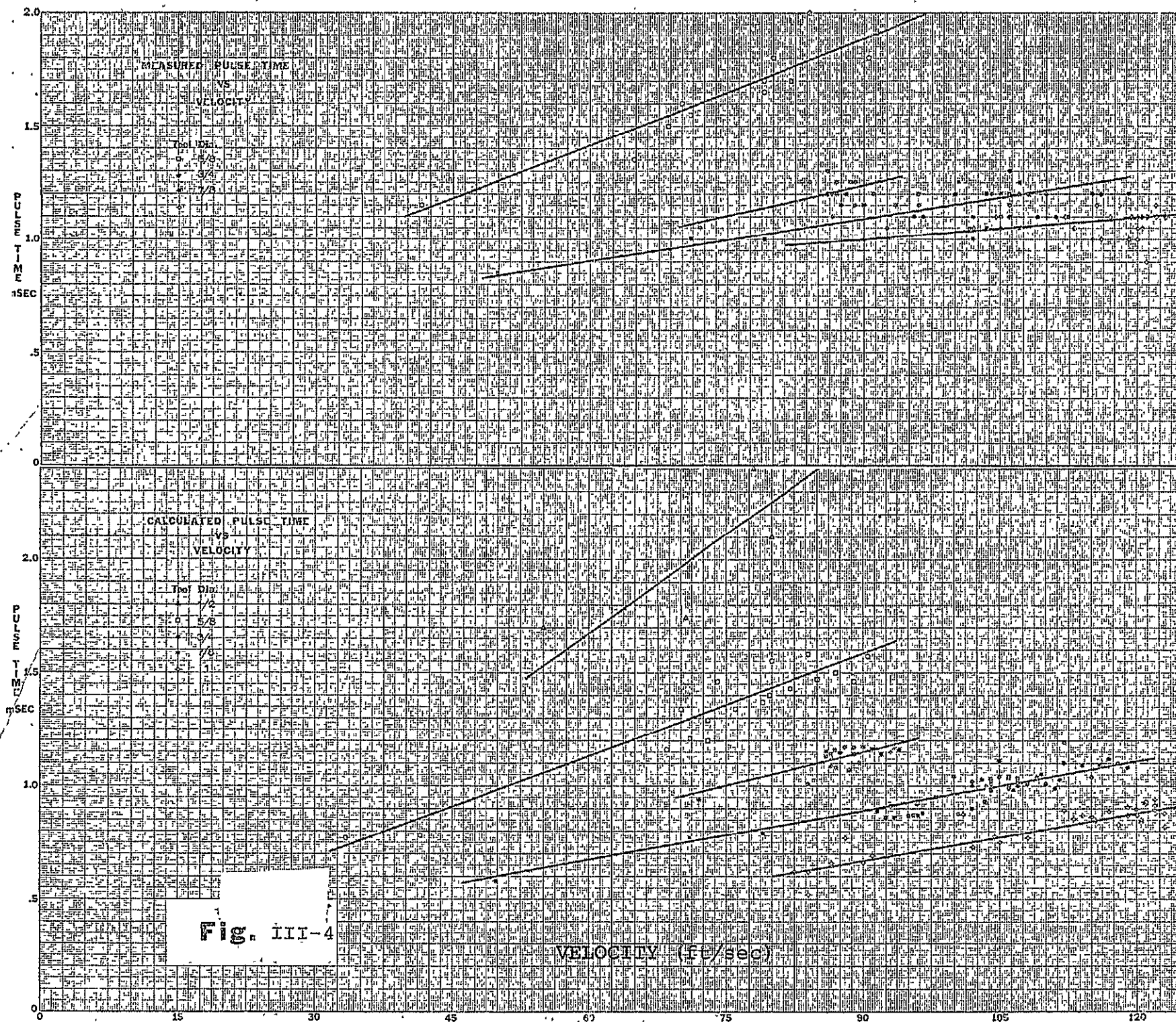
The point is that in saying the g-level is pri-
marily a function of tool diameter, we would expect
to see a g-level (for any given tool) that is
invariant with respect to velocity. We have varied
the test velocity for each tool and illustrated the
relative invariance of g-level.

c) Pulse Length vs Velocity

With a constant carriage mass we would expect that,
as a consequence of the above result, the pulse
length would be linearly related to the test velocity
($\int F dt = M\Delta V$). Figure III-4 illustrates this result.
The lines drawn in Figure III-4 indicate the degree
of sensitivity (pulse length as a function of
velocity) for each tool. Each tool has a different
sensitivity as we have shown it in Figure III-4 but
this is simply a result of including an actual area
function (d^2) within our third parameter tool
diameter (d).

6. Summary

We have developed a versatile impact testing machine
capable of evaluating most cell configurations within
the range of 1000g - 4800g and 0.8 - 2.0 msec. This has
been accomplished by changing only two variables -- tool
diameter and carriage velocity. The ability to cover

such a range this easily is of great convenience during

a given testing program. However, this in no way repre-

sents the limit ranges for this machine. Two other

prime variables (carriage mass and target materials)

have been held constant throughout the system develop-

ment described in this report. If desirable to study

the dynamic response of components to pulses of broader

length range, the additional capabilities of this

machine can be readily employed.

B. DETERMINATION OF THE MECHANICAL PROPERTIES OF Ni-Cd ELECTRODES

1. Introduction and Model Analysis:

The mechanical properties of battery electrodes must be known before the engineering design of an impact-resistant cell can begin. At a minimum, static force data must be available to permit reasonable cell configuration design. A more refined design must be based on dynamic force data. An optimum cell design may indeed hinge on a complete knowledge of the mechanical properties of the fundamental structural elements of the battery. Of prime concern are the electrodes themselves. Their response to a dynamic force input must be determined from a knowledge of their stress-strain-time relation. A major effort under the current Jet Propulsion Laboratory contract was expended in gathering the experimental data needed to describe the mechanical properties of these elements. At the beginning of the experimental work, it was valuable to propose a model for the structural element we were investigating. We made some assumptions about our battery plate material, formulated a model and made some preliminary predictions from that model.

If we neglect the electrochemical differences between the positive and negative plates, we can think about

metallurgical
materials division

their basic structure alone. Both positive and negative
plates begin as a sintered nickel structure called
plaque. This structure is basically a 20 mesh screen of
.007" diameter nickel wire to which particles of nickel
powder have been sintered. Applied primary to one side
of the screen, this sintered structure consists of par-
ticles of nickel powder sintered (fused) to each other
and, of course, sintered to the screen. A first impres-
sion might be to observe the similarity of this plate
to reinforced concrete. This comparison is not totally
valid since the sintered matrix of our plates is a
highly porous structure.

Although electrochemically very desirable, the porosity
of these plates makes structural analysis most difficult!
We have shown (2nd JPL QTR Report 1967) that depending on
positive or negative, cycled or sterilized, the total
porosity may range from 27% to 59%. It is apparent that
we are dealing with a highly complex structure having a
random distribution of various size openings. Some
recent pictures obtained by scanning electron microscopy
have illustrated the complexity and randomness of this
matrix or at least the surface characteristics.

Fortunately, for the development of our structural
model, these properties of the final plate are probably of

metallurgical
materials division

little consequence. We are assuming that only the original sinter structure (plaque, common to all plates) is of load carrying concern. In other words, we are assuming that it matters little from strength considerations that we fill this basic sintered porous structure to various degrees with active chemical material which has little reinforcement capability (especially in tension). Accepting this assumption, we need to be primarily concerned with only the description of the sinter matrix itself. It is this more highly porous structure that we wish to describe via a structural model. The model should allow us to calculate the actual load carrying area within this structure. Then, using the mechanical properties of nickel metal, we may calculate the strength and modulus associated with our model. We considered various cubic crystals as representative of the nickel matrix. The "atoms" (of radius "a") normally placed in the basic crystal, were considered to be hollow spheres; normal void space within the crystal was considered to be solid nickel metal. Three were considered because they offered models of a matrix having 74%· (FCC), 68% (BCC) and 52% (simple) porosity. Most emphasis was placed on the face centered cubic model.

The value of these porous models lies in our ability to look at various cross sections and calculate the load

bearing areas that are available. This was done for the three principal planes of each cubic structure. The overlapping of values obtained from such divergent models (of porosity) indicates something about the random distribution. Our real structure has been shown to contain a random number of various size pores. Therefore, one would expect to see mean values between the extremes of any crystal. This seems strengthened by the fact that the least dense (100) plane of a 52% porous model has a modulus lower than the mean plane (100) of a 74% porous model. We may modify our predictions further by three considerations: a) the real sinter structure (plaque) is 78-80% porous and is thus higher than the 74% porosity of the FCC Model, b) the "necks" carrying load between pores in the structure are essentially areas of infinitesimal gage length. Thus, elongation is impossible and considerable tension load bearing area can be expected to be lost very readily, c) plate material has many small cracks initially due to manufacturing processes. These considerations would tend to lower the apparent modulus and suggest that $E = 3.5 \times 10^6$ as predicted by the FCC (111) analysis would be most valid. This should be true especially in tension. In compression, however, we might suspect an increase. The model approach can also be used to predict values of plate strength. Using handbook values for

nickel metal these calculations were made. The previous consideration of premature yielding of infinitesimal "necks" indicates that some of these calculated quantities are of little value. Once yielding occurs, the matrix will be ineffective and total load should be carried by the nickel wires in tension.

Stress-strain curves were drawn to present upper and lower bounds of the real behavior. A curve for screen alone is completely valid as the lower bound since it assumes no strength associated with a matrix. The curve for FCC (111) is somewhat of an intuitive selection as the possible upper bound (primarily for tension). We expected then, to see experimental tensile data generate a curve very close to the upper bound.

Experimental Program Outline

The data required in support of a model for plate material covers a rather broad experimental program. We are immediately interested in obtaining a stress-strain curve in both tension and compression that will enable us to examine this model more closely and check the assumptions that have been made. Ni-Cd electrodes must be fully characterized with respect to their mechanical properties. What is essentially involved is a determination of the applicable stress-strain relation. However, there are a

metallurgical
materials division

great many areas and tests required to fully explore,
this relation and obtain the kind of information re-
quired to permit the analytical prediction of their
ability to withstand a shock environment. The scope
of the desired information is outlined below:

STRESS STRAIN BEHAVIOR:

    A.   Tensile

    B.   Compressive

        1)   Static

            a) Complete "Shape" of Curve

            b) Modulus of Elasticity

                (1) ΔE vs e-level

            c) Yield Strength.

            d) Ultimate Strength

            e) Poisson's Ratio

            f) Elongation

        2)   Dynamic

            a) Strain-Rate Effects

                (1) Yield Strength

                (2) Ultimate Strength

            b) Stress Amplification

            d) $\sigma\, y = f\,(\omega_n)$

    C.   Bearing Strength (Edge Crushing)

    D.   Thickness Compression of Pack

    E.   Coef. of Friction at Various Pressures

    F.   Buckling at Various Spacing & Pressures

2. <u>Mechanical Properties in Tensile Loading</u>

   a) Constant Deformation Static Testing

      The initial studies of the mechanical properties of
Ni-Cd electrodes involved the static determination
of "conventional" stress-strain curves in tension.
"Conventional" here means the engineering σ-ε curve
as established by constant deformation loading. All
test samples consisted of 1/2" wide x 6" long strips
containing exactly ten (10) longitudinal screen
wires. An Instron commercial testing machine was
used with a cross head speed of 0.1 in/min over a 4"
initial gage length for a constant strain rate, $\dot{\varepsilon}$,
equal to 0.0004" sec^{-1}. With cross head speed
related to chart speed, the x-axis as deformation was
established and with load cell output on the y-axis
we received initial data in the form of a direct load
vs deformation plot which was then easily converted
to a stress-strain curve. For positive plate, nega-
tive plate, positive plaque and negative plaque the
stress is simply the load divided by the actual
measured area of the specimen. However, for screen
specimens, an arbitrary apparent area of 0.013 in^2
was taken to permit strength comparisons with the
final plate material. What we sought from this type
of testing was the comparative strengths of the

metallurgical
materials division

screen alone, the reinforcement associated with the sintered nickel matrix and finally the actual strengths and differences in strength of positive and negative plate. Thus, the rough determination of modulus of elasticity, the engineering yield strength (0.2% ε), the ultimate strength, elongation (% in 4" G.L.) and most importantly, the complete shape of the stress-strain curve into the plastic region were of immediate concern. Several specimens were tested of each of the five "materials" of interest.

Reproducibility is excellent in this type of loading and the average results for each material are shown tabulated below with respect to important values describing the mechanical behavior:.

TABLE III B-1

	ANNEALED SCREEN	NEGATIVE PLAQUE (905)	POSITIVE PLAQUE (810)	* NEGATIVE PLATE (170)	* POSITIVE PLATE (176)
E (PSI)	0.18×10^6	0.23×10^6	0.47×10^6	0.41×10^6	0.58×10^6
ρ_{yield} (LBS)	2.9	5.1	11.1	10.0	11.05
σ_{yield} (PSI)	225	390	855	710	850
ρ_{ult} (LBS)	16.8	17.3	18.9	19.1	18.1
σ_{ult} (PSI)	1290	1330	1450	1360	1390
Elongation (%)	20.7	22.8	17.7	18.5	20.5

* Dry, as manufactured electrodes

In order to summarize the results of this study more clearly, Figure III-5 has been prepared to show the average stress-strain curve obtained for each material studied. The curve for screen alone essentially lays the foundation of comparison in this study. We can observe the progression of increased strength from the basic screen grid through negative plaque, negative plate, positive plate and finally positive plaque. It is desirable to compare these various materials with regard to three important quantities:

<u>Modulus of Elasticity</u> -- The values for each material were tabulated as an indication of relative strength. They were determined from approximate slopes of the initial portion of the σ-ε curves. They are valid as a confirmation of relative strength but tend to be low in absolute value. Section B.2.b of this report describes in greater detail the results obtained from a more precise method of determining this quantity.

<u>Yield Strength</u> -- The prime consideration in discussing yield strength is the degree of basic grid reinforcement that is attributable to the addition of the matrix. As first applied to the basic grid, this matrix of sintered Ni powder forms plaque. The first important result of this study was the significant difference in strength between positive and negative

FIG III-5

STRESS PSI X(10)^2

STRAIN (inches/inch)

STRESS VS STRAIN

STATIC TENSION

$\dot{\epsilon} = 0.0004$ /SEC

(1) POSITIVE PLAQUE (810-6)
(2) POSITIVE PLATE (Y6)
(3) NEGATIVE PLATE (170)
(4) NEGATIVE PLAQUE (005-3)
(5) ANNEALED (ND) SCREEN

III-29
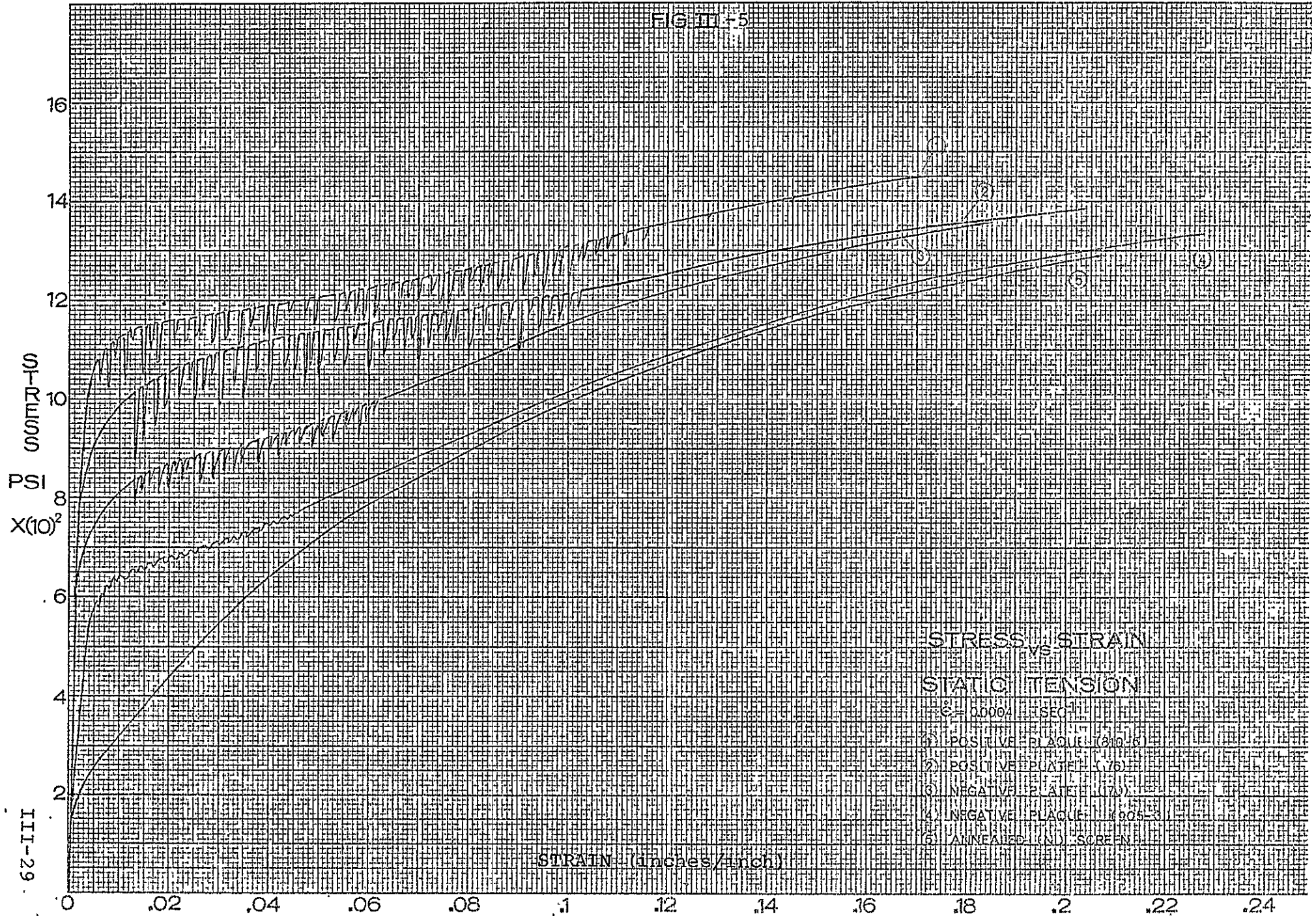
plaque. Positive plaque has a much higher yield
strength than negative plaque. Although both
materials are manufactured from the same slurry
formation and have the same thickness, the positive
has a higher area density than the negative. The
positive plaque has less total porosity than the
negative plaque and in addition, the sintering
temperature is higher for positive plaque than for
negative plaque. These facts explain very readily
the reason for the increased strength of positive
plaque.

The next significant effect shown is the reduction
in strength that occurs when positive plaque is
electrochemically formed into positive plate.
Porosity alone is certainly no indication of this
effect for it is not uncommon to reduce the total
porosity. The factor that is important is the
corrosion of the sinter matrix which occurs during
the process. It is true that positive active mate-
rial is deposited within the pores and results in
the lowered porosity, but it appears that this
material in hydroxide compound form adds little
strength to the material. The overriding effect,
then, is the significant weakening of the initially
strong positive plaque matrix by the extensive

metallurgical
materials division

corrosion associated with impregnation.

Equally significant is the reverse strength effect
we have observed associated with the manufacture
of negative plate. Negative plate material has a
higher yield strength than the initial negative
plaque. The total porosity is decreased during
this process but again, it is the manner in which
this change occurs that is important.

Firstly, however, the amount of sintered matrix
corrosion is less for the negative plate than for the
positive plate. Secondly, the negative active mate-
rial partially as a metal, has more strength than the
positive compounds. It is, therefore, apparent that
the lower amount of corrosion combined with the over-
riding factor of a stronger active material produce
the net strengthening of negative plate. It is shown
as a final result that positive plate material has a
higher yield strength than negative plate material.
This is obvious at the 0.2% ε point, by the higher
modulus of elasticity, and by the larger drop of load
as the matrix cracks. Not only is the positive plate
matrix stronger, but it continues to help support
load further into the high strain region. It seems
then, that even after considering the differences in

corrosion and impregnation phenomenon, the positive
Ni plate is stronger than the negative Cd plate
primarily because there is such a great difference
in their respective parent structures -- the posi-
tive and negative sinter material -- plaque.

Ultimate Strength -- Although the basic progressive
ineffectiveness of the matrix has been shown by the
reversion of plaque/plate strength to that of screen
alone, it is first important to note that the ulti-
mate strength of all four matrix materials remains
slightly higher than that of screen alone. This may
be accounted for by assuming that some of the nickel
powder has been effectively sintered to the screen
wires or in the immediate vicinity and permits this
small portion of the matrix to provide continued
reinforcement throughout elongation to fracture. If
this is indeed the mechanism acting, we can then also
explain the relative values of ultimate strength from
the corrosion consideration discussed earlier.
Firstly, it is reasonable to expect the higher den-
sity, higher temperature sinter of the positive
plaque to exhibit the highest ultimate stress which
indeed is the case. Secondly, we note that despite
a stronger matrix at yield, the positive plate has a
lower ultimate strength (absolute load) than the

negative. Here the greater corrosion of the
positive wires and proximate matrix would tend to
weaken and lower the ultimate strength below that of
the negative plate.

b) Constant Load Static Testing

Although the previous study is an excellent starting
point for an investigation of a material's mechanical
behavior and provides the usual engineering under-
standing, it may not provide the optimum information
for our purposes. Thus, we employed a constant load
test frame rather than the commercial constant
deformation type used in the preliminary studies.
This arrangement applied load to the specimen by
means of a water-fill technique. A container at-
tached to the specimen served as a dead weight
accumulator as it was filled with water at a con-
stant rate. Additionally, unloading at any point
along the stress-strain curve is easily accomplished
at a fairly uniform rate by draining water from the
accumulator. Load is measured by a strain gage proof-
ring and the signal plotted directly on the vertical
axis of an x-y recorder. Strain measurements are
taken more accurately by a strain gage extensometer
of 1" gage length mounted on the specimen. This
output is plotted directly on the horizontal axis of

the x-y recorder. This system provided a very
deliberate manner of loading to closely examine the.
region of yielding. Especially because of our
ability to unload very precisely, we were also able
to examine the modulus of elasticity of the material
and its relation to strain level. Again, the.
average results for each material are shown in Table
III B-2 with respect to the important values describ-
ing its mechanical behavior.

TABLE III B-2

	ANNEALED SCREEN	NEGATIVE PLATE *	POSITIVE PLATE *
E (PSI)	$0.8 \pm 0.2 \times 10^6$	$1.0 \pm 0.1 \times 10^6$	$1.2 \pm 0.2 \times 10^6$
P_{yield} (LBS)	3.1	9.9	11.2
σ_{yield} (PSI)	240	705	860
P_{ult} (LBS)	17.0	19.8	19.1
σ_{ult} (PSI)	1310	1420	1470

* Dry, as manufactured electrodes

Figure III-6 has been prepared to permit compari-
son of the average stress-strain curve associated
with each material studied. It is shown once again
that the screen alone forms the foundation and the

FIG III-6

STRESS STRAIN
vs
(static tension)
σ = constant

POSITIVE PLATE
POSITIVE PLATE HS
NEGATIVE PLATE
NEGATIVE PLATE HS
ANNEALED NICKEL GREEN

σ STRESS PSI

(ε) STRAIN   inches/ inch (10)⁻³

III-35
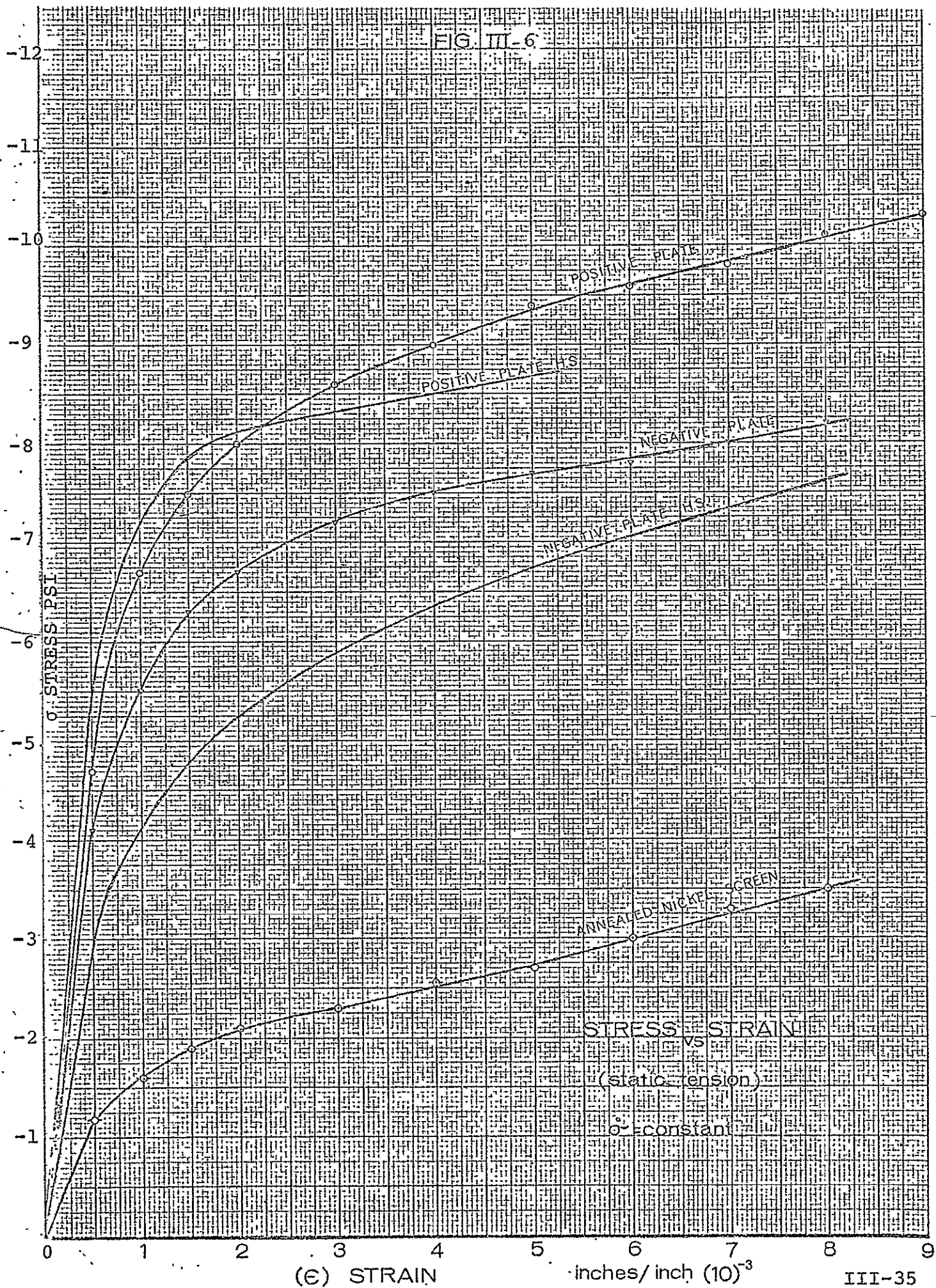
increased strength due to the matrix is very obvious in this region of low strain (<1%). The tabulated values of strength agree quite well with those obtained under the constant deformation type of loading. However, this description of strength was obtained in a different manner and it is best to consider each value separately.

Modulus of Elasticity

As the matrix becomes ineffective, (while cracks form as strain level progresses), we would expect to see a progressive decrease in the initial modulus value toward the lower value of screen alone. As indicated, the constant load technique allows us to unload and reload at any strain level we chose to determine the elastic modulus at that strain level. In practice, we were able to unload and reload at 400 μ in/in $< \epsilon < 6000$ μ in/in. Within this region, the experimental scatter is equal to the diminishing function which may exist. Some values were obtained near the 200 $\mu \epsilon$ level, and they were higher than the average reported. The values that have been given in Table III B-2 are the average values obtained from the unload-reload determinations within 400 μ in/in $< \epsilon < 6000$ μ in/in for each material. The tolerance is that of

III-36

experimental error combined with any diminishing
function that may exist within this region of strain.
We have, of course, plotted E vs. ε for each material
and can only say that three regions of interest seem
to exist: (a) E may be diminished rapidly in the
region $0 < \varepsilon < 200\mu$ in/in; (b) for the region 200μ in/
in $< \varepsilon < 2000\mu$ in/in there may exist a very small
diminishing of E; (c) beyond $\varepsilon = 2000\mu$ in/in there
seems to be no function of E vs ε level. In other
words we feel that a plastic deformation component
exists at very low strain levels ($<200\mu$ in/in) and
that yielding is complete @ $2000\mu\varepsilon$. This is con-
firmed by the fact that a determination of modulus of
elasticity by measuring the slope of the stress
strain curves will give a lower value than that ob-
tained by the more accurate unload-reload technique.
The values indicated in Table III B-2, therefore,
remain the best measure of true elastic response in
tensile loading. Aside from permitting future cal-
culations of dynamic response, they are important
measurements for several reasons: (a) the value ob-
tained for screen alone agrees well with that indi-
cated by the model; (b) at least for $\varepsilon < 6000\mu$ in/in
the modulus of plate material remains higher than
that of screen alone; (c) the strength (stiffness)

of the positive matrix is greater than that of the
negative matrix.

Yield Strength

As indicated, this type of precise loading was
meant to more accurately examine the region of
yielding $\varepsilon < 1\%$. Figure III-6 illustrates this
region in great detail. It is important only to
note that this value of yield strength @ 0.2% ε
agrees very well with the initial determination
given in Table III B-1. Thus, this series of con-
stant load tests fully supports the initial rela-
tions between positive and negative plates as
extensively discussed in the previous section.

Ultimate Strength

Although this type of testing was meant to closely
examine only the low strain region near yielding,
most specimens were taken to tensile fracture.
Load data was available up to the point of failure
and it is important only to note that the ultimate
strengths thus reported are essentially in agree-
ment with those first determined and reported in
Table III B-1. Thus, this series of constant load
tests essentially supports the discussion of
ultimate strength contained in the earlier section.

metallurgical
materials division

c) The Effects of Heat Sterilization and Electrolyte
    Saturation

All tabluated values and stress-strain curves shown in
the preceding sections were obtained from as-manufac-
tured, dry, unsterilized plate material. We were
interested, therefore, in the possible changes in
mechanical properties which might result from heat
sterilization and electrolyte saturation of this same
plate material. Tensile samples were thus prepared by
full heat sterilization ($135^{\circ}C$ for 64 hours) in the
saturated condition (30% KOH). These specimens were
then tested in the constant loading apparatus described
in Section B.2.b. The results are tabulated below and
should be compared to those in Table III B-2.

TABLE III B-3

SATURATED AND STERILIZED ELECTRODES

	Negative Plate	Positive Plate
E (psi)	$0.71 \pm 0.10 \times 10^{6}$	$1.35 \pm 0.25 \times 10^{6}$
P_{yield} (lb)	8.2	10.9
σ_{yield} (psi)	587	835
P_{ult} (lb)	19.2	22.0
σ_{ult} (psi)	1375	1690

The complete stress-strain curves have been included in

metallurgical
materials division

Figure III-6 in order to permit the comparison of as-manufactured vs saturated and heat-sterilized plates.

It appears that the mechanical properties of the positive plate material are not changed as greatly as those of the negative plate. The positive results indicate very small changes in the modulus of elasticity and yield strength. However, the ultimate strength has been found to be significantly higher.

The behavior of negative plate is changed a great deal by this saturated sterilization. The modulus of elasticity and yield strength of the negative has been significantly lowered along with a slight reduction in ultimate strength. The weaker of the two electrodes in our Ni-Cd system seems to be further weakened by the saturated sterilization treatment that is required.

d) Dynamic Tensile Testing

Considering the goal of the current effort to develop knowledge which will enable the design of impact-resistant Ni-Cd cells, it should be stated that the actual dynamic tests are of prime importance. In retrospect to what has been written, it should be stated that the reason for performing static testing is to establish a foundation of strength properties. What is necessary for a thorough understanding

metallurgical
materials division

is a knowledge of the actual transfer from static to

dynamic conditions. The static testing is valuable

since it can provide us with a complete picture of

stress vs strain which is not easily obtained under

dynamic loading. In fact, it will be shown that

only the yield point and ultimate load can be obtained

under dynamic conditions and that the static results

are of great value in establishing the complete mechani-

cal behavior.

Ultimate Strength:

From the static values we have obtained and a

knowledge of the plate's physical properties, we

might write --

$$\left(\frac{\text{Ultimate Force}}{\text{Unit Width}}\right) = \left[\frac{(\text{Length})\left(\frac{\text{Unit}}{\text{Width}}\right)\left(\frac{\text{Area}}{\text{Density}}\right)}{g}\right](N\ g)$$

and would find that --

$\ell \geq 3.3$ inch $\Rightarrow$ Failure

This mass, inertia-loading defines the method of

testing we have used to investigate dynamic proper-

ties. The essential concept is shown diagrammatically

below.

metallurgical
materials division
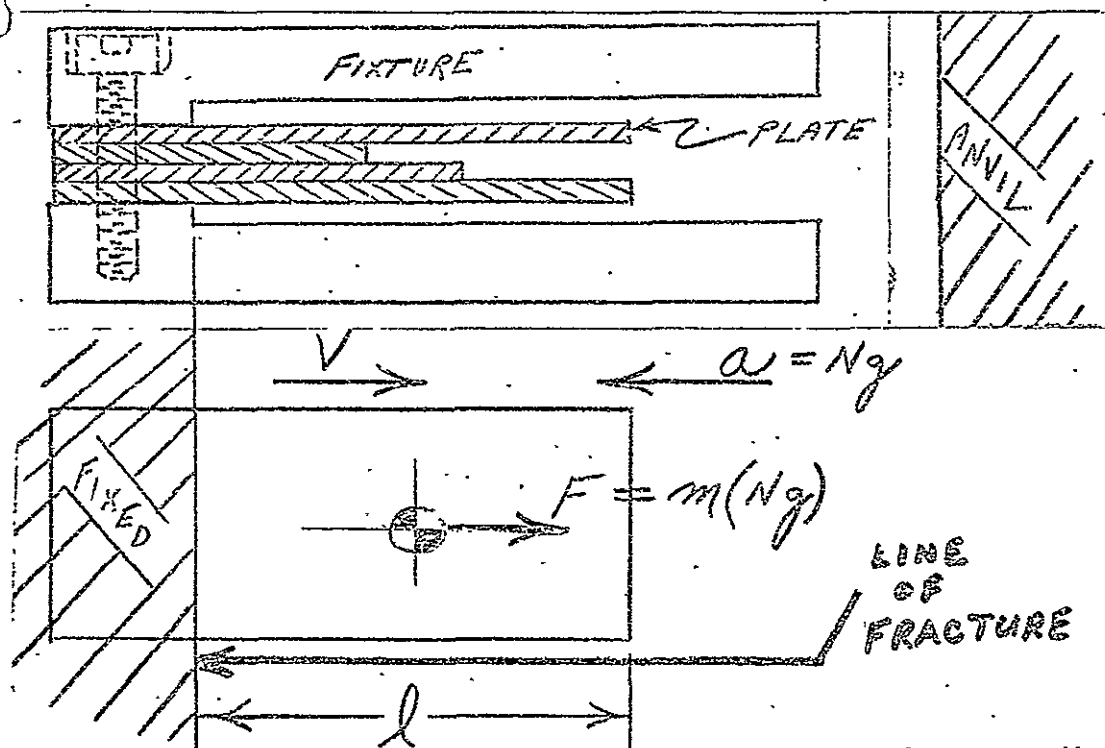
All specimens of positive and negative plate
material were constant width (2" or 40 wires) and
cut to various lengths (3-1/2" - 6-1/4").
Typically, four positive plates and four negative
plates, each of a different length, would be placed
in the fixture. Through suitable shims, friction
duplication techniques (support data of frictional
coefficients have been generated) and clamping
arrangements, we could consider one end fixed.
Then, knowing the effective free length, l, the
mass density, ρ, and the mean g-level at impact,
Ng, we could calculate for each plate the dynamic
tensile inertia force experienced. Therefore,
lengths were varied above and below the predeter-
mined static failure length and the value was

bracketed. Values of ultimate strength are tabulated below for comparison.

TABLE III B-4

#### ULTIMATE TENSILE STRENGTH (2" WIDTH)
(As-Manufactured Electrodes)

	Static $\overset{o}{\varepsilon}$ =Constant	Static $\overset{o}{\sigma}$ =Constant	Dynamic 7/8" Tool	Dynamic 1" Tool
Positive Plate	72#	76#	80#	107#
Negative Plate	76#	79#	90#	115#

What is apparent from this study is that the plate material can support greater loads under dynamic conditions and we indeed may use static strength determinations as a foundation or lower bound for design. In other words, the material is $\overset{\bullet}{\varepsilon}$ sensitive and under dynamic loading may support perhaps 120#. The reason that the dynamic tests as reported above are separated is due to the different pulse lengths involved. The calculated values shown are magnified to some degree by the dynamic loading. It is felt that we are in the area where the magnification is not constant and is dependent upon the natural and applied frequencies involved. This aspect is discussed in Section C.2.b of this report.

Yield Strength

In addition to bracketing the value of ultimate strength under dynamic loading, we are also able to determine the material's dynamic yield strength, as indicated by the onset of matrix cracking. For example, after impact loading a plate has the appearance shown in the following sketch and in Figure III-7.
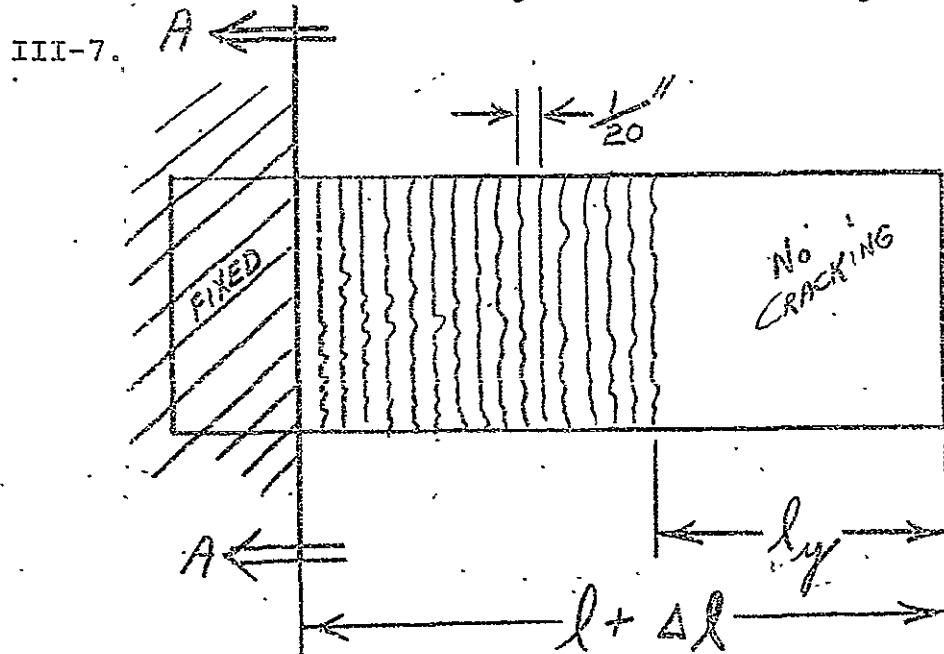

As stated previously, the value of effective length, l, will determine whether or not there is sufficient mass experiencing the test acceleration to produce a force sufficient to fracture the plate at Section A-A. There also exists for each plate a length, l_y, from the free end over which no matrix cracking occurs. Beyond l_y the matrix will have cracks uniformly spaced, each 1/20 inch (20 mesh screen). If we measure l_y for each plate, then, knowing the input

DYNAMIC TENSILE LOADING

VELOCITY

114.5 FT/SEC

L_{y1}

L_{y2}

L_{y3}
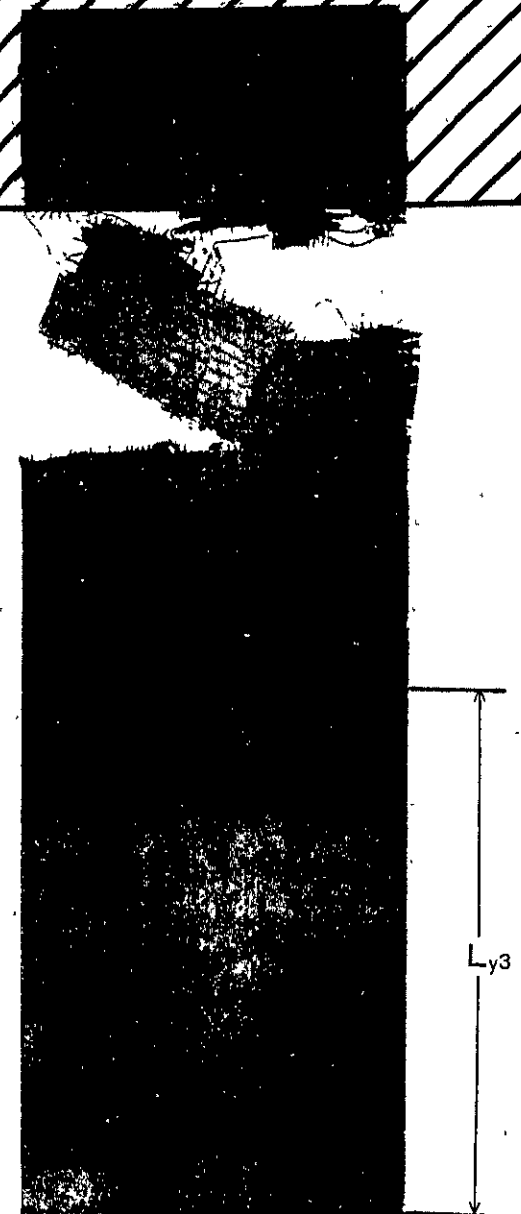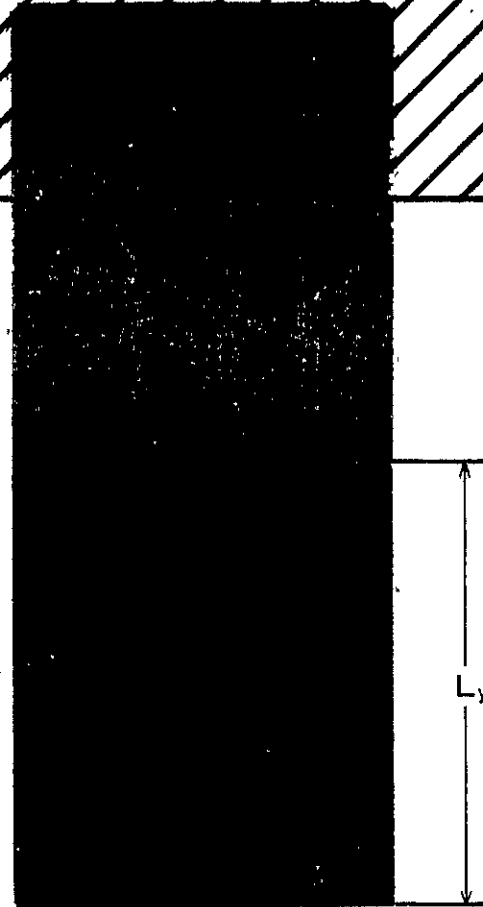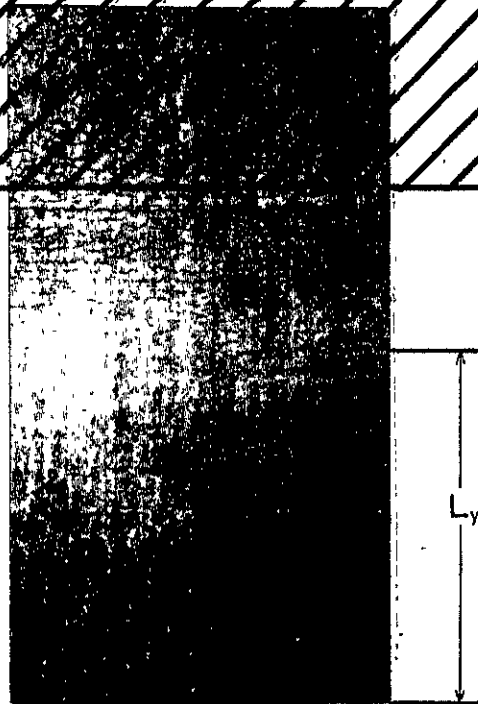
$L_{y1} < L_{y2} < L_{y3}$

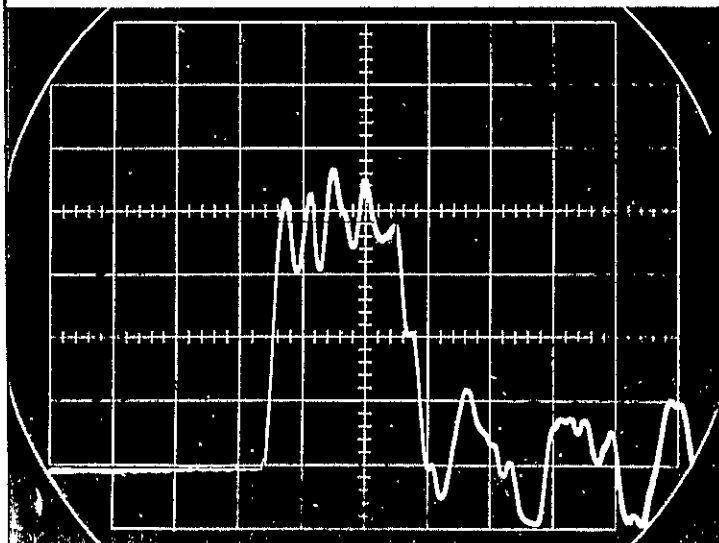1.05 msec   3850 g's mean

Figure III - 7

acceleration and the physcical properties of the
plate, we can calculate the dynamic force created
by this mass which was responsible for yielding
the plate or cracking the matrix. This dynamic
yield strength has been calculated for each plate
tested. We have plotted the yield force, ρy,
against the effective plate length, l, to demonstrate
the distinct linear function that exists because of
relative frequency - magnification considerations.
The effect is amplified by our failure to consider
the progressive nature of yielding. The range of
yield strength values are given in Table III B-5.

TABLE III B-5

YIELD STRENGTH (2" WIDTH) (AS-MANUFACTURED ELECTRODES)

	Static ε = Constant ρ_y @ 0.2% ε	Static σ =Constant ρ_y @ 0.2%	Dynamic 7/8" Tool ρ_y @ Crack	Dynamic 1" Tool ρ_y @ Crack
Positive Plate	44#	45#	60-72#	42-96#
Negative Plate	40#	40#	60-70#	48-78#

Again, it is apparent that yield strength as well
as ultimate strength is elevated by the higher
strain rate associated with dynamic loading. The

variation with pulse length (7/8" vs 1" tool) and effective plate length has been demonstrated. Rather complete static stress-strain curves have been established and the effect of strain-rate sensitivity has been shown:
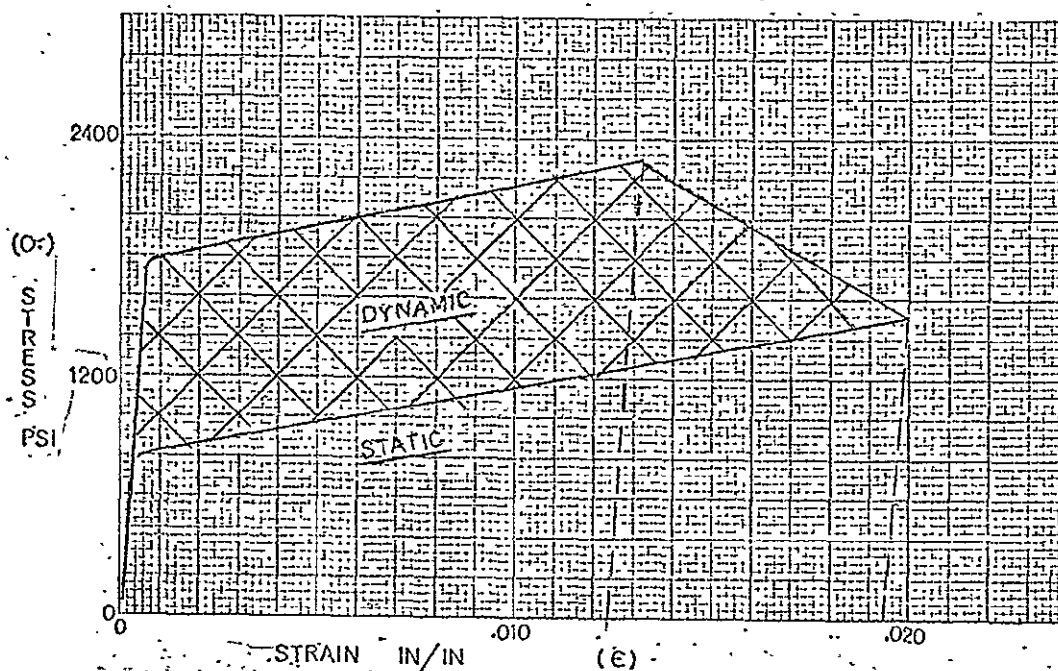
Dynamic strength behavior is elevated above that of the well-established static lower bound. However, the degree of this elevation (shaded area above) depends on a more well-defined relation between element response and the applied forcing function.

e) Poisson's Ratio

Extensive development of strain gage techniques was carried out under the present contract. The supporting data can be found in the 9th QTR JPL Report. The prime reason for development was the measurement

metallurgical
materials division

of dynamic strain during impact conditions as, dis-
cussed in Section C.2.b. These techniques also
offer the most appropriate method that can be used
for a determination of Poisson's Ratio. The static
determination employed an axial strain gage and an
identical transverse strain gage of the thin paper
foil type installed with Eastman 910 on each of
three ½" wide dry negative plate specimens.
Simultaneous strain readings were taken from each
gage and a commercial axial extensometer. Essen-
tially, we compared the slope ratio of the trans-
verse to the axial gage output within the region
of linear agreement between the axial gage and
the axial extensometer. The constant loading as
described in Section B.2.b was used for these
tests. The third specimen was subjected to one
unload-reload cycle to show the elastic behavior
more clearly.

The results are presented in Table III B-9. We
have indicated the modulus of elasticity, E, as
determined at various strain, ϵ, levels by unload-
reload cycles. The values obtained are in good
agreement with those previously determined by this
type of loading. We have also given the calculated
ratio of strain gage output to that of the

metallurgical
materials division

TABLE III-9

III-49

Negative Plate Specimen ½" Wide	E @ ε in/in (PSI)	$\left(\dfrac{\varepsilon \text{ axial gage}}{\varepsilon \text{ axial extensometer}}\right)$ ε-limits μ in/in	$\left(\dfrac{\varepsilon \text{ transverse gage}}{\varepsilon \text{ axial extensometer}}\right)$ ε-limits μ in/in	Poisson's Ratio ν
5-28	1.22×10^6 @ .0014 1.00×10^6 @ .0038	0.702 (50-300)	0.116 (50-350)	0.164
6-16	1.30×10^6 @ .0044	0.400 (100-600)	0.088 (100-700)	0.218
6-27 Initial Loading	------	0.364 (80-600)	0.068 (20->625)	0.186
6-27 Reload @ 0.0012 in/in	1.01×10^6 average @ .0012	0.733 (10->300)	0.124 (40->300)	0.169

extensometer. Next reported, are the values of
Poisson's Ratio, which were obtained from each
test. The average value is $\nu = 0.184$. However, more.
weight must be given to the values obtained at the
higher $(\frac{\varepsilon \text{ axial gage}}{\varepsilon \text{ axial exten.}})$ ratio since this indicates
a lower degree of matrix reinforcement. On this
basis, the best value of Poisson's Ratio is approxi-
mately 0.17 and should be used for subsequent calcu-
lations. This value is of course much lower than the
0.28 normally observed with pure nickel and indicates
a large degree of anisotropy. We had previously
observed the differences in tensile and compressive
strength, and this predicted anisotropic behavior
has been confirmed under this uniaxial loading study.

3. Mechanical Properties in Compression Loading

   a) Introduction

     The experimental program for evaluating the mechani-
     cal strength of Ni-Cd electrodes may be broadly
     separated into three (3) distinct methods of load-
     ing: tensile, compression, bearing. The behavior
     under tensile loading has been discussed in Section
     B.2. The studies of bearing strength are of prime
     design interest and will be discussed in Section
     B.4. This section describes the manner of loading
     and the strengths that have been measured in a com-

pression-buckling mode of failure. This area of investigation is similar to the tensile work in that it has primarily increased our understanding of our plates' behavior under load. In contrast, the bearing strength studies will be more clearly related to actual cell failure mechanisms. In other words, edge crushing of the electrode pack could be a prime cell failure mode under impact loading.
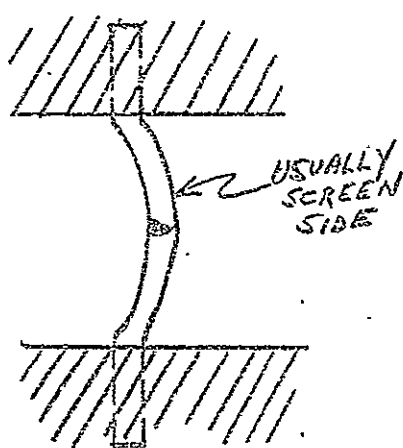
b) Constant Deformation Static Testing

The static compression loading was accomplished by the constant deformation method (commercial testing machine) as fully described in the tensile report. The manner of specimen loading is shown below:
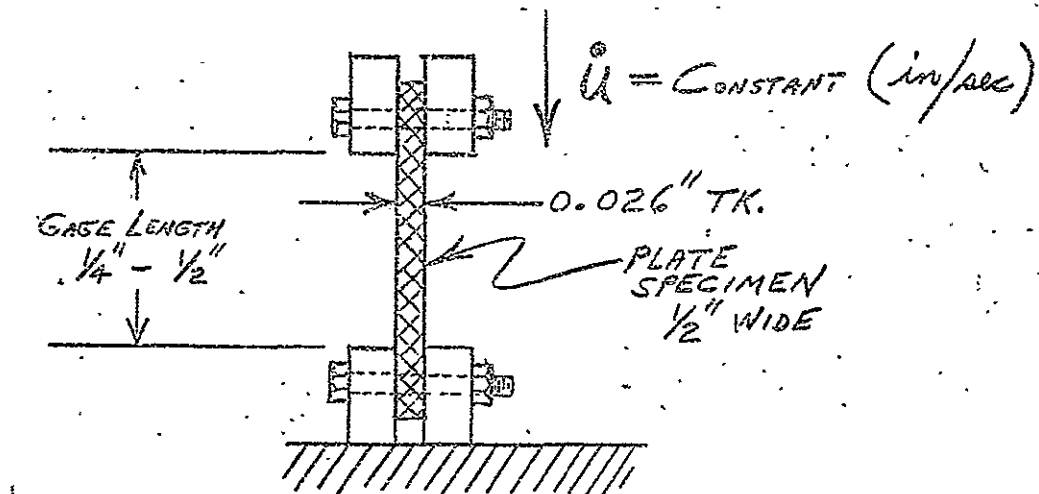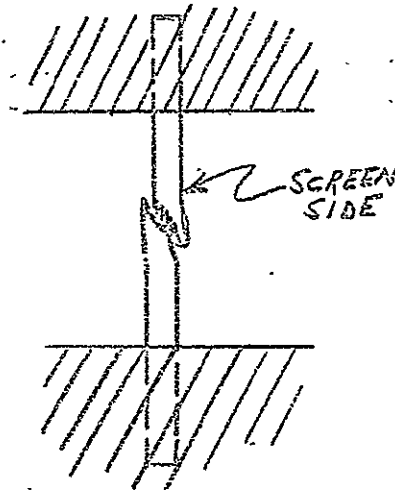
Two prime failure modes were observed, during the course of our investigation:

Since the loading system did not provide lateral support, buckling would occur whenever the effective column length was too large for the material strength available. If the material has sufficient strength, buckling is resisted and the higher compressional ultimate load is exhibited.

In the first series of tests, as-manufactured positive and negative electrodes 1/2" wide were loaded over a 1/2" initial gage length. In all cases, the buckling mode of failure was exhibited.

The second series of tests were performed on 1/2" wide specimens of positive and negative plaque over a 1/4" gage length. Again, the universal failure

metallurgical
materials division

mode was in buckling.

The third series of tests involved as-manufactured positive and negative plates 1/2" wide loaded over a 1/4" gage length. This was a sufficiently short gage length to permit the specimens to resist buckling and primarily exhibit compressional shear failure.

Reproduceability of stress-strain information for various specimens of the same material is poor when obtained by this manner of loading. Figure III-8 presents, therefore, average stress-strain curves for the three series of tests. The positive (both plate and plaque) is shown to be stronger than the negative in all cases. The very large increase of plate strength over that of plaque is shown. The absolute stresses shown in Figure III-8 are significant. Regardless of mode of buckling-compressional failure, we observe ultimate stresses of 3000-6000 psi as compared to 1400 psi tensile ultimate stress. What is needed for true compressional evaluation, however, is a measure of the uniform strain with a provision for positive lateral restraint.
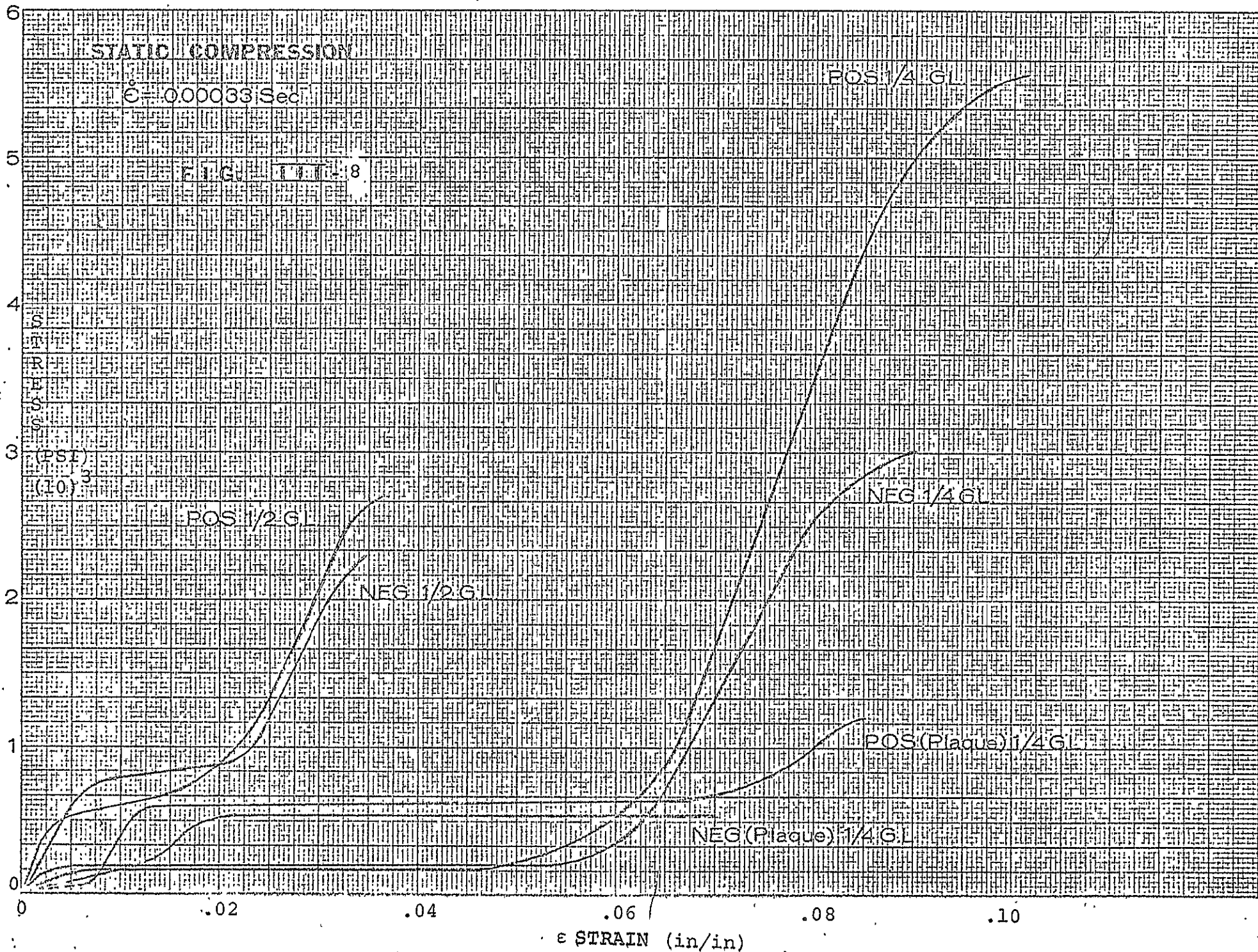
metallurgical
materials division

STATIC COMPRESSION

$\dot{\epsilon} = .00033$ Sec

FIG. III-8

STRESS (PSI)(10)³

POS 1/4 GL

NEG 1/4 GL

POS 1/2 GL

NEG 1/2 GL

POS (Plaque) 1/4 GL

NEG (Plaque) 1/4 GL

ε STRAIN (in/in)

Table III B-6 compares the experimental values
obtained with some fundamental buckling calculations.
E_1 represents the initial apparent modulus of elas-
ticity if significantly exhibited before yield.
Following the plastic elongation region, the final
"apparent modulus of elasticity" displayed during
ultimate loading is represented by E_2. The actual
failure load P, is next given but distinguished by
the associated mode of failure. Next we have
shown a predicted buckling load as calculated by a
modified E u ler equation which serves merely as a
very inaccurate lower limit for comparison purposes.

The absolute values of E_2 noted in this type of
testing are lower than those observed during con-
stant deformation tensile testing. It also appears
from this study, that a rather large amount of
plastic deformation is necessary before, the matrix
is able to support the load. Such factors suggest
that the initial bends in the screen play a very
significant role.

metallurgical
materials division

TABLE III B-6

		E_1 x 10^6 psi	E_2 x 10^6 psi	Static ⓟCritical Buckling #	Static ⓟ Ultimate Compression #	Calculated ⓟ Critical Buckling $2\left(\dfrac{\pi^2 E_2 I}{l^2}\right)$	Dynamic ⓟ Ultimate Compression #
Positive Plate	1/2"	0.24 ⟶	0.12	35	----	8	/
Negative Plate	G.L.	0.12 ⟷	0.12	32	----	8	/
Positive Plaque	1/4"	0.14 ⟶	0.05	15	----	12	/
Negative Plaque	G.L.	----	0.10	8	----	24	/
Positive Plate	1/4"	0.14	0.18	----	70	42	>34
Negative Plate	G.L.	0.16	0.16	----	42	36	34
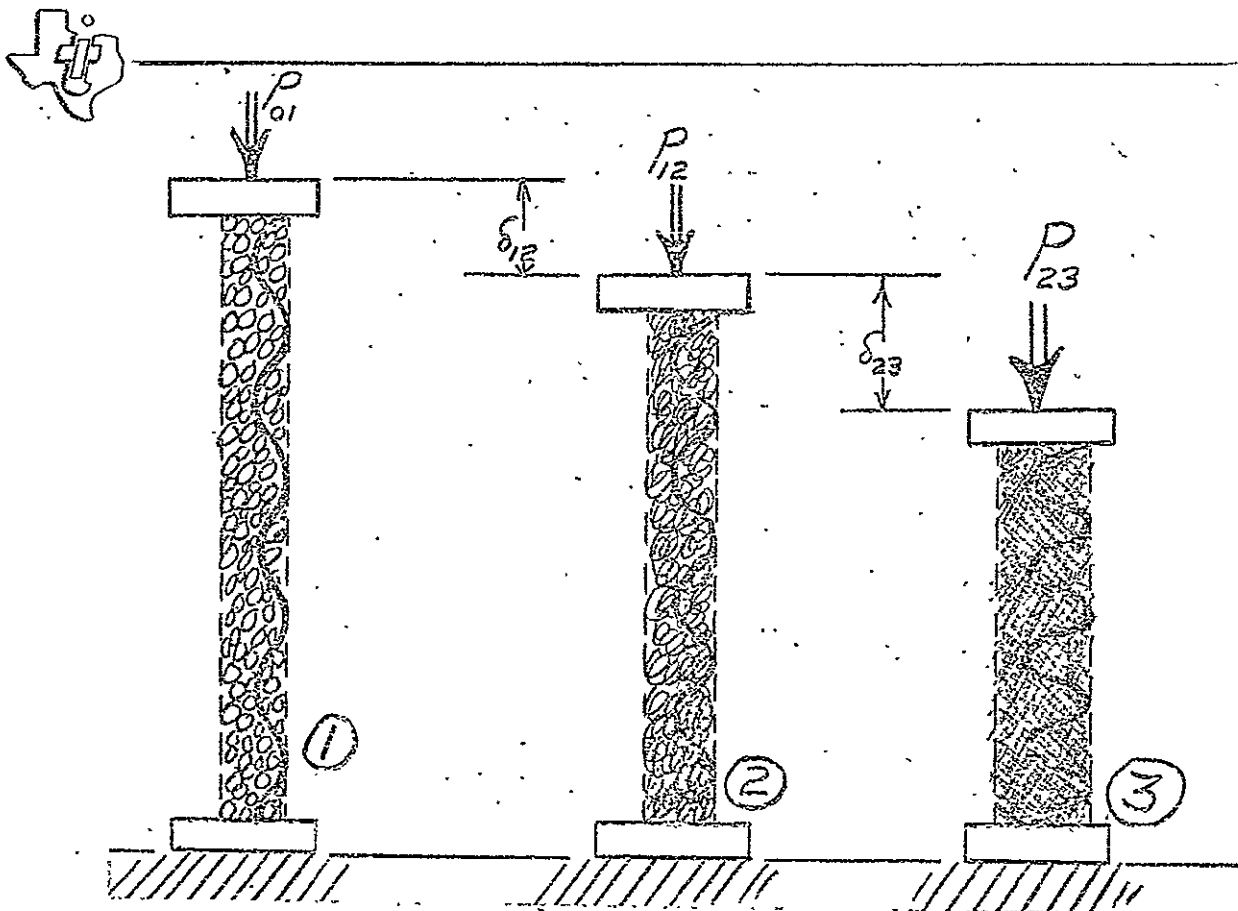
Porous structure uncrushed. Supporting initial load as in tension.

Porous structure has reached yield. Pores collapsing, wire bending.

Sufficient deformation & densification of collapsed pore structure to permit further load support.
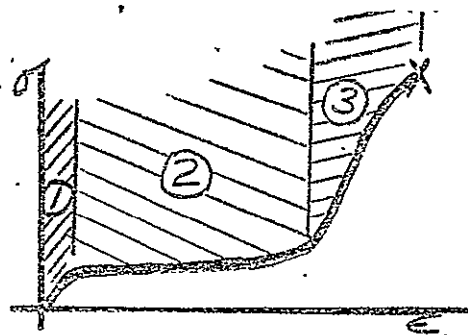
This understanding or explanation is supported by several experimental results. Yield strengths on the order of 100-600 psi have been observed in compression which are lower than those (225-850 psi) experienced under tensile loading. The extensive

plastic elongation region is then fairly well established. The modulus E_2 observed when load is again supported is $\leq$ the modulus of screen alone under tensile loading. This indicates that the contribution of screen under compression is reduced and that indeed from a modulus standpoint, the combination of corrugated screen and compressed sinter are scarcely equal to the screen alone in tension. The ultimate load carrying ability in tension was seen to rely primarily on screen alone since the matrix became ineffective or lost due to elongation. In contrast, however, compression appears to utilize the matrix as the major load bearing element up to the point of fracture.
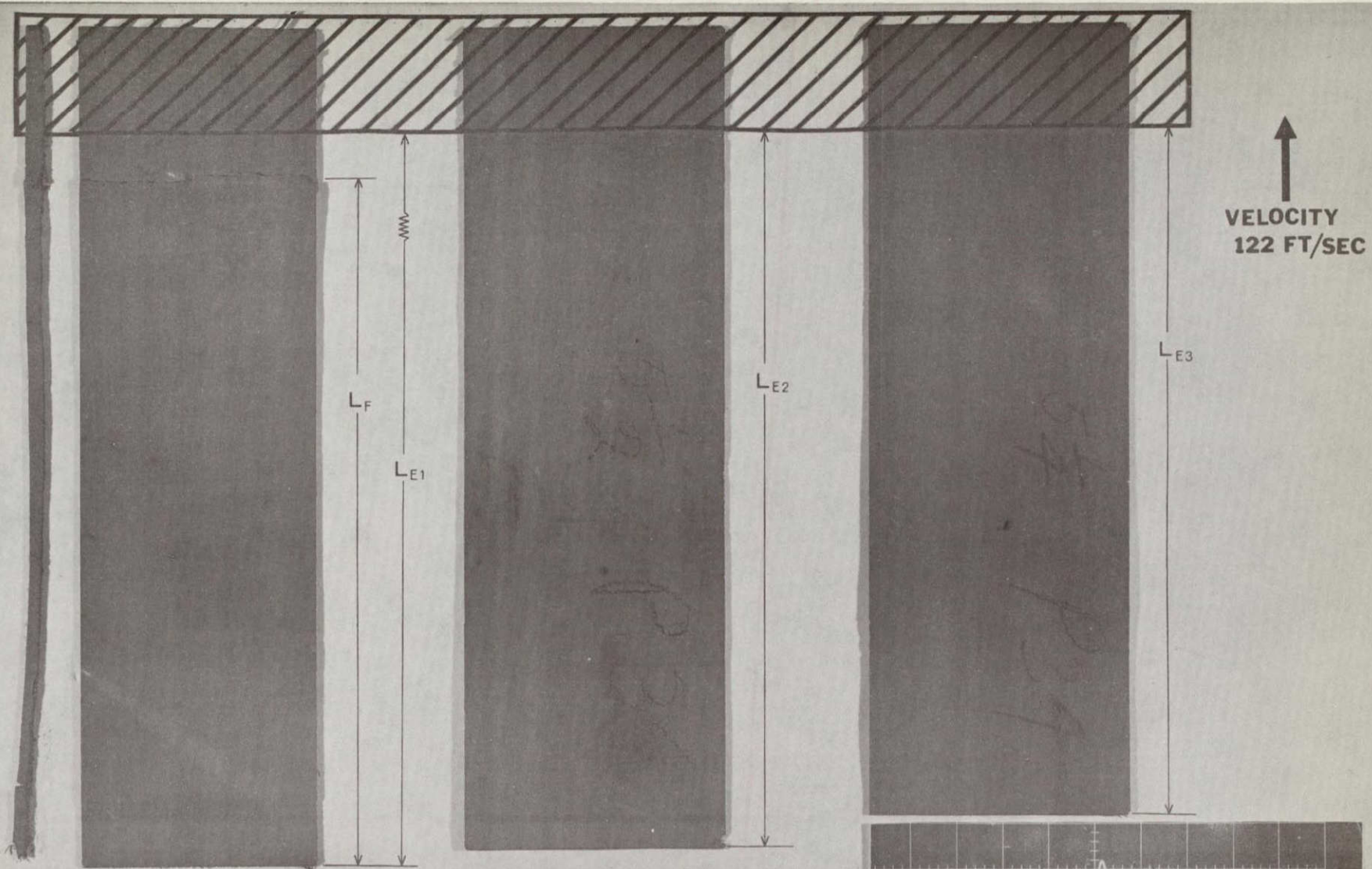
c) Dynamic Compression Loading

The dynamic test method used to evaluate Ni-Cd plates has been completely described in the tensile loading Section B.2.d. The method used for compression studies is identical except for a reversed mounting procedure which simply allows the plates to experience decelerating forces in the opposite direction.

metallurgical
materials division

V $a = Ng$

$FIXED$

$F = m(Ng)$

ℓ

LINE of FRACTURE
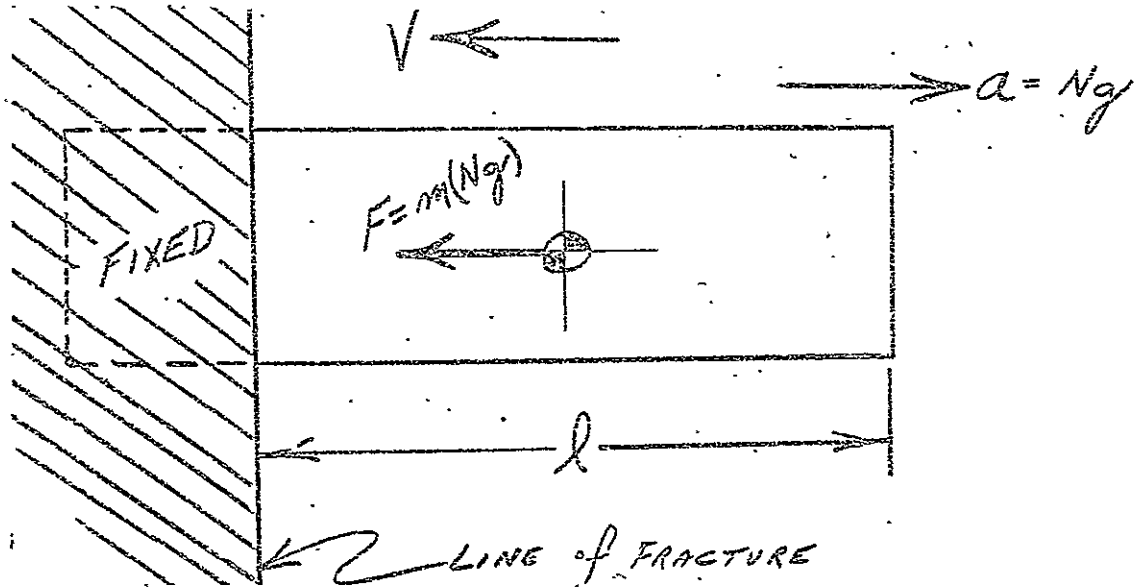
As in tension testing, the compressive specimens
were 2" wide and cut to provide various effective
lengths, l, for each impact. Through the use of
suitable clamping and friction elimination tech-
niques, each plate was essentially free to exhibit
its response to the input force. A buckling mode
-of failure was not permitted, and thus we observed
only compressional fracture as shown in Figure
III-9. If the effective length, l, was sufficiently
large, failure would occur at the associated load-
ing. A dynamic yield point is not observed in the
compression loading of the matrix as was seen in
tensile loading. Thus, we have merely a deter-
mination of the ultimate compression load.

Positive Plate could not be failed in a completely
dynamic compressional mode in our testing. We have

VELOCITY
122 FT/SEC

L_F

L_{E1}

L_{E2}

L_{E3}

$L_{E1} > L_{E2} > L_{E3}$

1000 G'S/CM (Y-Y)

1.25 MSEC/CM (X-X)
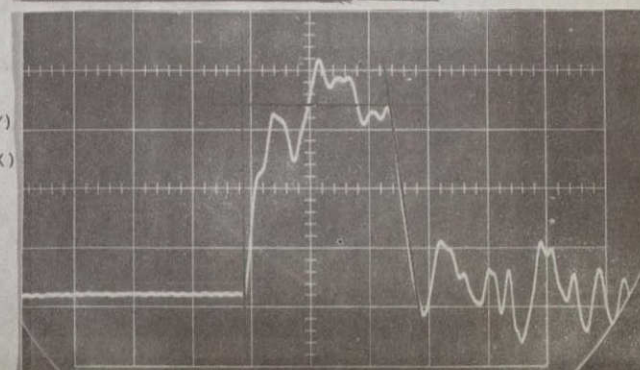
DYNAMIC COMPRESSIVE LOADING   Figure III - 9

observed plates of the maximum effective length
permissible (1 = 5-7/16") experiencing impact levels
of .3700 g with no apparent damage in pure dynamic
compression. Thus, we may only say that the P_{ult} >
134# or σ_{ult} > 2600 psi. Indications are then, that
the positive is stronger than the negative which is
in agreement with the very obvious result of static
testing.

<u>Negative Plate</u> material has been found to have a
fracture load of 135 lbs for the 2" width (2400 psi).
This is slightly lower than the average value
obtained in static testing (recall 168 lbs or 3000
psi). Even recognizing that the static data con-
tained a great deal of scatter, we may assume that
some dynamic phenomena are being observed. If our
deformation model for compression is valid, it
would imply that the Ni metal screen wires are not
available at ultimate load to carry significant
stress and therefore the strain rate, $\dot{\varepsilon}$, effects
observed in tensile loading will not appear in com-
pression. In other words elevation of σ_{ult} in ten-
sion at elevated $\dot{\varepsilon}$ was an observable and reasonable
effect but we now have reason to expect very little
difference in compressional σ_{ult} as a function of $\dot{\varepsilon}$.

metallurgical
materials division

4. Mechanical Properties of Electrodes in Bearing Loading

a) Introduction

The determination of the mechanical properties of Ni-Cd electrodes under tensile and compressive loading has been discussed. This section describes the third and final method of loading employed to complete the strength characterization of this material. Bearing tests, although certainly related to the study of compression loading have been distinguished here as a separate method. The main reason is that we did not insist upon any one failure mode. Instead, we attempted to shift from one failure mode to another in a controlled fashion. A second reason for distinguishing this series of tests is that the present manner of loading more closely approximates the type of freedom and failure that might be experienced in an actual battery. It was envisioned that under high gravitational fields our plate material might exhibit any one of three failure modes:
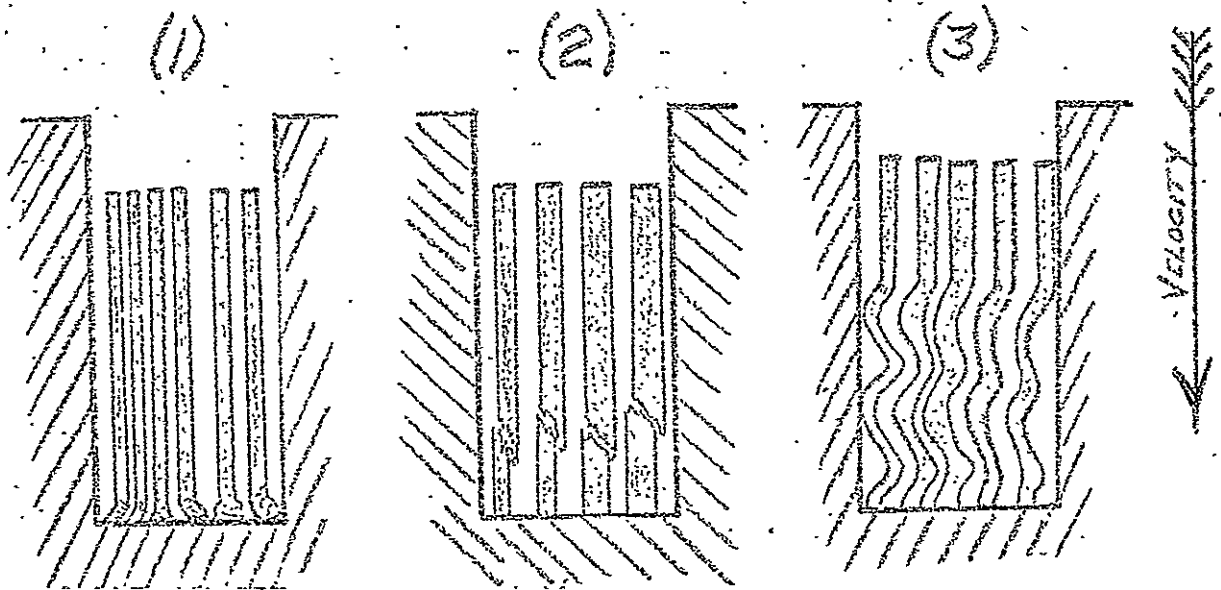
(1)   True Bearing Failure: The bearing failure

mode would be exemplified by edge crushing of

the plate material at the fixed impact surface.

If this failure mode were exhibited, it would

occur at a lower value of inertial stress than

that maximum required to cause true compres-

sional failure. This failure mode has signifi-

cant implications to the battery manufacturer

since it is most likely to cause separator

penetration and shorting of the cell.

(2)   Compression-Shear Failure: The true compres-

sion failure mode would be exhibited if ulti-

mate bearing stress exceeded ultimate compres-

sion stress. If this is the case, then the

value observed would represent the maximum

inertial stress that can be supported by this

metallurgical
materials division

material. It is obvious, therefore, that the battery designer would be extremely interested in this determination.

(3) Buckling Failure: The buckling mode of failure will be observed at a lower stress level than that associated with either failure mode (1) or (2) and is obviously to be avoided. Hence, the determination of the degree of lateral restraint necessary to prevent this transfer of failure mode is of prime design importance.

With these considerations and goals in mind, the experimental program was outlined to investigate the occurance of all three failure modes under controlled lateral restraint at both static and dynamic rates of loading.

b) Constant Deformation Static Testing

The static bearing loading was accomplished on a universal testing machine at a constant deformation rate ($\dot{\epsilon} \approx 0.0007$ sec^{-1}). The manner of specimen loading is shown on the proceeding page:

metallurgical
materials division
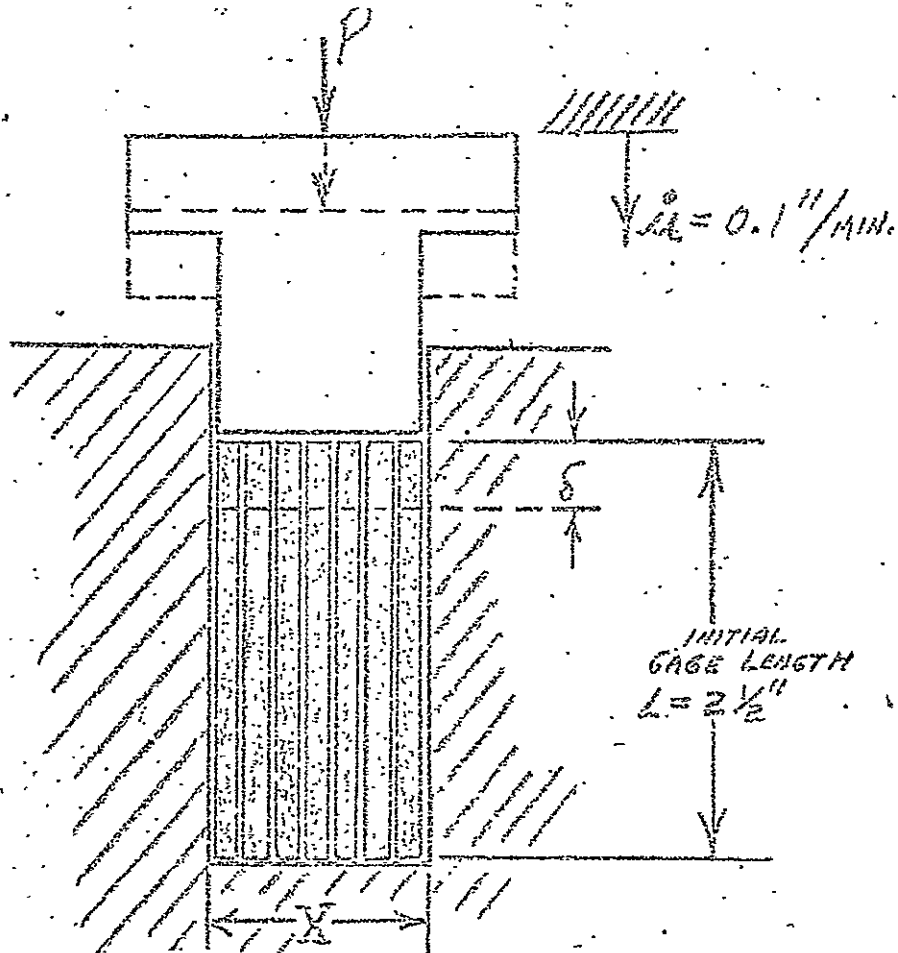
The essential characteristic of this loading
arrangement was the controlled lateral restraint.
The degree of lateral restraint was normalized for
all tests to a value of additional space allowed
for each electrode.

$$S = \frac{X - \left[(t_{p1} + t_{p2} + \ldots + t_{pn}) + (n + 1)t_s \right]}{n}$$

S = excess deformation space permitted per
plate (in)

X = constant dimension of fixture

t_{p1} = thickness of plate (Typ. 0.026")

t_s = separator thickness

n = number of plates

Thus, stress, σ, could be defined as:

$$\sigma. = \frac{P}{w(t_{p1} + t_{p2} + \ldots + t_{pn})}$$

where the denominator is simply the area of plates
being compressed and P is the total force as
recorded from the load cell of the machine on the
y-axis. Strain in this study was taken as $\varepsilon = \frac{\delta}{L}$
and again $\delta = \overset{o}{\mu}$ t. was directly displayed on the x-axis
of our recorder.

The static bearing tests carried out under this
type of loading were conducted on positive and negative
plates at spacing values ranging from .000"/plate -
.009"/plate. The specimens are shown in Figure III-10.
The progression from left to right illustrates the
complete transfer of failure mode from true compres-
sional-shear to buckling as the spacing is increased.
We observe the ultimate loads decrease to that mini-
mum level associated with pure buckling. Important
to note is the total absence of edge-crushing or.
true bearing failure. What is observed then, is an
ultimate bearing stress which seems to be greater
than the ultimate compression stress for this material

metallurgical
materials division

under <u>static</u> conditions.

Ultimate strain levels were fairly uniform regardless of failure mode mainly due to our definition of an overall apparent macro-strain. The stress levels are important however and large differences have been exhibited in direct relation to the spacing allowed and our ability to restrain buckling. The values of buckling stress and ultimate compression stress obtained in this study agree very well with the values determined earlier under strict compression loading as demonstrated in Table III B-7.

TABLE III B-7

Material	Static Buckling Stress		Ultimate Comp. Stress	
	Compression (1/2"G.L.)	Bearing (Max. Spac'g.)	Compression (1/4" G.L.)	Bearing (Min. Spacing)
Pos. Plate	2700	3000	5600	6500
Neg. Plate	2300	2300	3000	4900

c) Dynamic Bearing Loading

Having established a static strength foundation, we were interested in observing possible changes in these values because of increased loading rate. Dynamic bearing tests were performed by use of a loading fixture as shown on the proceeding page:

metallurgical
materials division

Figure III - 10

STATIC BEARING

NEGATIVE   MAXIMUM STRESS (S)

.000"/PLATE   .001"/PLATE   .0025"/PLATE   .0045"/PLATE   .009"/PLATE

S = 4910 PSI   S = 4000 PSI   S = 3715 PSI   S = 2760 PSI   S = 2290 PSI

POSITIVE

.000"/PLATE   .0025"/PLATE   .001"/PLATE   .0045"/PLATE
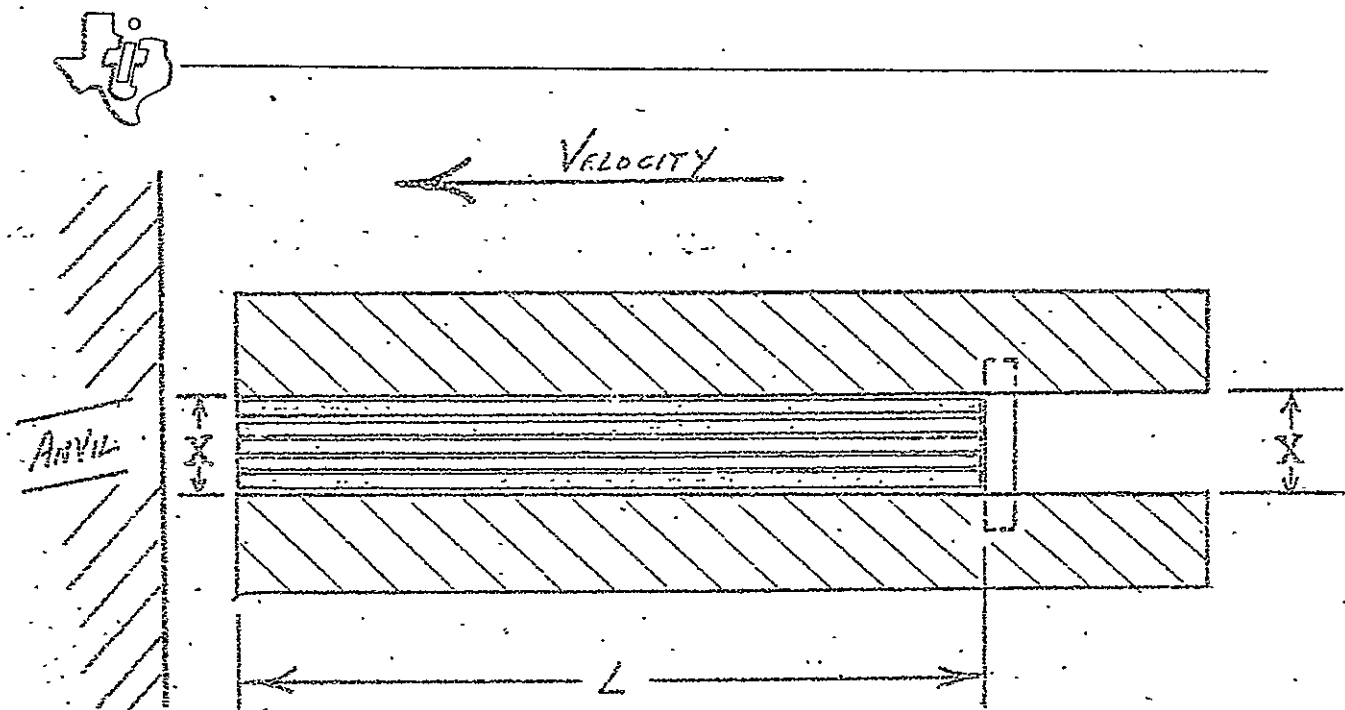
S = 6500 PSI   S = 4585 PSI   S = 5480 PSI   S = 1385 PSI

VELOCITY

ANVIL

X

X

L
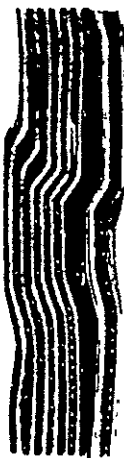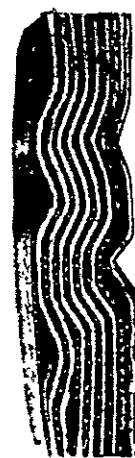
In this arrangement the plates were not "fixed" as in the compression fixture but were free to move and to crush at the ends if sufficient force was applied. Controlled spacing/plate, however, through the use of shims, was the essential feature of this fixture in order to duplicate the static conditions of loading. Initial plate length and impact level could be varied and thus maximum stress, $\overline{\sigma}_{max}$, has been defined here as:

$$\sigma_{max} = \frac{P}{A} = \frac{m(Ng)}{(t \cdot w)} = \frac{(w \cdot L \cdot \rho)(Ng)}{g(t \cdot w)}$$

$$\sigma_{max} = (\frac{\rho}{t})(LN)$$

where: ρ = area wt. density (#/in^2)

   t = plate thickness (in)

   L = plate length (in)

   N = number of g's accel. (-)

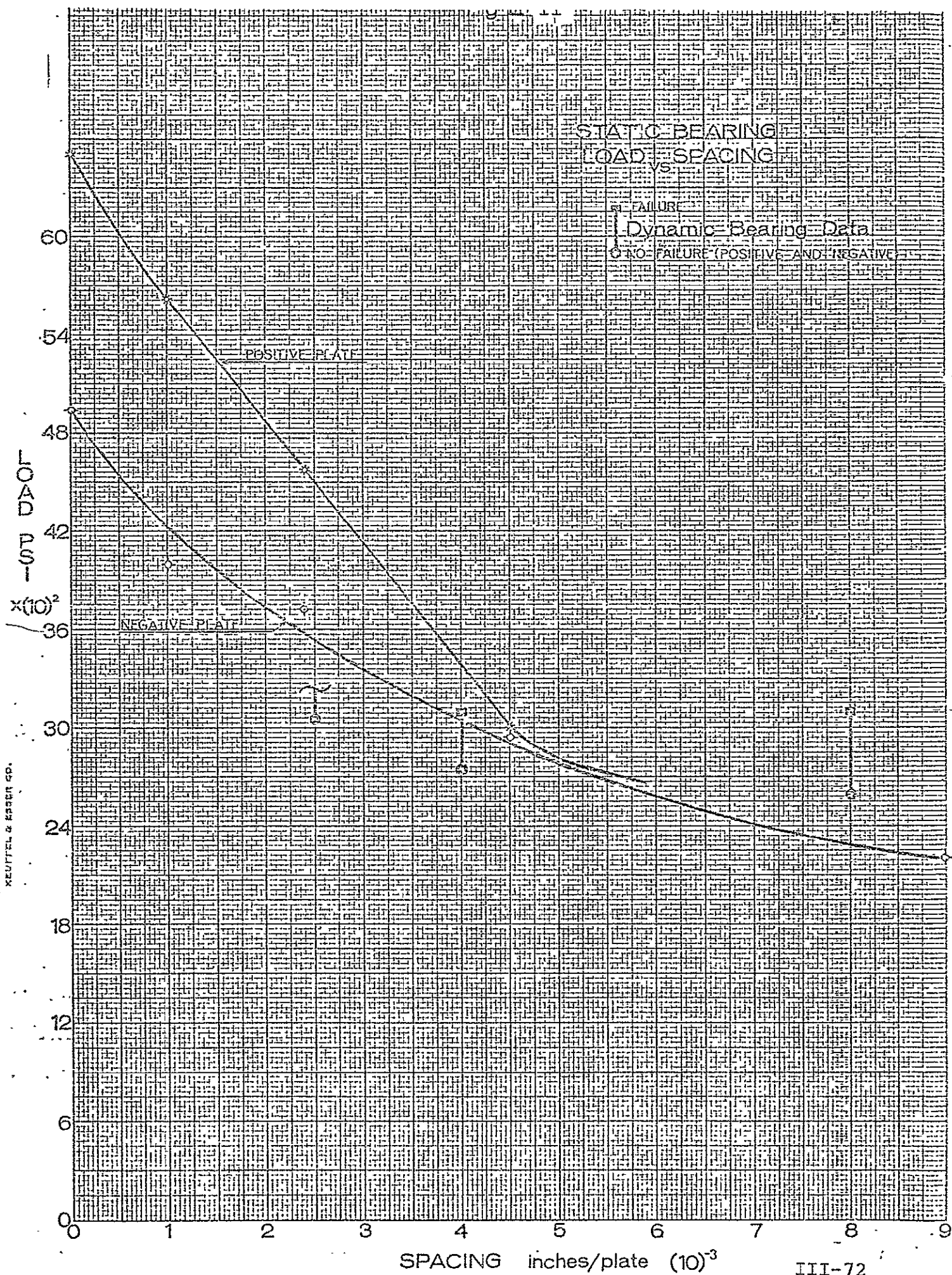III-69

metallurgical
materials division

Thus, for a given test at a controlled spacing/
plate, the maximum stress would be calculated from
the measurement of plate dimensions and applied
deceleration. This max. stress would either cause
visual failure at the end of the plates or it would
not. If this max. stress was sufficient to fail
the plates, we would lower the value to find the
point where the material would not fail. If the
same max. stress was not sufficient to fail the
plates, the level would be raised to the point of
failure. This partly explains the span lines of
experimental determination of failure-non-failure
shown in Figure III-11. This procedure was fol-
lowed for each value of spacing selected. Figure
III-11 presents the values of dynamic failure loads
superimposed on the static failure loads as a func-
tion of plate spacing or degree of lateral
restraint. The static curves are well behaved and
exhibit the greater strength of the positive elec-
trode and show both electrodes tending toward a
nearly common buckling stress asymptote. This is
again in agreement with the earlier static compres-
sion study. These curves display the need to main-
tain a high degree of lateral restraint if exces-
sive loading must be endured.

The dynamic load levels that are indicated as span
lines on Figure III-11 are not solely the limits of
two experimental levels. We have included in these
lines the results of both positive and negative
plates. Several of each type were placed in each
fixture and the difference in stress was very small.
This was essentially as expected since it agreed
with the static results observed -- that at larger
spacing, buckling is dominant and there is thus
little distinction between the two electrodes.
This is shown by the joining of the two static
curves and their tending toward a common asymptote.

As lateral restraint was increased, however, we
reached a point where we were unable to produce
failure in either electrode (single point on Figure
III-11 @ .0025" spacing). In other words, taking
the longest plate (6-5/8") that could be accommo-
dated in our fixture, and employing the highest
impact level (meas. mean 4000g) for 1.1 msec from
110 ft/sec). Available at that time, the maximum
stress developed (3100 psi for NEG.; 2900 psi for
POS.) was not sufficient to produce failure. Thus,
only a lower bound could be established at this
degree of lateral restraint (see Table III B-8).

metallurgical
materials division

STATIC BEARING
LOAD vs SPACING

Dynamic Bearing Data
☐ FAILURE
○ NO FAILURE (POSITIVE AND NEGATIVE)

POSITIVE PLATE

NEGATIVE PLATE

LOAD PSI x(10)²

SPACING inches/plate (10)⁻³

III-72

It appears, however, that the dynamic curve, if able
to be completed, would have a shape or character
similar to the static curve. The dynamic values of
ultimate stress are nearly equal to those obtained
statically and reinforces our position that $\overset{\circ}{\varepsilon}$
effects may not be as important in compression.
This is valuable information in that it makes the
transfer from static to dynamic results less compli-
cated.

The failure modes exhibited in the dynamic study
included all three mechanisms to some degree. In
the case of minimum lateral restraint, the onset of
buckling at the impact end was dominant as expected.
As we increased the degree of lateral restraint,
both compression-shear (very close to the impact
edge) and bearing failure (edge crushing of the
impact surface) were displayed in nearly equal
amounts. It appears, therefore, that in high rate
loading the ultimate bearing stress nearly coincides
with the ultimate compression stress.

It is valuable as a final summary to tabulate the
dynamic results obtained in this study and compare
them with previous determinations of dynamic ulti-
mate strength.

TABLE III B-8

|	Dynamic σ_{ult} Tension	Dynamic σ_{ult} Compression	Dynamic σ_{ult} Bearing @.008"	@.004"	@.0025"
Pos. Plate	2000	>2600	2800	2800	>2900
Neg. Plate	2000	2400	3000	2800	>3100

C. DYNAMIC RESPONSE OF ELEMENTS TO IMPACT LOADING

1. Theoretical Predictions of Dynamic Response

a) One Degree of Freedom Analysis of Natural Frequency:

The natural frequencies, f_{N_n}, of a vibrating system or

element are a most important parameter in the study of

the transient as well as the steady state response of

that system. Therefore, our preliminary analysis

effort was directed toward a modified single degree of

freedom approach to approximate the natural frequencies

of our system. With this approximation, we could then

examine the consequences of the value of f_{N_1} so obtained

with respect to the shock spectra of the specified

deceleration pulse.

The single degree of freedom system employed is shown

below:

metallurgical
materials division
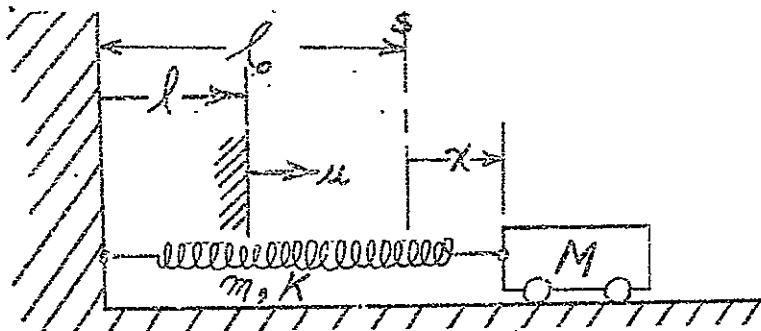
l_o = unstressed length of spring

S = static equilibrium position

χ = dynamic displacement of body

M = mass of body

> 1 = length along spring
>
> μ = dynamic displacement of dl
>
> m = mass of spring
>
> K = spring constant

This system permits the mass of the spring to be con-
sidered and $\omega_{N_1} \approx \sqrt{\frac{K}{M}}$ as in the simple case. Thus we
can use this system to reduce our distributed-mass
(infinite degree-of-freedom) element (battery elec-
trode) to a lumped-parameter system utilizing the con-
cept of vibrational transfer of potential and kinetic
energy. This method has been accurately described in
the literature and for this system it has been shown
that the natural frequency (undamped) is:

$$\omega_{N_1} = \frac{\pi}{2} \sqrt{\frac{K}{2M+m}} \quad \text{for } M << m$$

(Rad./Sec.)

Thus if $M \to O$, we have the case of a spring alone without concentrated end mass and:

$$\omega_{N_1} \approx \frac{\pi}{2} \sqrt{\frac{K}{m}} \quad \text{for } M = 0$$

or for our elastic spring element of length, l, apparent cross-sectional area, A, and apparent modulus of elasticity, E, we have:

$$f_{N_1} = \frac{\omega N_1}{2\pi} \approx \frac{1}{4} \sqrt{\frac{AE}{lm}} \quad (\text{cy/sec})$$

Now for battery electrodes we may write for convenience:

A = width x thickness = wt

$$m = \frac{\text{weight}}{g} = \frac{\text{length x width x area density}}{g} = \frac{l \cdot w \cdot \rho}{g}$$

where: ρ = area weight density

$$f_{N_1} = C \sqrt{\frac{E}{l}} \quad \text{Where: } C = 1/4 \sqrt{\frac{t \cdot g}{\rho}}$$

Specifically for our Ni-Cd electrodes:

t = thickness (.025"-.028") = 0.0265 in.

g = acceleration of gravity = 386 in/sec^2

ρ = area weight density = 3.2 x 10^{-3} #/in^2

(2.8-3.2 x 10^{-3} #/in^2 positive)

(3.3-3.5 x 10^{-3} #/in^2 negative)

Variables:

E = modulus of elasticity

0.1 x 10^6 psi negative plate in compression

1.0 x 10^6 psi positive plate in tension

l = length of electrode
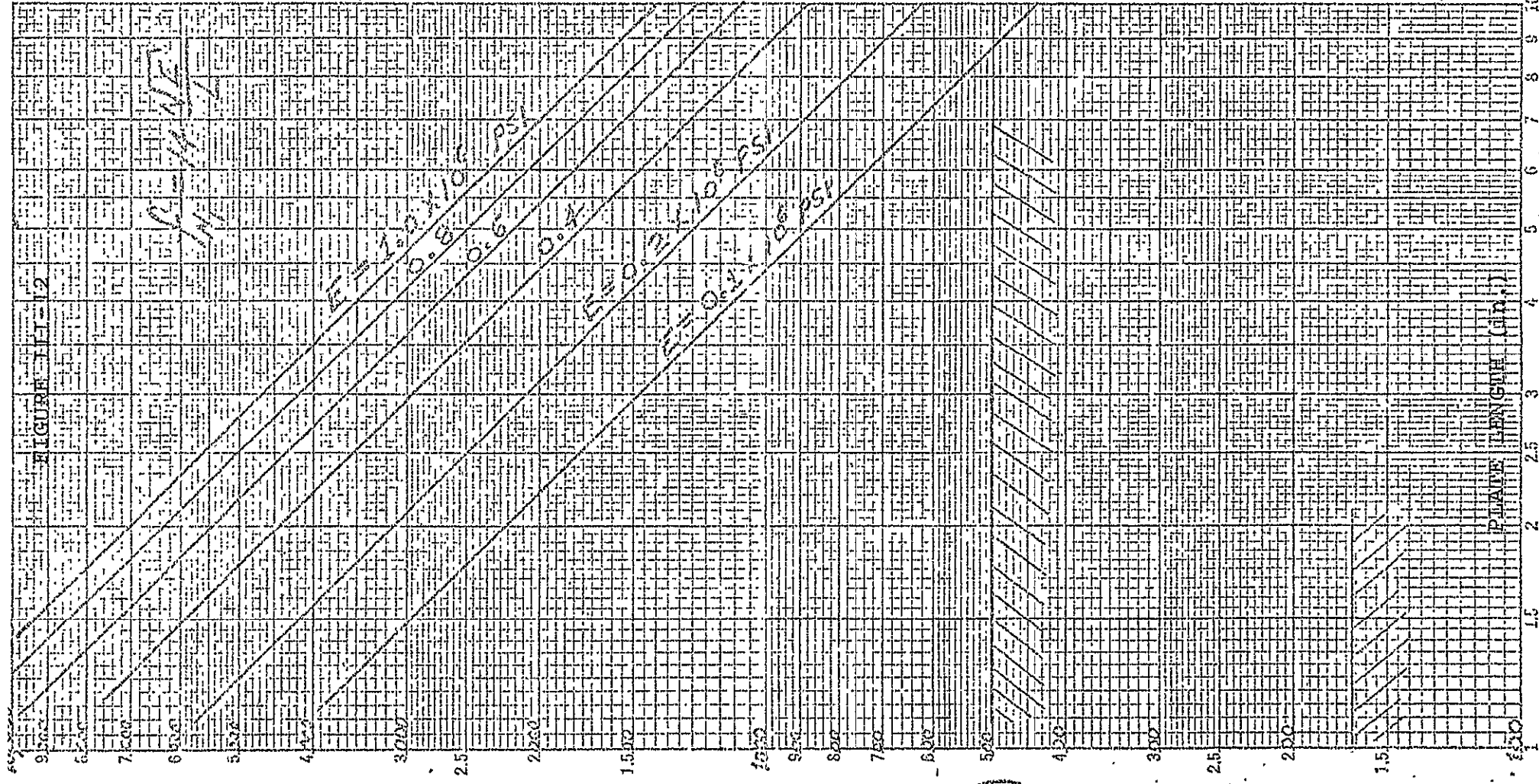
normally 3" - 8"

Thus: C = 14

and the fundamental frequency of longitudinal vibration

for sintered Ni-Cd electrodes is given by:

$$f_{N_1} = (14)\ \frac{\sqrt{E}}{l}$$

This fundamental natural frequency has been calculated

for various plate lengths and values of E and is plotted

in Figure III-12.

b) Shock Spectra Implications:

A shock spectrum is a plot showing the peak response of

a variable-frequency, single degree of freedom oscillator

to a specific shock pulse as a function of the natural

frequency of the oscillator. (It is important to under-

stand from the start, that the shock spectrum tells us

what a given shock pulse will do; not what it is.) This

is much different from a Fourier spectrum or plot of the

Fourier analysis performed to describe a given shock

pulse. It has been found that when a single degree of

freedom, linear, undamped system with a distinct natural

frequency is subjected to a mechanical shock, its re-

sponse motion will be determined by the magnitudes, shape,

and time duration of the shock pulse. In fact, the

amplification spectrum as it is sometimes called, is

metallurgical
materials division

FIGURE III-12

NATURAL FREQUENCY (cy/sec)

$E = 1.0 \times 10^6$ PSI
$E = 0.2 \times 10^5$ PSI
$E = 0.1 \times 10^6$ PSI

PLATE LENGTH (in.)

rather insensitive to the exact time-history of the
pulse. Rather, the rise-time of a given pulse is the
most important factor which distinguishes the maximum
amplification factors for various pulse shapes. The
total impulse and rise time are the two main damage
criteria. As will be seen, the rapid rise time of
our square pulse implies the highest maximum value of
any pulse shape (theoretically = 2X). In general, the
shock spectrum will not have frequency alone as the
abcissa because of the above considerations, rather a
ratio of the shock pulse length (t_o) to the natural
period of the oscillator (T) is more useful $\frac{(t_o)}{T}$.
Depending on the value of this ratio, however, we find
that the system's response <u>during</u> application of a
given shock pulse may differ considerably from the mo-
tion <u>after</u> the shock pulse has ended ($t = t_o$). It is
therefore common to plot a "primary" spectrum (response
during shock input $o<t<t_o$) and a "residual" spectrum
(response after shock input $t_o<t<\infty$) to fully generalize
the behavior of various elements to various shock dura-
tions of a certain pulse shape. However, it is more
useful to provide the designer of shock-resistant ele-
ments with a single "maximax" spectrum plot arrived at
by taking the greater value from the "primary" or the
"residual" plots throughout the frequency ratio range
of interest.

It is not appropriate to reiterate the derivations and
analyses of various spectra characteristics that can
be found in the literature. The value of using this
concept is well recognized and it is only important
that we understand the fundamentals in order to apply
the information that can be obtained. Thus, the
character of the maximax shock spectra can be obtained
directly from the literature. In our case, we wish to
consider a <u>single</u> shock input:

$$t_o = 1 \, msec$$
$$\Delta V = 129 \, ft/sec.$$
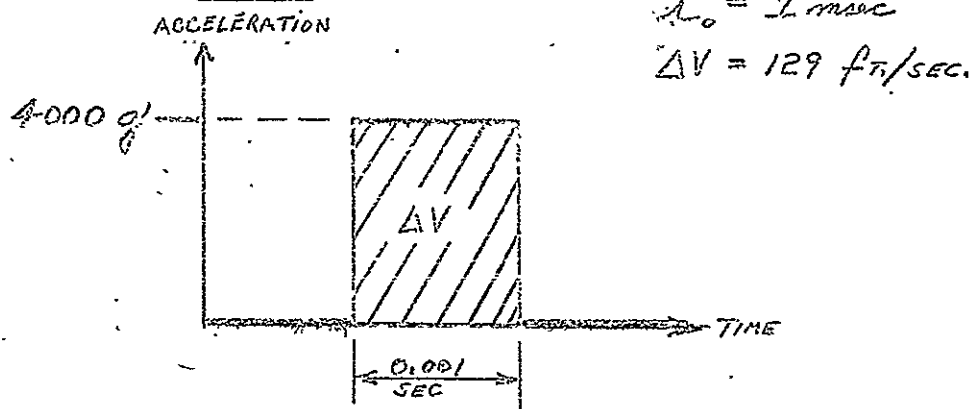
Thus, we can establish the abscissa directly as the
natural frequency of our Ni-Cd electrodes rather than
as a time ratio.

The ordinate is simply the relative response and can
be scaled directly in numerical <u>dynamic amplification
factors</u>. It must be remembered that the response can
be thought of as displacement, acceleration, etc.
(If this same quantity describes the input pulse). More
useful to the designer is the concept of force or
stress (indirectly strain) amplification over that of a

static loading equal to the amount of input acceleration.

The shock spectrum for the pulse illustrated above is given in Figure III-13 with the ordinate and abcissa scaled as discussed for optimum use in our problem. The basic implications are: (1) Any Ni-Cd electrode with a natural frequency greater than 167 cy/sec will experience an amplification of the nominal input forces under dynamic loading. (2) Any Ni-Cd electrode with a natural frequency greater than 500 cy/sec will experience twice the nominal input forces under this dynamic loading situation.

From a design point of view, the calculation of natural frequencies in the previous section now has more value. It may be instructive to outline the design considerations that have been formulated:

    (1)   The manner of loading must first be identified and this will dictate the modulus of elasticity and strain-rate effects from previous determinations of the mechanical properties of our electrode.

    (2)   Space considerations may indicate a trial size of our electrode.

    (3)   The design pulse magnitude will be used to calculate the static stress applied to this size and weight electrode.

FIGURE III-13

SHOCK SPECTRA for PULSE
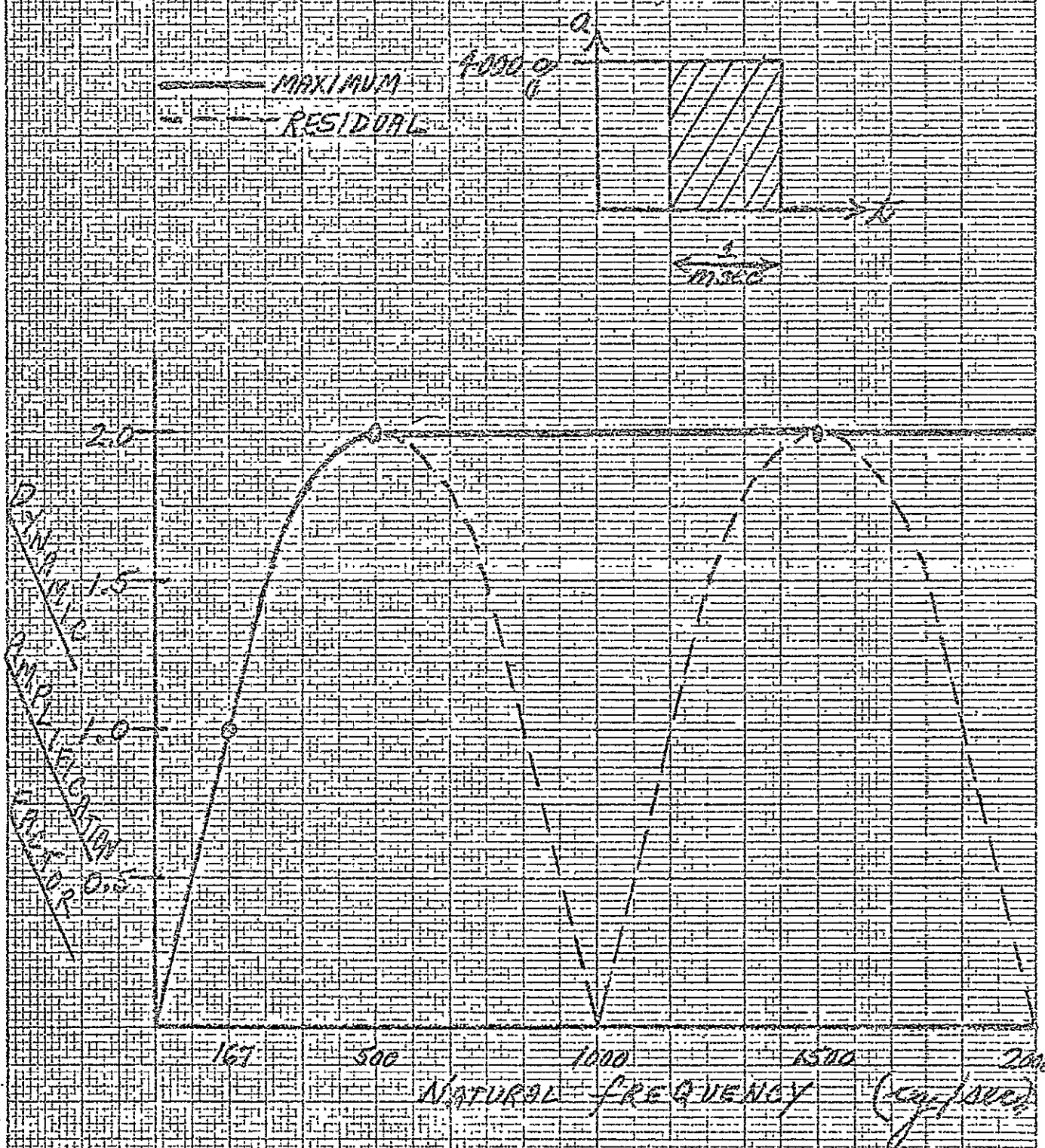
(4) The natural frequency of this specific
     electrode is determined.

(5) The shock spectrum (for the design
     pulse) is used to determine the dynamic
     amplification factor which applies.

(6) The· actual stress which this electrode
     will experience under this design pulse
     loading can now be calculated.

(7) The effect of this stress on the elec-
     trode is now determined from previous
     determinations of this electrode's
   mechanical properties under the same
     manner of loading.

The importance of determining complete experimental
information concerning the mechanical properties of
Ni-Cd electrodes is now obvious. Without such
information, design can neither begin (Step 2) nor can.
a valid judgment be made (Step 7) concerning the actual
damage that may or may not occur to an electrode in a.
specific loading situation.

c) Analysis of Displacement and Stress for Distributed-
    Mass Element:

The frequency-shock spectra analysis is quite straight-
forward and can provide valuable information to the
designer. It does not permit a direct calculation of
the stress within the element, however, and it does. not

give us a description of the deformation process. What
we would like is an insight into the actual displacements
within an electrode and the stresses that are applied
during impact. We seek an accurate description of stress
and strain as a function of location and time. This type
of information can only be obtained by a more rigorous
analysis of our distributed-mass element. To explore the
possibility of solution, we have formulated the problem
as a long, slender element of uniform cross-sectional
area, A, and constant initial velocity (rigid body
motion), -V, which is subjected to a sudden longitudinal
deceleration at time t = o. The problem is shown below:
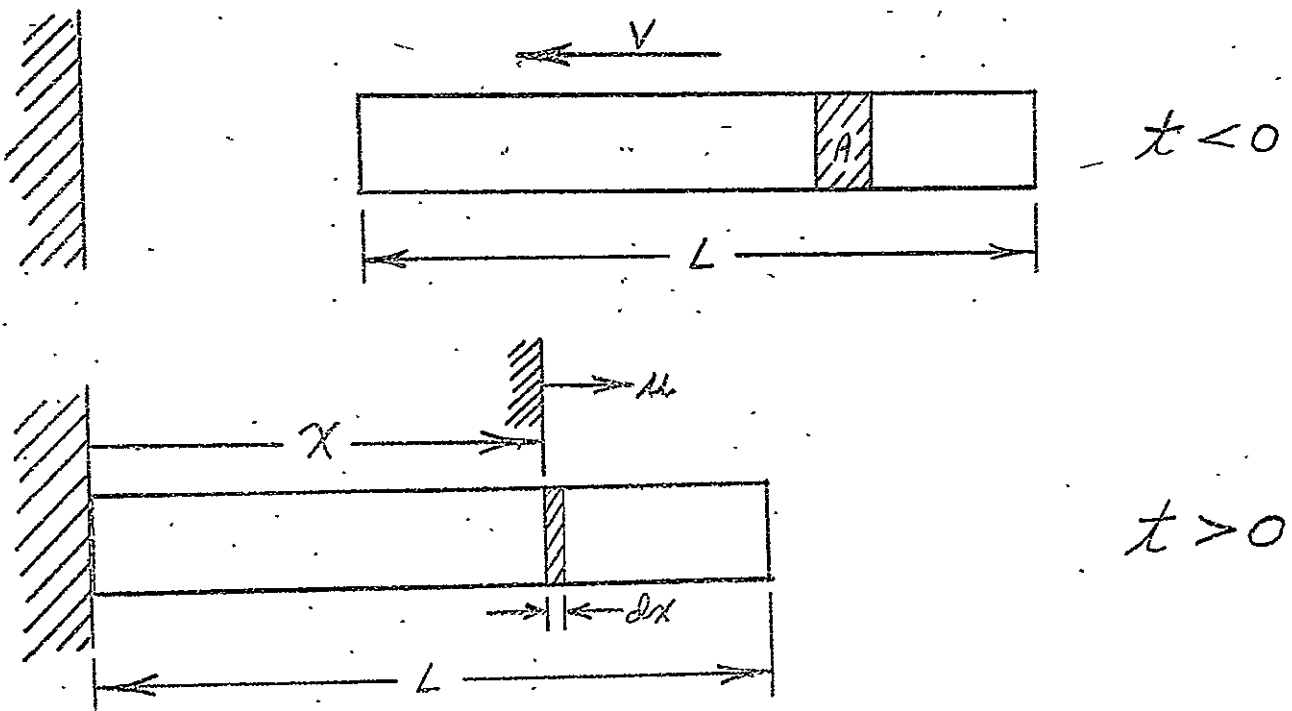
We find that the governing differential equation is:

$$\frac{\partial^2 u}{\partial t^2} = a^2 \frac{\partial^2 u}{\partial x^2} \tag{2}$$

which is the general "wave equation" in which:

$$a = \sqrt{\frac{E}{\rho}} \qquad \text{where:} \quad \rho = \text{mass density}$$

We have for our case:

Initial Conditions	Boundary Conditions
$u(x,o) = o$	$u(o,t) = o$
$\frac{\partial u}{\partial t}(x,o) = -v$	$\frac{\partial u}{\partial x}(L,t) = o$

imposed by our considerations of constant initial velocity, rigid fixed end and free unstressed end.

Following the method of separation of variables we assume the general solution of EQ. (2) may have the form:

$$u(x,t) = X(x)\, T(t) \tag{3}$$

Now we may write EQ. (2) as:

$$X\, T'' = a^2\, T\, X''$$

$$\frac{T''}{T} = a^2 \frac{X''}{X} = -\lambda^2$$

the component ordinary differential equations will be:

$$T'' = -\lambda^2 T \qquad \& \qquad X'' = -\frac{\lambda^2}{a^2} X$$

and whose solutions are known:

$$T = A \cos \lambda t + B \sin \lambda t$$

$$\&$$

$$X = C \cos \frac{\lambda}{a} x + D \sin \frac{\lambda}{a} x$$

Therefore, the general product solution EQ.3 can be written:

$$u(x,t) = (C \cos \frac{\lambda}{a} x + D \sin \frac{\lambda}{a} x)(A \cos \lambda t + B \sin \lambda t) \quad (4)$$

Examining the first boundary condition in EQ.(4):

$$\implies C = 0 \text{ in general for all } t$$

Examining the second boudary condition in EQ.(4):

$$\implies (D \frac{\lambda}{a}) \cos \frac{\lambda}{a} L = 0 \quad \text{in general for all } t$$

Hence: $\lambda_n = \dfrac{(2n-1) a\pi}{2L} \quad n = 1,2,3,\ldots\ldots$

Now the general solution EQ.(4) has been reduced to a series of product solutions:

$$u(x,t) = \sum_{n=1}^{\infty} \sin \frac{(2n-1)\pi}{2L} x \left[A_n \cos \frac{(2n-1)\pi a}{2L} t + B_n \sin \frac{(2n-1)\pi a}{2L} t \right] \quad (5)$$

Examining the first initial condition in EQ.(5):

$$\implies A_n = 0 \quad \text{in general for all } x$$

Examining the second initial condition in EQ.(5):

$$\frac{\partial u}{\partial t}\bigg)_{t=0} = \sum_{n=1}^{\infty} B_n \left(\frac{(2n-1)\pi a}{2L} \right) \sin \frac{(2n-1)\pi}{2L} x = -V \quad (6)$$

We recognize a similarity between EQ.(6) and a half-range Fourier Series expansion. Hence, the problem of determining B_n in EQ.(6) is really the problem of expanding the given function $f(x)$ in a half-range sine series expansion over the interval $0<x<L$.

Performing the required expansion and integration to determine the coefficients we find:

$$B_n = \left[\frac{-8\ VL}{(2n-1)^2\ \pi^2\ a} \right] \qquad (8)$$

Now we may write the final general equation for displacement from EQ.(5):

$$u\ (x,t) = \frac{-8VL}{a\ \pi^2\ } \sum_{n=1}^{\infty} \frac{1}{(2n-1)^2} \sin \frac{(2n-1)}{2}\ \pi\ \frac{x}{L} \sin \frac{(2n-1)}{2}\ \pi\ \frac{at}{L} \qquad (9)$$

which fully describes the elastic displacement at any time and any longitudinal location along the electrode. The natural frequencies of this sinusoidal displacement u(t) or vibration are:

$$f_{N_n} = \frac{\lambda n}{2\pi} \quad \text{(cycles/sec)} \quad n = 1,2,3,\ldots\ldots$$

therefore:

$$f_N = 1\ (\frac{a}{4L}),\ 3\ (\frac{a}{4L}),\ 5\ (\frac{a}{4L}),\ \ldots\ldots\ldots\ldots \qquad (10)$$

Examining the fundamental natural frequency:

$$f_{N_1} = \frac{a}{4L} = \frac{\sqrt{E/\rho}}{4L} = \frac{\sqrt{Eg/\gamma}}{4L} = \frac{1}{4}\sqrt{\frac{tg}{\rho}}\ \frac{\sqrt{E}}{L}$$

We find that it is equivalent to the "approximation" we had obtained earlier in Section III C.1.a. in our consideration of the single degree of freedom system. This is not actually surprising since the earlier approximation employed sine functions as "guesses" for both the normal function and the time function. This means now that Figure III-12 gives us the true natural frequency, f_{N_1}, as confirmed by a rigorous analysis.

Having obtained a complete solution (EQ.(9)) for elastic
displacement, we can now investigate the general stress
solution:

$$\sigma = E \varepsilon = E \frac{\partial u(x,t)}{\partial x}$$

If this initial assumption of elastic material behavior
is retained, the general stress solution is:

$$\sigma (x,t) = \frac{-4EV}{a\pi} \sum_{n=1}^{\infty} \frac{1}{(2n-1)} \cos \frac{(2n-1)}{2} \pi\frac{x}{L} \sin \frac{(2n-1)}{2} \pi\frac{at}{L} \qquad (11)$$

which fully describes the elastic stress within the
element at any time and any longitudinal location along
the electrode.

We are interested in the expression for maximum stress
which occurs at the fixed end (x = 0):

$$\sigma_{\underline{max.}} (0,t) = \frac{-4EV}{a\pi} \sum_{n=1}^{\infty} \frac{1}{(2n-1)} \sin \frac{(2n-1)}{2} \pi \frac{at}{L} \qquad (12)$$

Numerical Analysis:

We have attempted to numerically evaluate the maximum
stress (EQ.(12)) for a few values of time, t. It is
apparent that we have simply the summation of the
fundamental and all the odd sinusoidal harmonics which
is of course a square wave. The coefficients of the
odd harmonies appear to imply a $\frac{\pi}{4}$ multiplier for the
fundamental. At the fixed end where stress is a maximum,

metallurgical
materials division

we have a state of compression for the time interval,
$0 < t < \frac{2L}{a}$, followed by a state of tension for the time
interval $\frac{2L}{a} < t < \frac{4L}{a}$. This process is then cyclic at a
frequency of $(\frac{a}{4L})$ cycles/sec.

Conclusion:

The sole limitation of the general solution obtained
in this section is the one assumption that made the
solution possible -- elastic material behavior. If
we do not impose this material limitation and allow
stress to be some general function of strain, we do
not obtain EQ.(2) as the governing differential equa-
tion.

Rather:

$$\frac{\partial \sigma}{\partial \epsilon} (\frac{\partial^2 u}{\partial x^2}) = \rho \frac{\partial^2 u}{t^2} \tag{13}$$

whose general solution is unknown. EQ.(13) therefore
introduces the most significant portion of non-
linearity into our system. We understand that JPL has
devoted some effort to the treatment of this and large
displacement non-linearities. Recent literature has
discussed ways of introducing empirically the non-
linearities implied by plastic and strain hardening be-
havior. This area is in need of further analysis. The
research indicated for a more complete understanding of
dynamic response is in the introduction of these material

metallurgical
materials division

behavior non-linearities into the general governing differential equation (13) and the physical interpretation of its solution with the aid of computer analysis.

One further point does not concern the validity of the solution given, but concerns the exactness of its applicability to our experimental loading situation. In question is the first boundary condition which was used in our solution to describe the rigid fixed end.

We should go back and examine the effect on our solution of imposing a condition of uniform deceleration during the time interval of impact:

$$u(o, t) = -Vt - \frac{a}{2} t^2 \qquad o < t < .0001/sec.$$

This more accurately describes the displacement of this end of the bar during the time of loading and could thus make the existing solution conservative in its prediction of stresses which may be higher than those actually experienced in our testing.

2. Experimental Determinations of Dynamic Reponse

   a) High Speed Photographic Analysis

   Following an analysis or theoretical prediction of mechanical behavior, we most desired an experimental verification of that prediction. One method to experimentally obtain the actual displacements of an element

during a loading situation is to visually observe and measure them. We have, therefore, used high speed photography to examine the motion of our electrodes during impact. It appears that a great deal of information concerning the description of dynamic displacements can be gained by this method.

b) Dynamic Strain Measurements

Some work has been done in the measurement of dynamic strain under impact conditions using the strain-gage techniques we have developed. The basic circuitry and instrumentation system was simply a wheatstone bridge employing a single active strain gage with zero balance:

Hewlett Packard Constant Voltage Power Supply Mod.#6215A

Tektronix 1A7 Plug-In
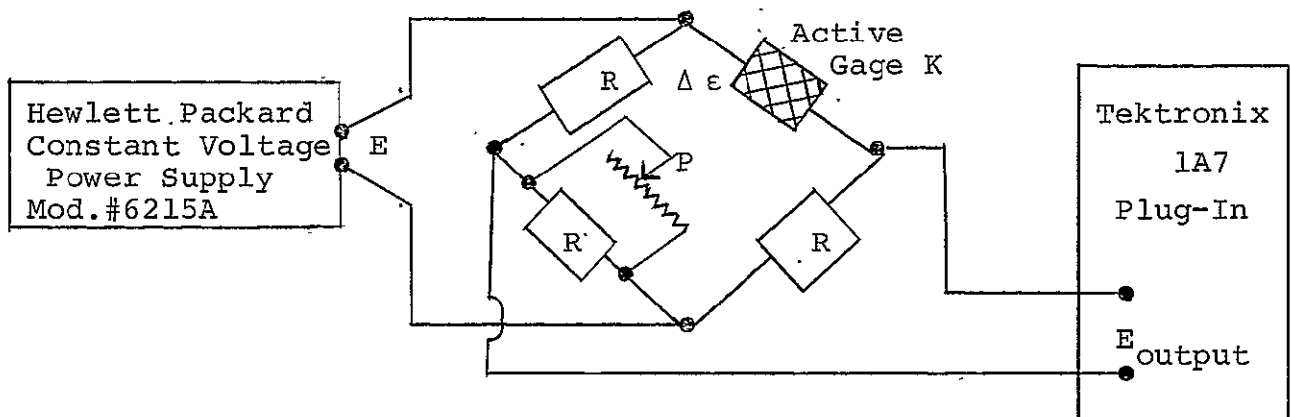
E_{output}

K = Active Gage Factor (2.0)
R = Fixed Resistor (120 Ω)
P = Zero Balance Potentiometer
E = 12 Volt Supply

$$E_{output} = \frac{R^2 KE}{(R+R)^2} (\Delta \epsilon) = 6.0 (\Delta \epsilon)$$

This circuit was used for all the experimental data contained in this report. Some work was done near the end of the experimental program involving two active strain gages to explore the dynamic strain distribution along the plate length, $u = u(\underline{X}, t)$. This data was very limited, however, and rather inconclusive. Some correlation with our theoretical predictions of strain distri-

metallurgical
materials division

bution with time, u = u (x, T), was indicated before the experimental work ended. This portion of the report indicates the relation of these preliminary findings to the theoretical predictions that have been made.

(1) Aluminum Plates:

The mechanical properties of the aluminum alloys are well established and readily available. An aluminum plate loaded within its elastic region is obviously a more well-behaved system than our porous plate material. Thus, our initial experimental work was aimed at confirming our theoretical analysis by the use of an aluminum plate:
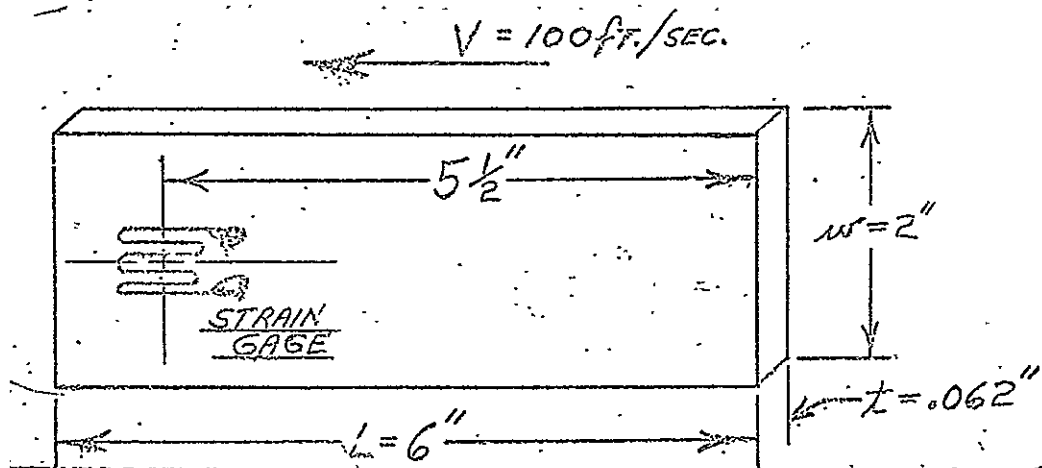
6061 - T6 Alloy:

$E = 10.0 \times 10^6$ psi
$\sigma_y = 40,000$ psi
$\sigma_{ult} = 45,000$ psi
$\gamma = 0.0976$ #/in^3
$\rho = 0.00605$ #/in^2
$a = 16,600$ ft/sec

Single Strain Gage:

$R = 120\ \Omega$
$K = 2.0$
$E = 12.0$ Volts
$\Delta E = \dfrac{R^2 KE(\Delta\epsilon)}{(R\&R)2} = (6.0)\Delta\epsilon$

We could first calculate the natural frequency, f_{n_1}, of this element by either of the two equivalent equations we have given earlier:

$$f_{n_1} = \tfrac{1}{4}\sqrt{\frac{tg}{f}}\ \frac{\sqrt{E}}{L}$$
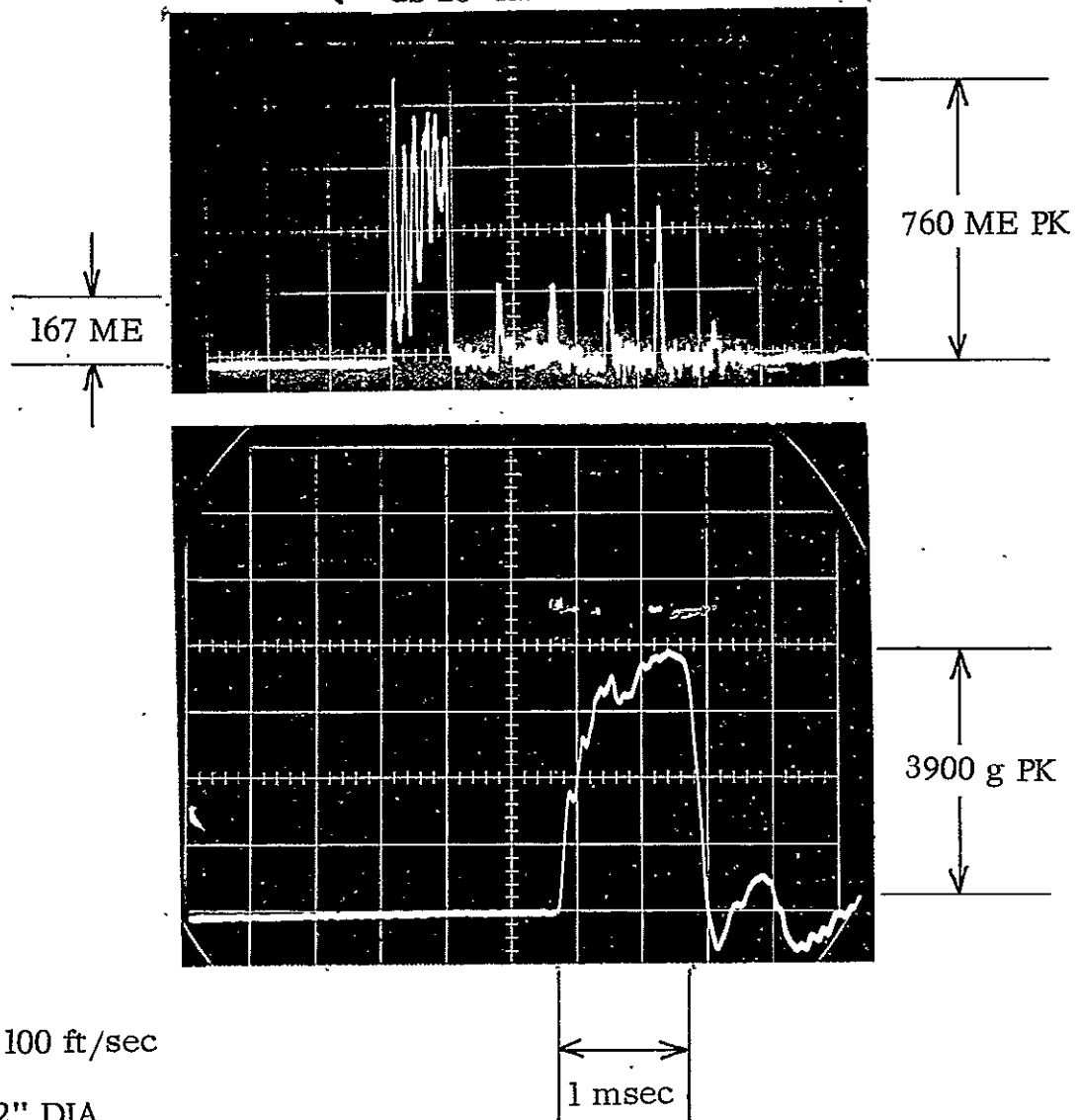
Figure III - 14

UPPER TRACE:

DYNAMIC STRAIN - 1 msec/cm; 1 mo/cm

LOWER TRACE:

ACCELERATION PULSE - 0.5 msec/cm; 1000 g/cm

6,500 cy/sec

dS 28 Al

760 ME PK

167 ME

3900 g PK

1 msec

V = 100 ft/sec

1 1/2" DIA.

DYNAMIC STRAIN OSCILLOGRAPH OF AL PLATE

or $f_{n_1} = 1 \left(\frac{a}{4L}\right)$

and we find $f_{n_1} = 8{,}300$ cy/sec.

The lower trace of Figure III-14 shows the accelera-
tion time history of loading imposed on this plate
during impact. We note that the pulse length (t_o)
is 0.001 sec. The shock spectrum given in Figure
III-13, therefore, applies directly. Since the cal-
culated $f_{n_1} = 8{,}300$ cy/sec $>>500$ cy/sec, we can
only conclude from this spectrum that a dynamic am-
plification factor equal to 2.0 must be used.
Due to simple inertia loading, the static stress
level (L=6") may be calculated:

$$\sigma = \frac{ma}{A} = \frac{(L' \cdot w \cdot t \cdot \gamma)}{g \, (w \cdot t)} \; (Ng) = L'\gamma N \implies \sigma_{static} = 2300 \text{ psi.}$$

Employing the dynamic amplification:

$$\sigma_{dyn.} = 4600 \text{ psi}$$

And: $\varepsilon_{dyn.} = \dfrac{\sigma_{dyn.}}{E} = 460 \; \mu\varepsilon$

is the expected gage output under this loading con-
dition. We now note that the upper trace of Figure
III-14 has recorded an experimental peak strain of
$\varepsilon = 760 \; \mu$ in/in. In the experimental record, it is
possible that the subsequent peaks which indicate a
more uniform 668 μ in/in peak strain level are truly
more significant. The difference between measured
and calculated strain is then 210 μ in/in. This is
quite encouraging as a very preliminary experimental
result. The predicted natural frequency (f_n) of the
cyclic displacement within our element was 8,300
cy/sec and should be recorded by the strain gage.
The upper trace of Figure III-14 shows this cyclic
strain behavior within the plate at a frequency
of approximately 6,500 cy/sec. Again, it is
encouraging to see this preliminary correlation
but we cannot account for the discrepancy

III-93

(1800) cy/sec) at this time. We may now look at
the experimental results and the predictions from
our detailed analysis. It appears that our series
in the max. stress equation (12) converges to $\frac{\pi}{4}$.
We may, therefore, calculate the max. elastic stress
predicted:

$$\sigma_{max.}(o,t) = \frac{-4EV}{a\pi}\left(\frac{\pi}{4}\right) = \frac{-EV}{a} = -60,000 \text{ psi}$$

Now:

$$60,000 \text{ psi} > 40,000 \text{ psi} = \sigma_{yield}$$

In fact not only plastic deformation is implied but
$60,000 \text{ psi} > \sigma_{ult}$!

Even if we assume that a high strain-rate sensi-
tivity elevates the dynamic yield stress and the
elastic modulus still applies we have:

$$\epsilon_{predicted} = \frac{\sigma}{E} = 6,000 \text{ } \mu\epsilon$$

This value is $>0.2\%$ ϵ normally taken as the yield
point; yet there was no observation of plastic
deformation after repeated loading at this impact
level. Furthermore, the experimental strain trace
showed no residual strain (plastic or lack of zero
return); yet the fact remains:

$$\begin{array}{ccc} 760 \text{ } \mu\epsilon \text{ PK} & & 6,000 \mu\epsilon \text{ PK} \\ \text{Experimental} & << & \text{Predicted} \end{array}$$

Our only conclusion must be that our analytical
prediction is nearly an order of magnitude con-
servative! The fault must lie in the first boundary
condition we have assumed:

$$u \ (o,t) = o \text{ implies no carriage displacement}$$
$$\text{during the loading period}$$

What we really have is the situation that the car-
riage and the end of the element have an absolute
displacement during the loading period. Thus, we
must modify our analytical prediction to account
for this boundary condition. Consideration of
this, of course, will reduce the predicted magni-
tude and have a strong effect on the discrepancy
that has been brought out by our preliminary experi-
mental results. Time did not permit the introduc-
tion of this aspect during the current investigation.

(2) Cadmium Electrodes:

Following our study of the aluminum plate, we have
obtained some preliminary results on the negative
electrode.

V = 64 ft./sec.

$L' = 4\frac{3}{4}''$

$w = 2''$

STRAIN GAGE

$t = .026''$

$L = 5''$

Negative Cd Plate	Single Strain Gage
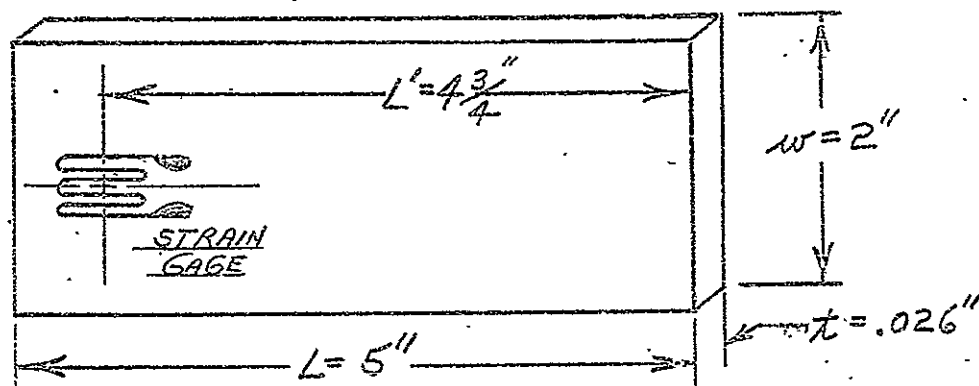
$E_{comp.} \approx 0.5 \times 10^6$ psi   AF-7-1-56 (E-910)

$\sigma_{ult.} \approx 3000 - 5000$ psi $\Delta E = (6.0) \Delta E$

$\qquad = 0.127$ #/in^3

$\qquad = 0.0033$ #/in^2

$a \approx 3250$ ft/sec

Again, it is first useful to determine the natural
frequency of this element either by calculation as
before or directly from Figure III-12.

$$f_{n_1} \approx 2000 \text{ cy/sec}$$

The upper trace of Figure III-15 shows a cyclic
strain behavior within the electrode at a frequency
of approximately 2500 cy/sec. This is in good
agreement with our predicted 2000 cy/sec. Further-
more, it implies that the governing elastic modulus
may be higher:

$$E = \left(\frac{f_n L}{14}\right)^2 = 0.8 \times 10^6 \text{ psi}$$

The lower trace of Figure III-15 shows the accelera-
tion-time history of the loading and the pulse length
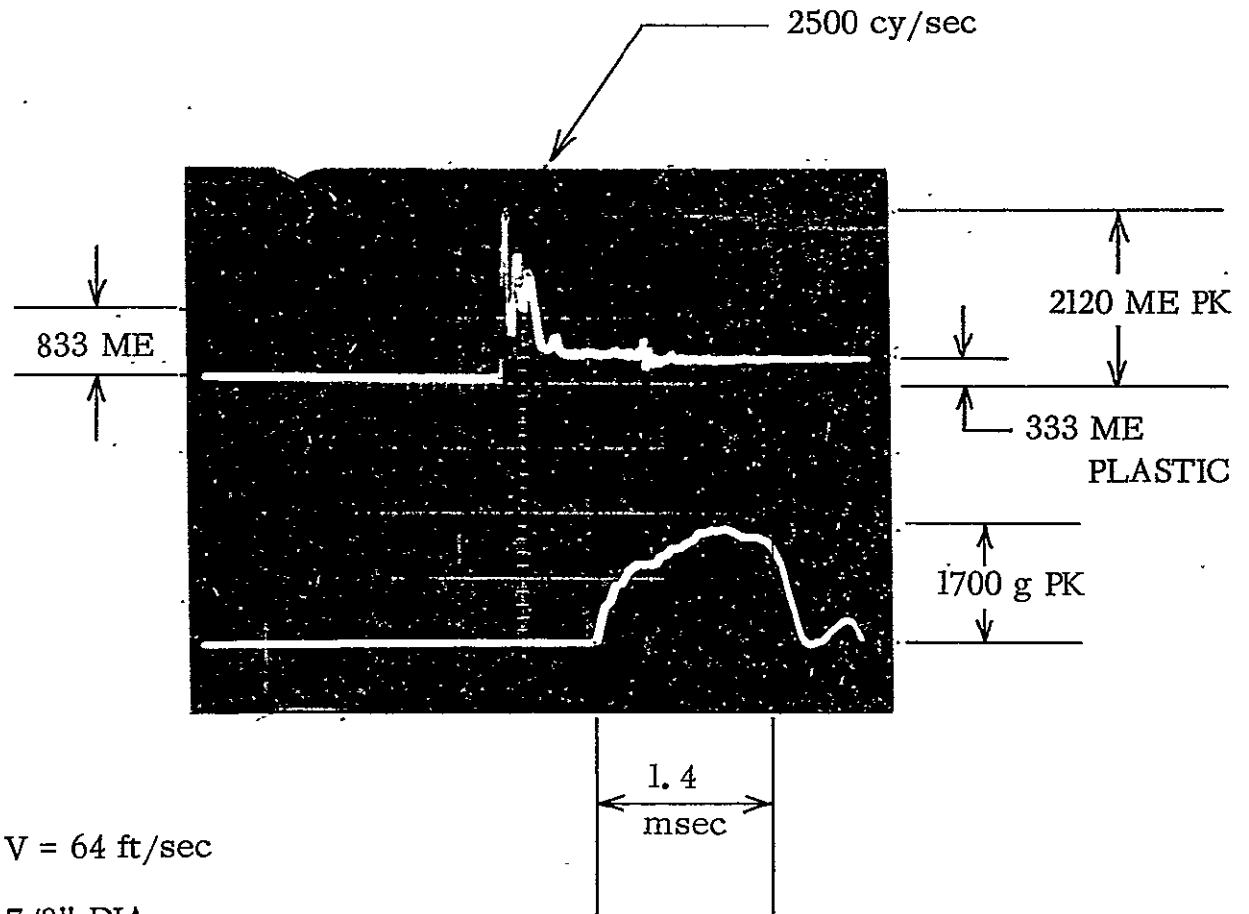
metallurgical
materials division

Figure III - 15

UPPER TRACE:

DYNAMIC STRAIN - 2 msec/cm; 5 mo/cm

LOWER TRACE:

ACCELERATION PULSE - 0.5 msec/cm; 1000 g/cm

V = 64 ft/sec

7/8" DIA.

d = 0.367"

DYNAMIC STRAIN OSCILLOGRAPH OF Cd ELECTRODE

t_o is approximately 1.4 msec. Thus, we cannot use the
shock spectrum of Figure III-13 directly ($t_o \searrow .001$ sec).
However, the amplification factor of 2.0 will apply to
any element with a $f_{n_1} > 356$ cy/sec for this loading
pulse if we assume it is square. If is obvious that
$f_{n_1} = 2000$ cy/sec >> 356 cy/sec and the maximum amplifi-
cation factor will apply. The maximum will apply for any
shape pulse of this duration. However, we could question
the use of the square wave for this low velocity impact
level and assume the experimental record more closely
approximates a half-sine pulse. If this is true, a
maximum amplification factor of 1.8 will apply.

We may now calculate the maximum stress due to simple
inertia loading:

$$\sigma = \frac{ma}{A} = L\gamma N = 1080 \text{ psi}$$

Employing the 1.8 x amplification factor:

$$\sigma_{\text{dyn.}} = 1940 \text{ psi}$$

which implies: $\varepsilon = \dfrac{\sigma_{\text{dyn.}}}{E=0.8 \times 10^6} = 2430\mu$ in/in PK.

The upper trace of Figure III-15 has recorded an experi-
mental peak strain level of only 2120μ in/in. There is
one consideration that might help explain this
discrepancy although we have no experimental confirmation
at this time. We know that if a material is one-half
critically damped ($^{c}/_{c}c = 0.5$), its maximum amplification

factor for a half-sine pulse is only 1.1. If this factor is taken into account we would predict a peak strain of only 1470μ in/in. This is lower than the recorded peak yet equal to the approximately 1450μ in/in strain level recorded by subsequent peaks.

This is important enough that it should be investigated if work were continued since it is a very beneficial material property of this porous electrode.

It is important to note the lack of zero-return in the upper trace of Figure III-15. This indicates a residual plastic strain of 333μ in/in.

Considering the complete analysis, we could evaluate the stress by equation (12) as we did for aluminum:

$$\sigma_{max.}(o,t) = \frac{-4EV}{a\pi} \left(\frac{\pi}{4}\right) = 9850 \text{ psi}$$

If our original values $E = 0.5 \times 10^6$ psi and a = 3250 ft/sec are used for our 64 ft/sec impact. This value of $\sigma_{max.} >> \sigma_{ult.}$ as was the case for the aluminum plate analysis. The reasons for this discrepancy have been discussed in the previous section.

(3) Summary:

The experimental measurement of dynamic strain during impact loading has been accomplished. The frequency

metallurgical
materials division

data of elastic wave propagation that has been obtained may be our most valuable tool for determining the value of the dynamic modulus of elasticity. The ability to measure the residual plastic strain component in a total strain level has also been demonstrated. This ability will allow us to very accurately determine the dynamic σ-ε curve from a number of tests. Information well beyond the empirical yield point 0.2% ε seems very possible. The preliminary magnitudes that have been recorded are satisfactory at this time. Agreement was good and it is felt that the experimental data would correlate very well with the predictions that could be made from the detailed analysis with proper boundary condition modification. The interplay of: (1) strain-gage reinforcement, (2) amplification factor based on pulse shape as well as frequency, (3) viscous damping of the porous material, (4) accuracy of E value, and (5) the compressional strain-gage behavior, have been briefly described. With an accurate experimental determination of E, σ may be accurately calculated from Equation (12) if we have made the analytical modifications indicated. Then we are confident that the dynamic amplification could be accurately determined for future use.

D. IMPACT TESTING OF Ni-Cd CELLS

1. Failure Criteria

True "failure" may be electrochemically defined as the
cell's inability to deliver suitable discharge capacity fol-
lowing an impact environment. Since we have monitored a
cell's open circuit voltage during impact, we can use this
as an indicator of electrical damage. Typical of the informa-
tion provided by this failure indicator are the phenomenon
shown in Figure III-16. The upper traces display a cell's
open circuit voltage from 5 msec.before impact to 15 msec
after impact. The three oscillographs presented indicate
the classifications of impact-induced damage:

(a) no cell damage   (N) $V_2 = V_1$ no ΔV @ impact

(b) questionable damage   (P) $V_2 = V_1$ ΔV @ impact (momem-
                                               tary shorting)

(c) failure   (f) $V_2 < V_1$ ΔV @ impact (complete
                                               shorting or loss of
                                               plates

The type of behavior exhibited in (b) is of very question-
able damage electrochemically. We assume that such a
momentary short will have little effect on the following
discharge capacity and certainly not prevent the cell from
subsequent cycling. However, we will distinguish this ob-
served behavior from that of a complete satisfactory per-
formance.

metallurgical
materials division

UPPER BEAM:

OC VOLTAGE OF CELL
VERT: 1 VOLT/CM
HORIZ: 2 msec/CM

LOWER BEAM:

ACCELERATION
VERT: 1000g/CM
HORIZ: 0.5 msec/CM

a)

NO CELL DAMAGE →

b)

**MOMENTARY
SHORTING
DURING IMPACT** →

c)

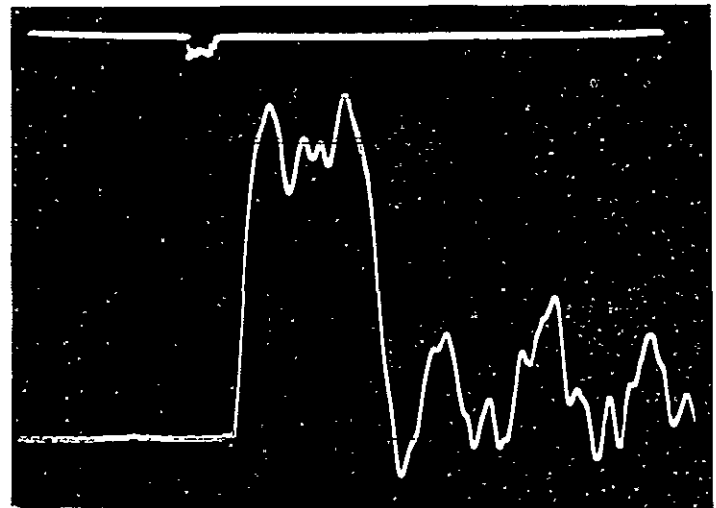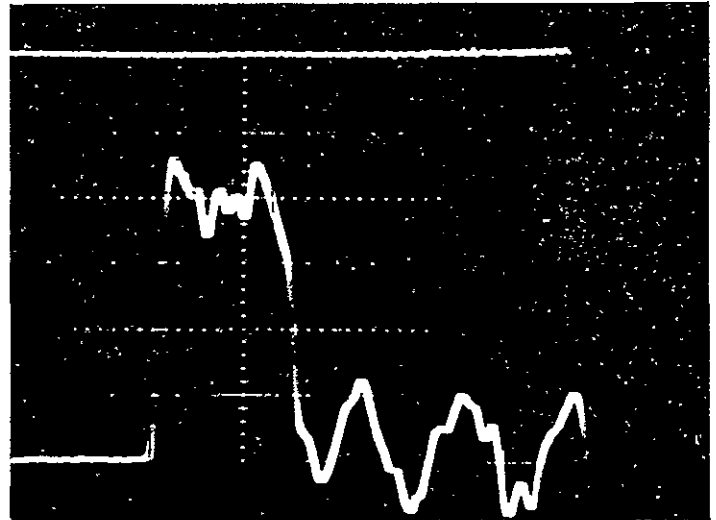**COMPLETE
CELL FAILURE
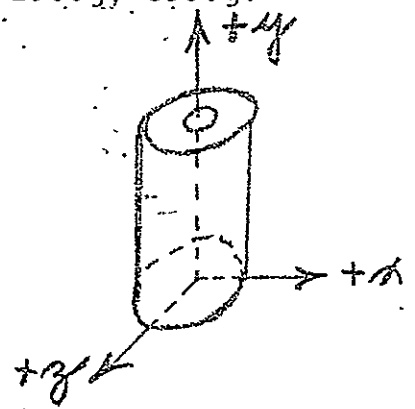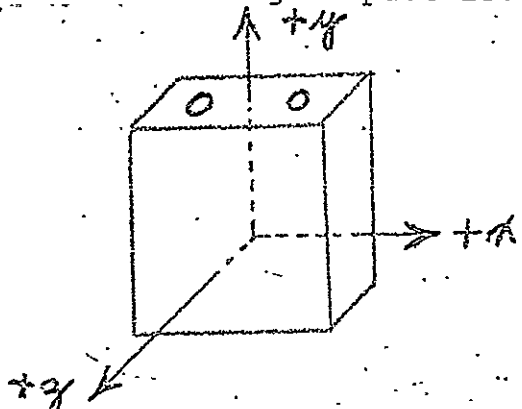AT IMPACT** →
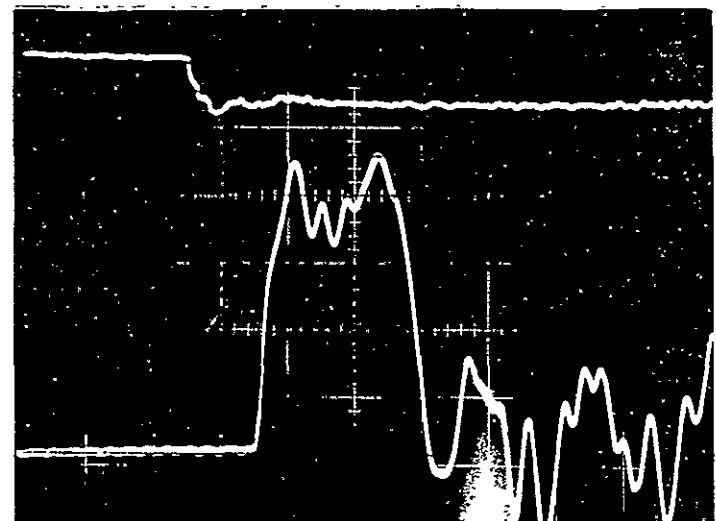
Figure III - 16

2. Existing Ni-Cd Cells (<5AH)

The total study of existing cells involved 52 impact tests to evaluate the performance of four (4) types of Ni-Cd cells:

(1) C Sub-C without spindle (Part #006200)

(2) CS Sub-C with spindle (Part #003800)

(3) LC Long Sub-C without spindle (Part #005500)

(4) P Prismatic 4 AH (Part #003500)

Each type of cell was tested in each non-redundant direction at three average impact levels: 2300g, 2960g, 3950g.

NOTE: Impact in +y direction implies:

$\vec{v}$ in +y direction

$\vec{a}$ in -y direction

impact surface -- terminal end (+y)

Each cell was fully characterized physically and electrochemically before impact testing. The cell was in the charged state and voltage was monitored during impact. Following impact and discharge, each cell is further examined physically and electrochemically (post-

characterization) before complete failure analyses.

Table III D-1 summarizes the results of the complete study. Each type of cell is shown with the directions of impact included. The actual impact (meas. mean g-level and velocity) is stated and the observed cell behavior. It must be emphasized that none of these cells was designed specifically for impact-resistance. The inherent impact resistance exhibited (or the lack of it) is not meant to imply the actual shock resistance that can be attained by any of the configurations that have been studied. The obvious example is the prismatic cell where great gains could be expected for the ±y direction with a minimum of design improvement.

In general, we were encouraged by the preliminary-analysis of this study. The cylindrical cells performed quite well, however, the Sub-C with spindle seems to have more potential damage in the x direction than the same cell configuration without a spindle. The long Sub-C seems to have experienced more difficulty in the -y direction than in the +y direction. Similarly, the prismatic results in the ±y directions were anticipated, but not the relatively poor behavior in the z direction at the highest impact level.

3. Testing of High-Capacity Cells (25 AH)

In addition to the programmed testing of smaller production

metallurgical
materials division

TABLE III D-1

Cell Type & Impact Direction		Low Impact Level (g)	(V) ft/sec.	Behavior	Med. Impact Level (g)	(V)	Behavior	High Impact Level (g)	(V)	Behavior
Sub-C	x	2000	(87)	N	2800	(106)	N	3800	(118)	N
Without	-y	2350	(86)	N	2700	(107)	N	4170 / 4100	(122) / (113)	P / N
Spindle	+y	2350	(---)	N	3400	(102)	N	3500 / 4200	(120) / (115)	P / N
Sub-C	x	2000	(88)	N	3400	(106)	N	3600 / 3600	(122) / (123)	F / P
With	-y	2520 / 2050	(89) / (86)	N / N	2750	(106)	P	4600	(121)	P
Spindle	+y	2400	(87)	N	2800	(108)	P	4800	(119)	N
Long	z	2100	(89)	N	2700	(107)	N	3500	(122)	N
Sub-C	x	2350	(88)	N	3400	(106)	N	3500	(121)	N
Without	-y	2450	(86)	P	3120 / 3000	(105) / (105)	P / P	3700	(119)	P
Spindle	+y	2300	(90)	N	2700	(106)	N	3700 / 4600	(117) / (116)	P / P
Prismatic	z	2250	(89)	N	2500	(104)	N	4070 / 4020 / 3800	(114) / (111) / (120)	P / P / F
4 A.H.	x	2300	(89)	N	2850	(105)	P	4400	(120)	P
	-y	2300	(88)	F	2800	(104)	F	3100	(112)	F
	+y	2600	(87)	F	3200	(102)	F	3800	(113)	F

CELL BEHAVIOR CODE: N - no damage
P - possible damage
F - failure

metallurgical
materials division

cells, 25 AH cylindrical prototype cells have been tested.
It must be emphasized that these cells were heat-sterilizable
but not designed for impact resistance. The tests were
meant solely to study the design techniques and practical
aspects that might occur with the larger cells.

a) Description of Large Capacity Cells

Since it was decided that a cell specifically designed
for impact resistance would not be manufactured under
the current contract, we felt it would be of value to
study the large heat-sterilized Ni-Cd cells. Three
cells of the approximately 25 AH size were available.
Again, it must be emphasized that these cells were not
designed for impact resistance but were of geometric
value in supporting some of our data on plate strength.

Cell #PR38

(12) Positive Plates 6.6" lg. x 2.8" wd. x .0255" tk.
1.46 gm/in^2, 0.0596#/plate

(13) Negative Plates 6.6" lg. x 2.8" wd. x .026" tk.
1.61 gm/in^2, 0.0656#/plate

(26) Separator   0.005" tk.

Case 7-5/8" high x 2.925" wide x 0.832" tk. internal

Spacer 0.5" @ top

free SPACE:

Thickness --
Approx. 0.002"/plate

Width --
Approx. 1/16" each side

Height --
   Approx. 7/16" Top
   Approx. 1/16" Bottom

from: $\sigma = \dfrac{F}{A} = \dfrac{W(N)}{w \cdot t}$

4000 g $\Rightarrow \sigma_{\substack{max \\ pos}} = 3{,}340$ psi

(assume no
   dynamic amplification) $\sigma_{\substack{max \\ neg}} = 3{,}610$ psi

Cell #PR114

(10) Positive Plates   5.4"lg. x 2.8"wd. x 0.030" tk.
                        1.67 g/in² 0.0557 #/plate

(11) Negative Plates   5.4"lg. x 2.8"wd. x 0.032" tk.
                        2.04 g/in², 0.0680 #/plate

(22) Separator   0.005" tk.

   Case   6.31"high x 2.925" wd. x 0.832" tk. internal

   Spacer 0.5" tk. @ Top

         free SPACE:
                   Thickness -- Approx. 0.0018"/Plate
                   Width   -- Approx. 1/16" each side
                   Height   -- Approx. 1/4" @ Top
                                Approx. 1/8" @ Bottom

from: $\sigma = \dfrac{W(N)}{w \cdot t}$ (assume no dynamic ampl.)

4000 g $\Rightarrow \sigma_{\substack{max \\ pos}} = 2{,}650$ psi

$\sigma_{\substack{max \\ pos}} = 3{,}040$ psi

Cell #C33

(3)   Positive Plates   18"lg. x 4.2"wd. x 0.0255" tk.
                         1.465 g/in², 0.244 #/Plate

metallurgical
materials division

(4) Negative Plates   18"lg. x 4.2"wd. x 0.026"tk.
                        1.61 g/in^2, 0.268 #/Plate

(6) Separator   0.005" tk.

     Case 2.931" I.D. x 5.532" int. height

     Spacer 0.5" tk. @ Top

                    free SPACE:

                            Thickness -- Approx. 0.01"/Plate
                            Height -- Approx. 11/16"-13/16" @ Top
                            Approx. 3/16"-1/4" @ Bottom

from: $\sigma = \dfrac{W(N)}{w \cdot t}$ (assume no dyn. impl.)

        4000 g $\Rightarrow \sigma_{\substack{max \\ pos}}$ = 2120 psi

                $\sigma_{\substack{max \\ pos}}$ = 2290 psi

One cell of each configuration had been previously

cycled and only cell #PR114 was shorted prior to our

testing. Initial indications were that the plates in

all these cells would support the loading imposed by a

4000 g - 1 msec impact! The stresses that have been

calculated do not exceed the values obtained during

static bearing tests for plates with the same degree of

lateral restraint. Dynamic bearing stress values gave

excellent correspondence with the static values and

indicated that a significant dynamic amplification fac-

tor is not required. The plates used in these cells

are much longer than those used in static bearing tests

and approximately equal in length to those used in

dynamic bearing tests. This implies a lower natural

metallurgical
materials division

frequency and therefore even less concern for requiring
a dynamic amplification factor. Thus our only conclu-
sion from previous evaluation of the mechanical proper-
ties of Ni-Cd electrodes would be that the plates in
any of these cells would survive impact.

b) Analysis of the Impact Process:
The preliminary conclusions are indeed founded on
design data. However, we must examine the manner of
loading. There is reason for concern over the amount
of free space permitted within these cells. It will
be shown that this is the main reason for emphasizing
that these cells were not designed for impact resistance.

It is instructive to ask: Is a mere 1/16" vertical
free space dangerous to a large cell's capability for
impact resistance?

$$\underrightarrow{\dfrac{V}{120 \ \text{ft./sec.}}}$$

CELL #PR 38

$\frac{1"}{16}$ free space
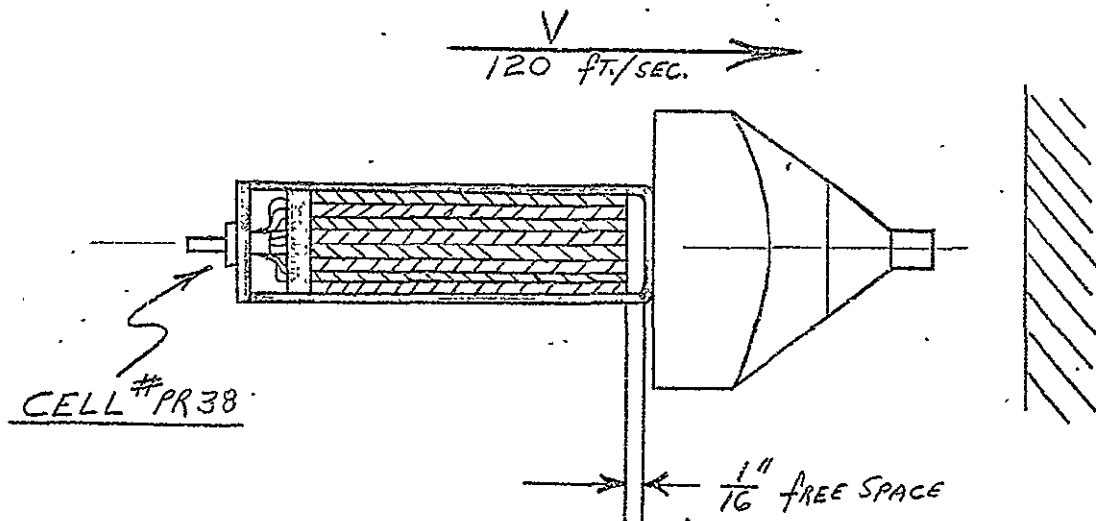
When impact occurs, the carriage, cell, and individual

electrodes experience a 4000g gravitational field for

1 msec. The resultant force exerted on a negative elec-

trode is:

$$F = ma = 262\#$$

This force will accelerate the electrode to some higher

velocity which will be limited by the distance (and

thus time) over which this acceleration force can act:

$$S = v_i t + 1/2 \ a \ t^2$$

$$t = 35\mu \ sec$$

With this time available to cover the 1/16" free space,

the final electrode velocity at impact will be:

$$v_f = v_i + at = 124.5 \ ft/sec$$

Now during the same time interval, the carriage and cell

case have to be decelerated to a velocity of:

$$v_f = v_i + at = 115.5 \ ft/sec$$

Diagramatically we have:

$\frac{1}{16}''$ FREE SPACE

120

120

$t < 0$

120⁻ → ... 120⁺

$t = 0$

115.5 → ... 124.5

$t = 35 \mu sec$

0 → ... 0

$t = 1000 \mu sec$
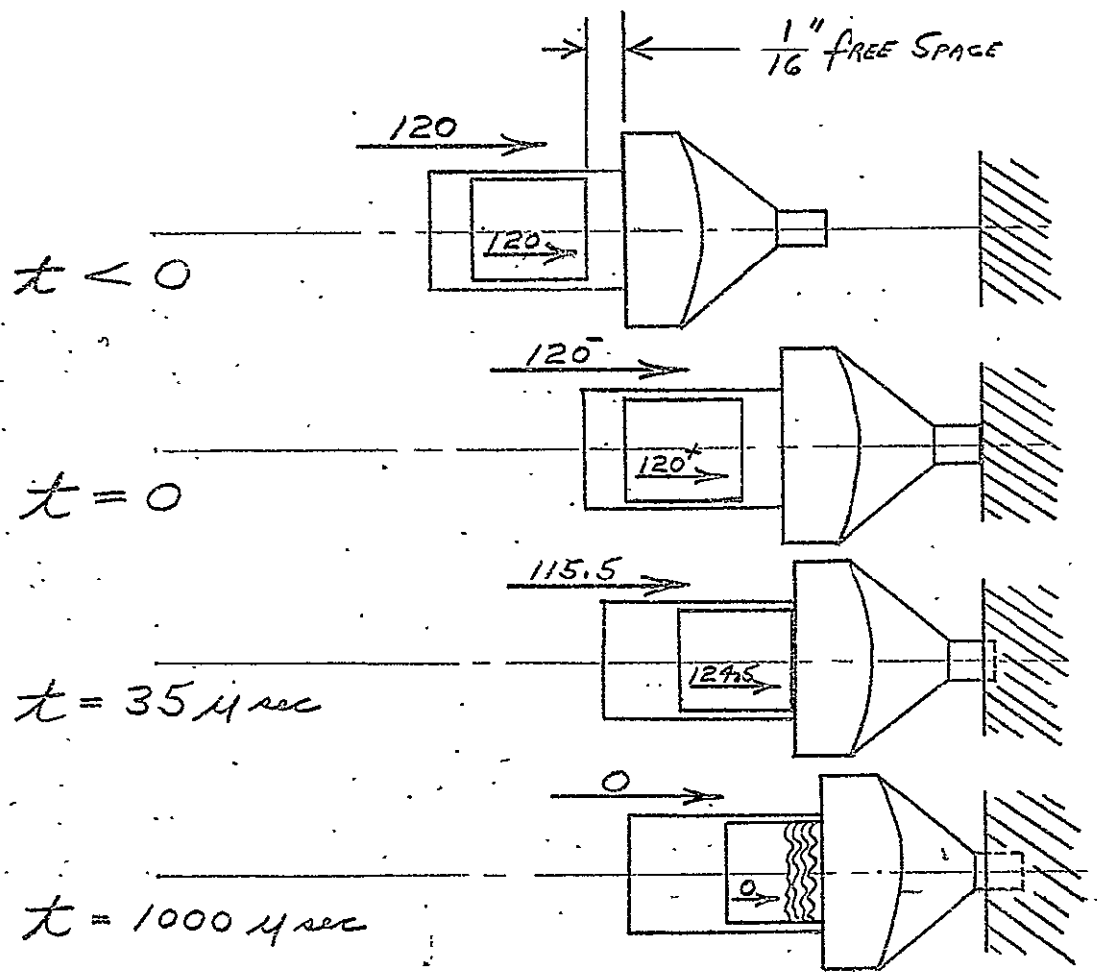
In reality therefore, we have the carriage and cell case experiencing entirely different loading than the electrodes:

P MAGNITUDE

TRUE ELECTRODE LOADING

IDEALIZED ELECTRODE LOADING

CELL CASE LOADING

6000 g

4000 g

"TIME"

2000 g

"MAGNITUDE" & "TIME" CANNOT BE INDEPENTLY CALCULATED

35 μ SEC.

0.5

1.0 msec

t
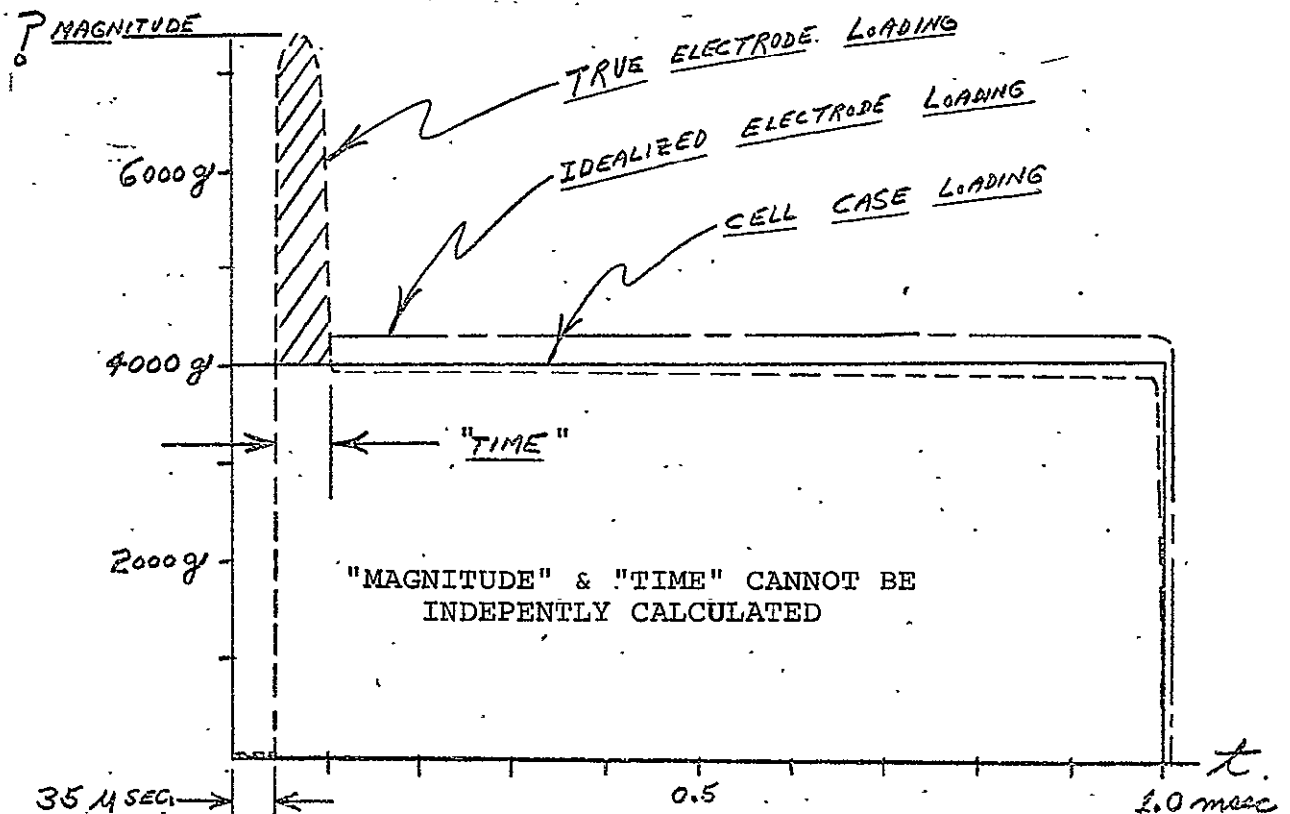
The cell case of course experiences the uniform, deceleration loading. The electrode, however, has a relative velocity at its impact of 9 ft/sec which must be diminished before movement with the carriage (and 4000 g loading) can occur. Rapid deformation of the electrode will occur at this point, as loading increases for a short time. We can calculate the energy involved.

$$\int F \cdot dt = m \ (\Delta v) = (9 \ ft/sec)$$

or the shaded area of the spike. Unfortunately, we cannot determine the "magnitude" or "time" involved without additional experimental information describing the deformation process.

We can only assume that this is a small amount of energy and question if the electrode can accommodate it by deformation at maximum load for the remainder of time available. If the static bearing values are valid, the maximum stress that a negative electrode can support at .002"/plate lateral restraint is 3750 psi. Thus the maximum force is:

$$F = \sigma \ (w \cdot t) = 274\#$$

The amount of time required (by uniform force) to accomplish the total velocity change from 124.5 ft/sec → 0 ft/sec is:

$$F \cdot t = m \ (\Delta V)$$

$$t = 0.926 \ msec$$

metallurgical
materials division

This amount of time is < 0.965 msec still available and implies the deceleration could be accomplished safely (with a margin of only 39 μ sec!).

This exercise was performed for a specific plate (2.36 length: width ratio) and assumed a mere 1/16" free space; yet, it dramatically illustrates the very fine distinction between failure and survival. Several points regarding this analysis must be noted:

1. The additional weight of electrolyte saturation was not included in the mass of the electrode.

2. The total area of the end of the electrode was presumed to be available for supporting load.

3. Prior to initial impact, the electrode pack was presumed stationary -- maintaining its 1/16" relative distance to the cell case impact surface.

4. Most importantly, the effect of a damaging peak force at electrode impact was neglected in our final statement of apparent survival.

c) Results of Testing:

We shall now look at the results of impact tests performed on these cells and see that failure to achieve the above conditions will have rather obvious consequences.

metallurgical
materials division

The orientation of each cell during impact is shown below:

#PR38   #PR114   #C33
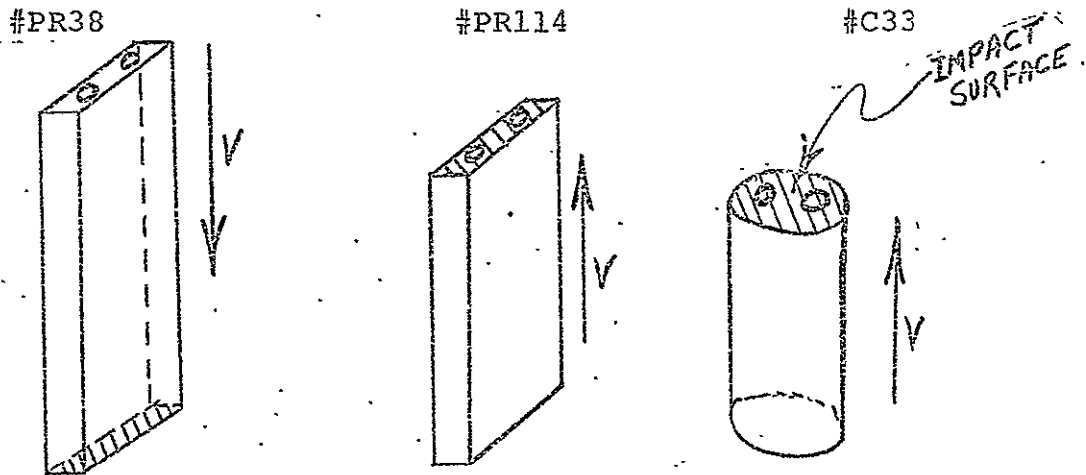
The description of the impact parameters for each cell (velocity, g-level, time) is given in Figure III-17 (a), (b), (c). The time history of open circuit voltage during impact is also shown. All three cells failed under the imposed impact. X-rays taken of each cell immediately after impact are shown in Figures III-18, III-19, III-20. Upon disassembly of each cell, photographs were taken of the electrode deformation and are shown in Figures III-21, III-22, III-23. The visual evidence of failure depicts quite vividly the kinds of deformation that can occur when some of the earlier design points are not realized. We may discuss these tests individually:

Cell #PR38:

The large prismatic cell failed in buckling of the electrodes. It was our decision to test each cell as

Figure III - 117

UPPER TRACE: 2 msec/cm   LOWER TRACE: 0.5 msec/cm

(a) CELL #PR 38

V = 105 ft/sec

1.2 VOLT

1000 g
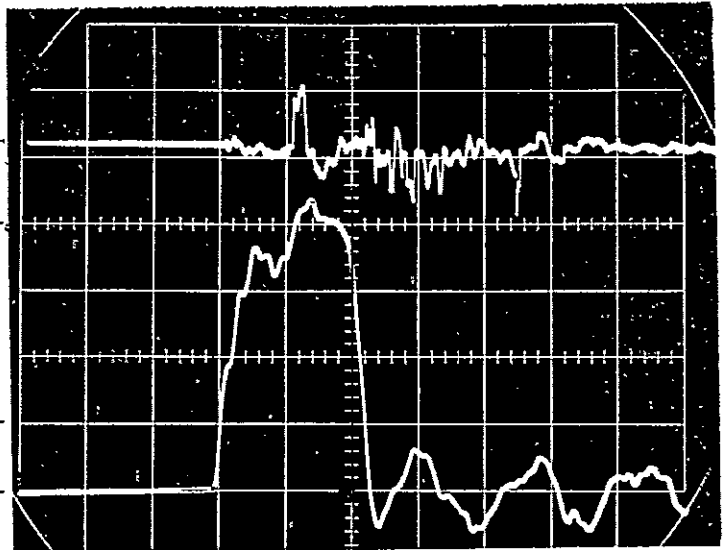
(b) CELL #PR 114

V = 104 ft/sec

EXTRANEOUS SIGNAL
NOT CONNECTED
TO SHORTED CELL
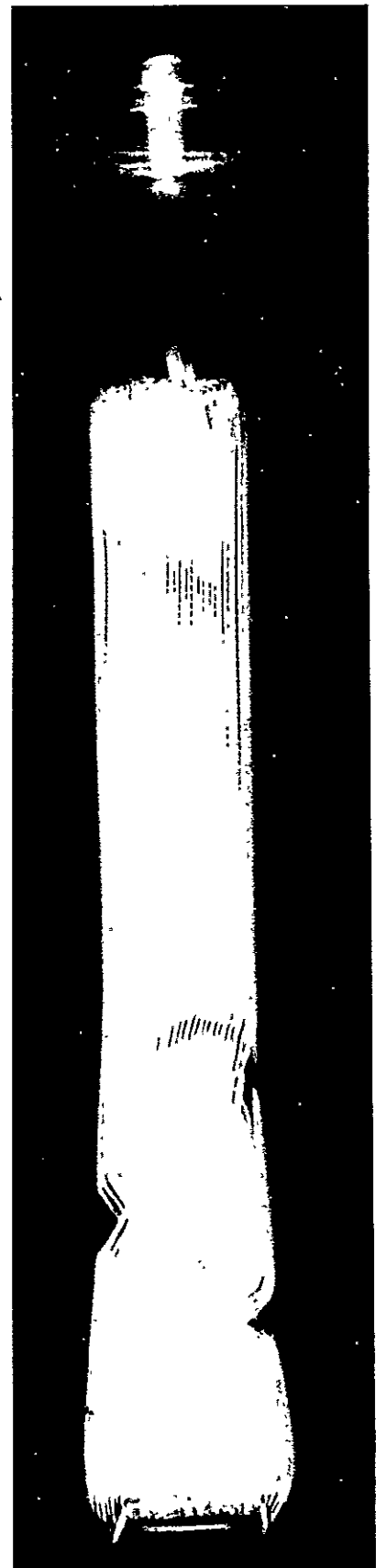
1000 g
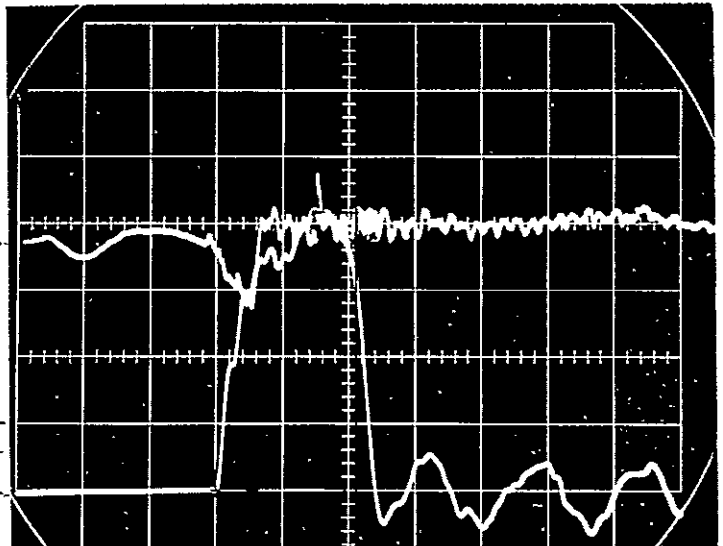
(c) CELL #C 33
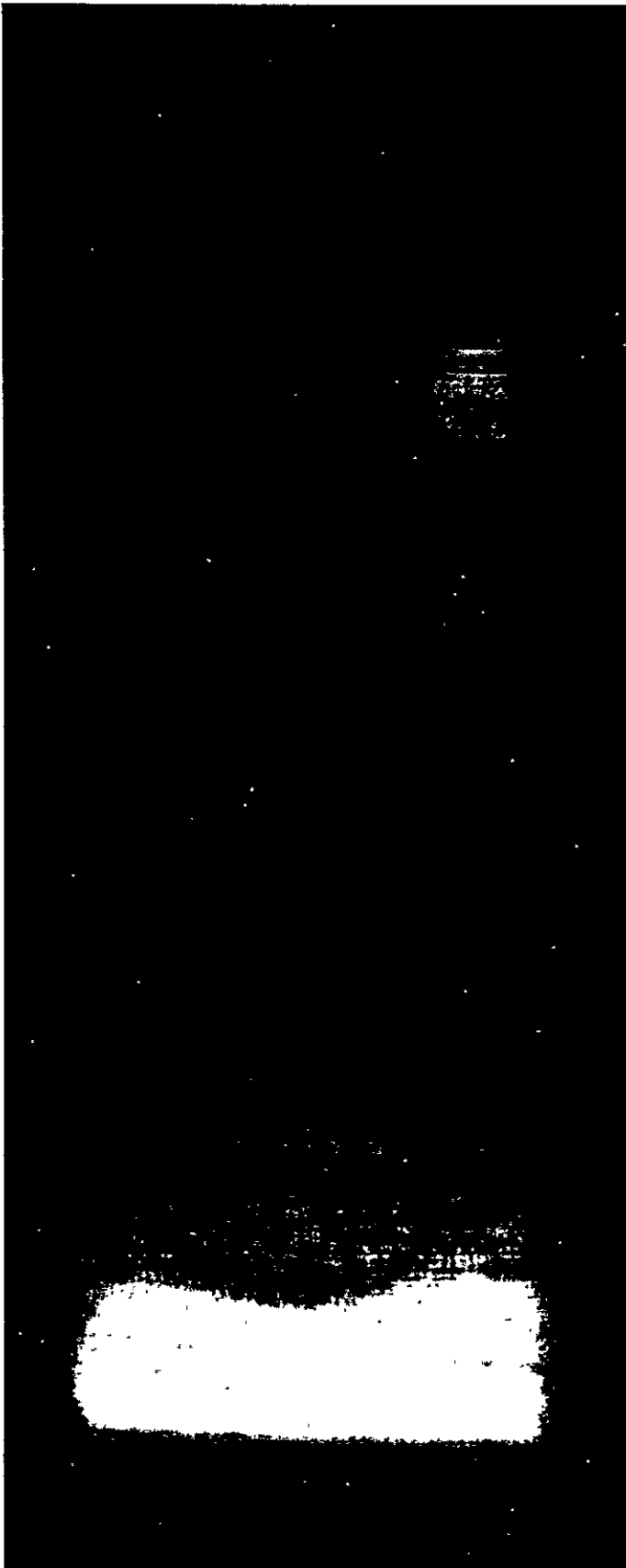
V = 104 ft/sec

0.7 VOLT

1000 g

III - 115
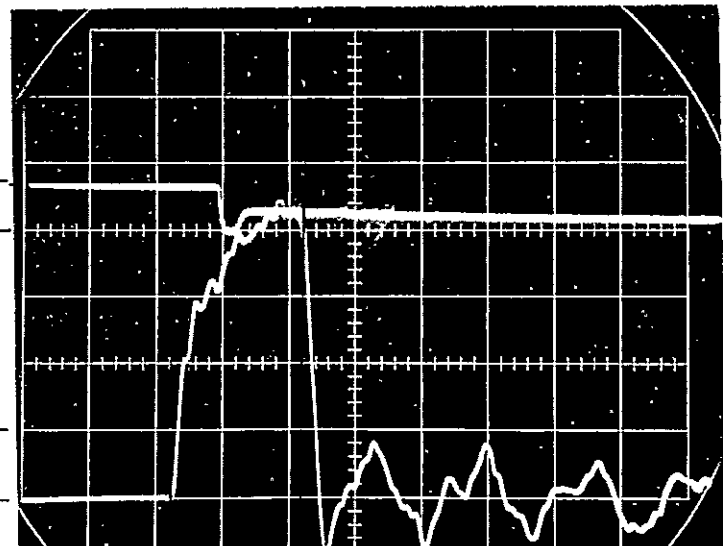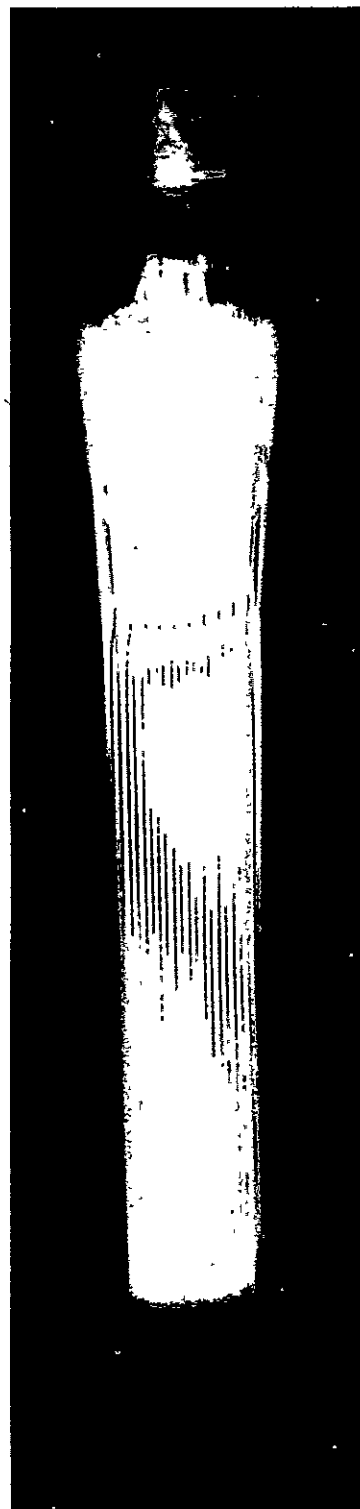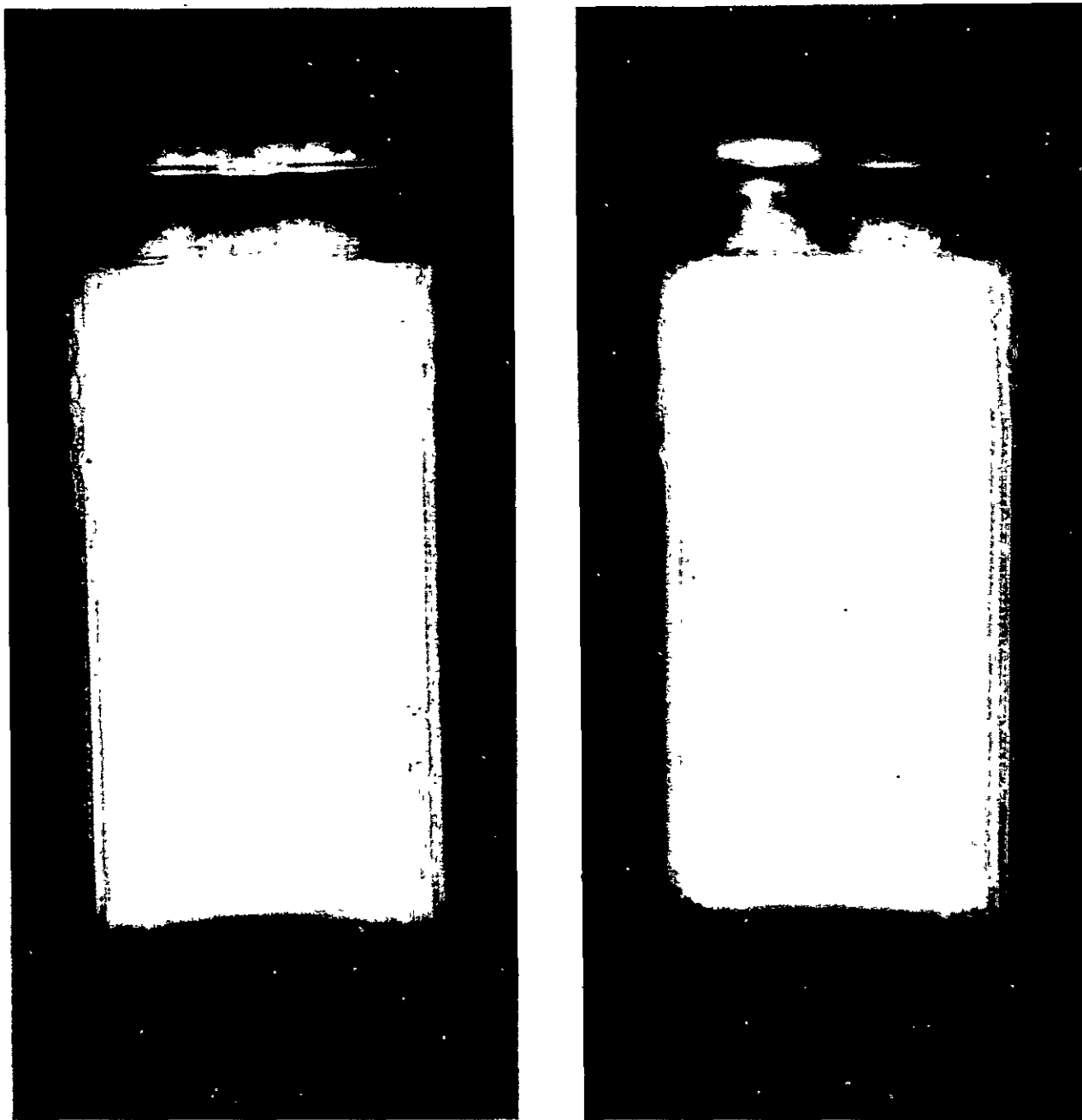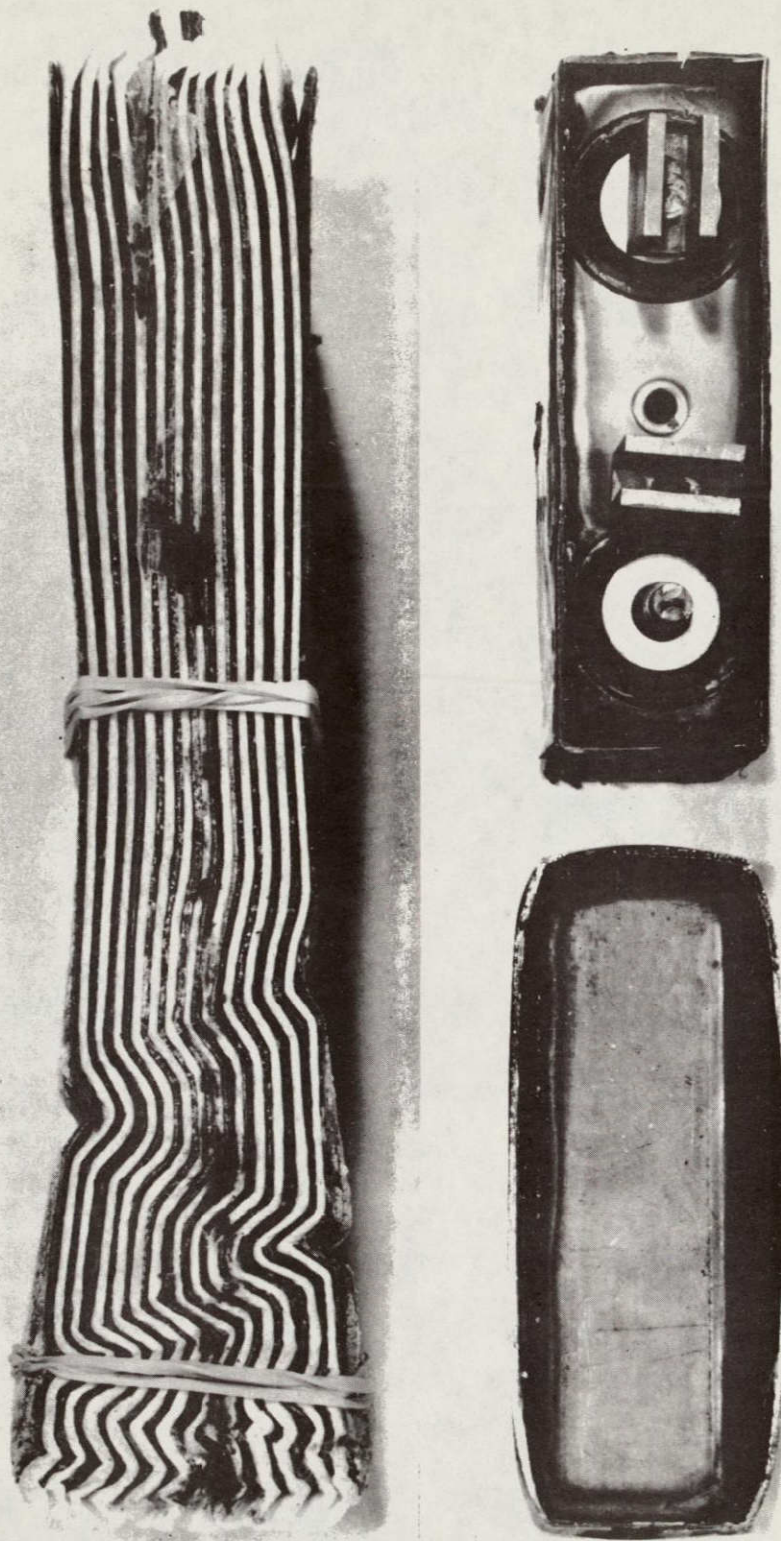
Figure III - 18

CELL #PR 38   POST-IMPACT

Figure III - 19

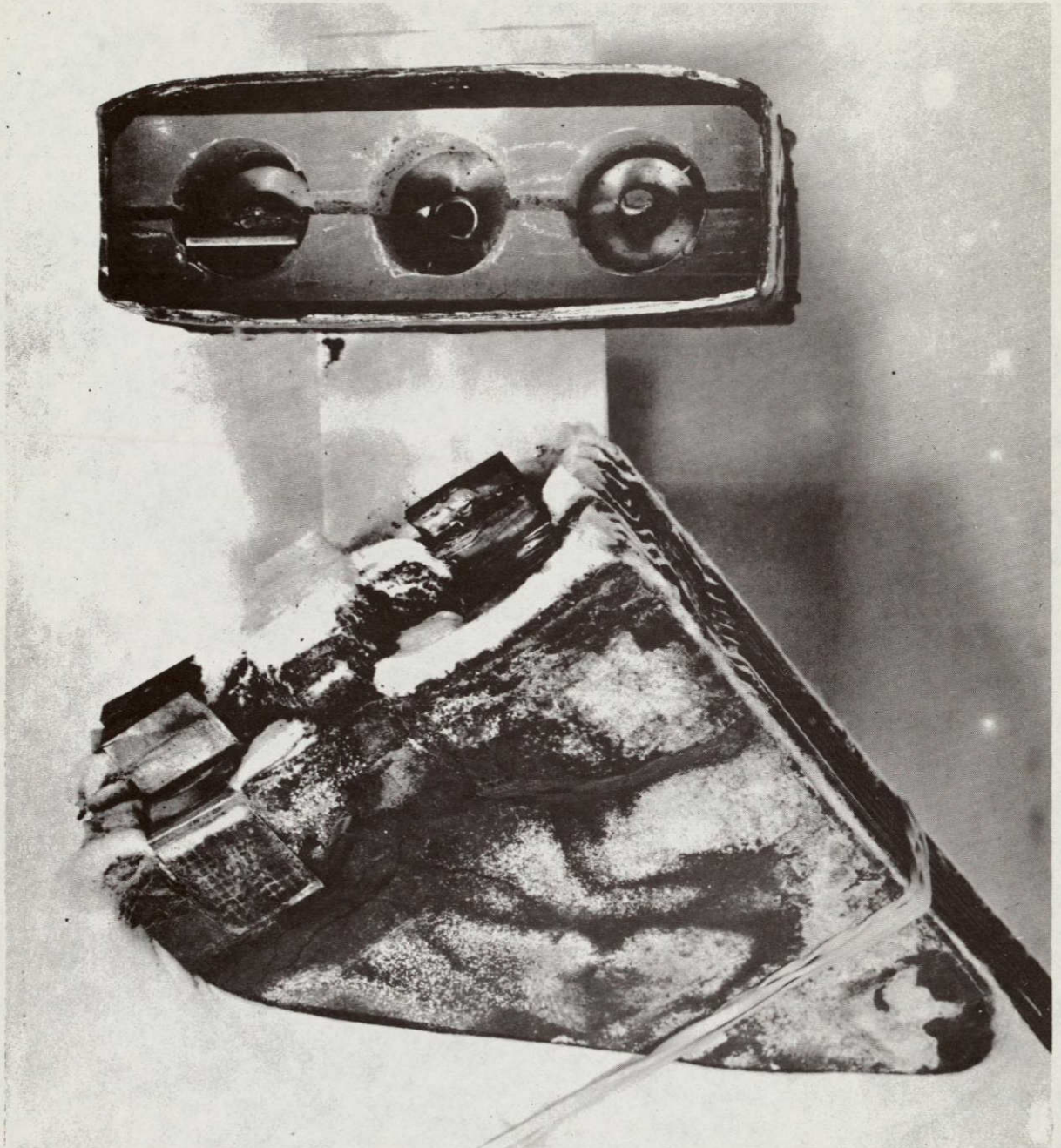CELL #PR 114   POST-IMPACT

Figure III - 20

CELL #C 33   POST-IMPACT
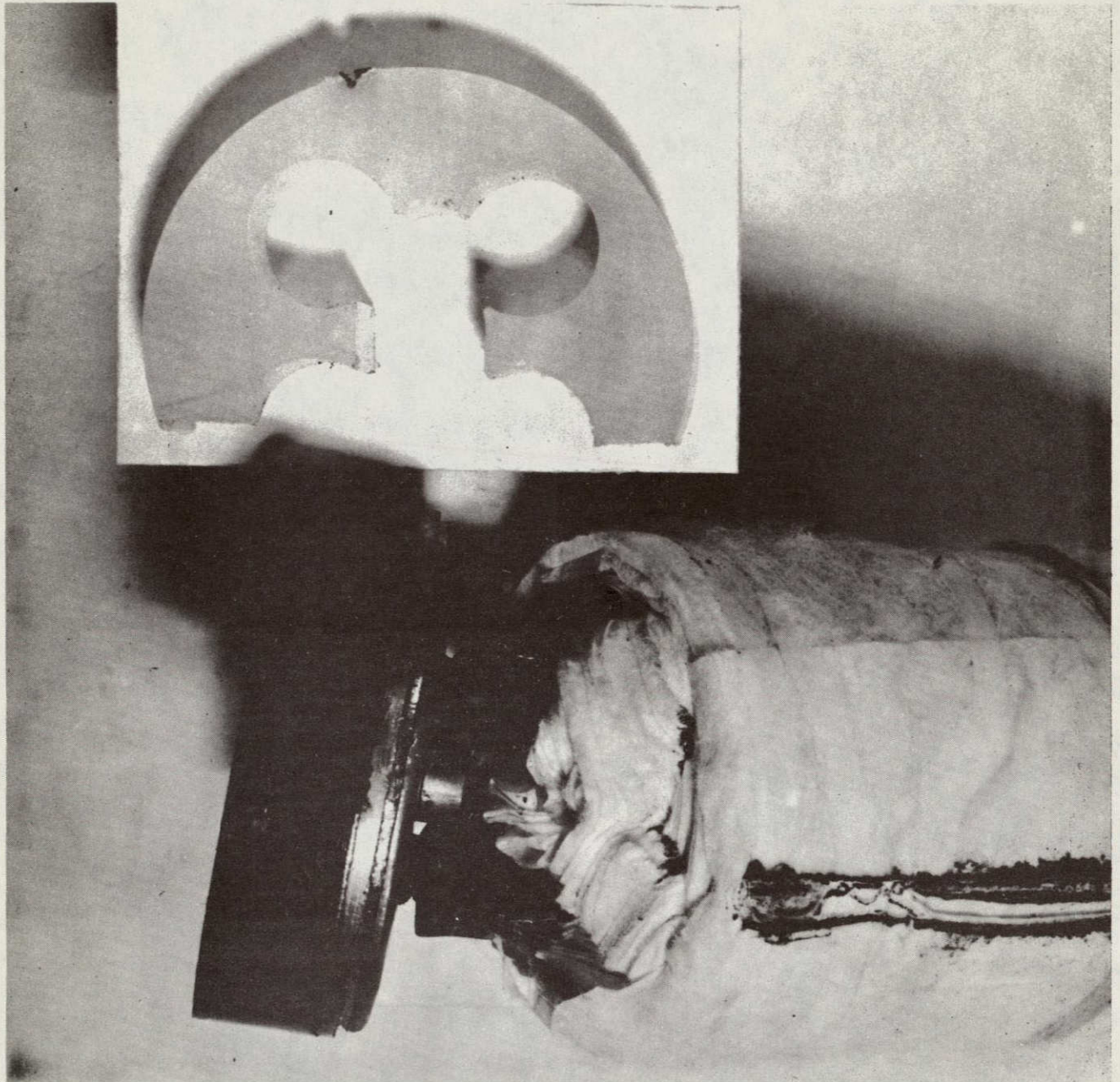
Figure III - 21

CELL #PR 38

Figure III - 22

CELL #PR 114

Figure III - 23

CELL #C 33

an entity in the sense that external restraints would not be used. This lack of restraint showed that the cell case alone is not of sufficient strength to support its own weight under inertial load and the lateral pressure imposed on it by the deforming electrode pack. The electrode pack apparently had sufficient lateral restraint and support from its terminals to withstand the loading during acceleration. This is both a visual observation and the presence of full voltage at impact. Under deceleration a much lower degree of lateral restraint was available from the cell case, and the electrodes had little difficulty in buckling (Figure III-18 & 21). The electrodes could not reach the full value of stress which they are capable of supporting. The post-mortem failure analysis also showed that one terminal collector had apparently not been welded. This is the most likely cause for the erratic voltage trace shown in Figure III-17(a). We note, however, that voltage was maintained on this cell despite the defective terminal and the extensive deformation. It is our contention that this cell would not have experienced failure if thicker axial spacers and lateral restraining plates had been used.

Cell #PR114:

The smaller prismatic cell had the largest free space

at the impact end of any cell and this is largely
responsible for the damage. We cannot make a judgment
on the motions during acceleration. Although there is
no visual damage to the bottom of the electrode pack,
we do not have a trace to indicate the voltage at im-
pact. During deceleration both terminal collectors
were fractured. The most significant lesson in the
study of this cell is the total ineffectiveness of the
spacer design.

$\Rightarrow$ *1.35 in²*

63% of ELECTRODE
PACK BEARING
AREA
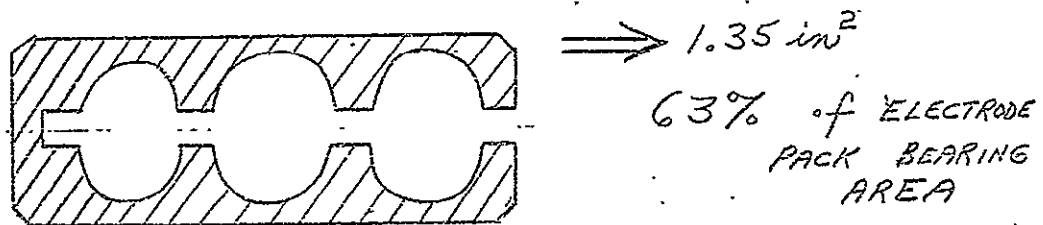
The predicted stresses for this cell become meaningless
under this situation and failure is the obvious conse-
quence. The visual observations of the top of the elec-
trode pack dramatically show the areas which supported
load (Figures III-19 & 22). The spacer vent hole area
is quite emphatic. We note that the failure mode in
supported areas is again buckling. This again indicates
that low lateral restraint (static plate spacing and
dynamic cell case expansion) prevented the electrodes
from reaching their ultimate compression stress.

Cell #C33:

The cylindrical cell developed direct shorting in the

terminal areas of the cell (Figure III-17(c)) as electrode motion was severe during impact. Again, the spacer design was solely responsible for this failure.
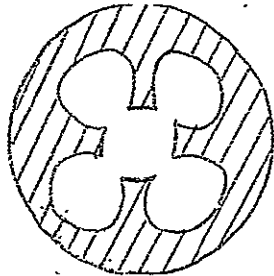
$\Longrightarrow$ 2.60 in^2
59% of electrode pack bearing area

As shown in Figure III-20 and Figure III-23, the plates moved forward into the open areas of the spacer. The open core in particular had large axial excursion. Again, there was no damage to the cell during acceleration (visual observation and cell voltage trace). It is significant that this cylindrical configuration has resisted nearly totally the buckling mode of failure. Even in the areas where severe bearing loads were possible, the x-ray analysis shows only traces of buckling. The stability of the cylindrical cell is apparent mainly because of the inherent cell case design. What we have seen is that the cell cases in the two prismatic designs (without the benefit of restraining plates as normally used on batteries) were the prime cause of lowering lateral restraint under impact conditions. This confirms our contention that our electrodes themselves will

resist buckling and go on to the true ultimate compressional stress that we have established.

In conclusion, the study of these cells has provided the design emphasis that we desired. The importance of static assembly plate spacing, the use of spacers that maximize effective bearing area and axial thickness, and the cell case contribution to pack integrity have been adequately demonstrated. In short, we have stated the precautions that must precede the use of our design data to predict a cell's behavior under impact loading.